University POLITEHNICA of Bucharest
ROMANIA

Optimization of the 3D space trajectory by using the neural network and kinematics, dynamics and Fourier spectrum

ICMAS

8-9 November 2012

Bucharest, ROMANIA

Prof.univ.Ph.D.Eng.Adrian OLARU
Fellow member of International Association of Computer Sciences and Information Technology (IACSIT) Singapore
Member of IEEE Robotics and Automation Society (IEEE-RAS), USA
Fellow member of the Mechanical Engineering Society (MES), Singapore
Fellow member of Robotics and Automation Association (ARS), Singapore
Fellow member of Science and Technology Institute (SCIEI), USA
President of the International University Association for Science and Technology (UASTRO), Romania
Member of the American Nano Society (ANS), USA
Member of Romanian Robotics Society (RRS), Romania
University “Politehnica” of Bucharest (UPB), Romania

Optimization of the space trajectory

- *By using the control law and transfer function method* – controlling the servo driving;
- *By using the artificial intelligence, proper neuronal network* and direct and inverse kinematics and dynamics results;
- *By using the intelligent smart damper and proper neural* network for controlling the Fourier spectrum;
- **By using the complex control** with proper neural network, the kinematics, dynamics and Fourier spectrum;
- ***research for the future;*** By using the intelligent damper and smart panel mounted in some sections for the control of all structure;

- By using the control law and transfer function method – controlling the servo driving;

Assisted optimization of the servo driving by using virtual LabVIEW instrumentation and the elementary transfer functions method

Adrian Olaru[1], Serban Olaru[2] and Aurel Oprean[3]

[1]University Politehnica of Bucharest, Romania,

[2] Romsys Mechatronics Company, Romania

[3]Vice President of the Mechanical Branch of the Romanian Academy of Technical Sciences

E-mail address: olaru_robotics@yahoo.com .

I NT R O D U C T I O N

- The transfer functions theory applied to the elements and the systems **using the LabVIEW** non linear components assure one very easily mode of the **modeling, simulation and validation** of the elements and systems, finally to obtain by sinthesys one integrated and intelligent system;
- In the paper will be presented **one virtual LabVIEW propre library** for the assisted research of the electrical and hydralic elements and systems with many results what will be possible to use in the curently research;
- In the optimising field was used some neural network and the **on-line research** of the network influences to the finally target of the servo driving system;
- With applied this theory was possible **to design one proper smart system to decrease the vibration** of the robot end-effector and optimise the space trajectory;
- With designed LabVIEW VI-s will be possible **to choose the optimal values of the constructive- functional parameters** of the components of the system.

Table 1. Some expressions and virtual LabVIEW instruments of transfer functions

Type	Expresion of transfer function		Virtual LabVIEW instrument
PT_1	$H(s)=\dfrac{k}{T_1 s+1}$		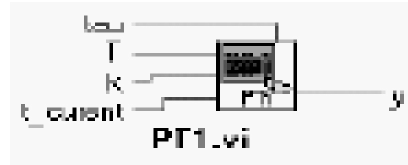
PT_2	$H(s)=\dfrac{k}{(s+a)(s+b)}$	$\xi>1$	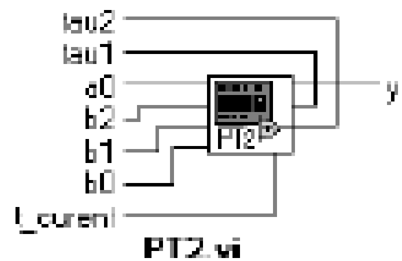
	$H(s)=\dfrac{k}{s^2+a^2}$	$\xi=0$	
	$H(s)=\dfrac{k}{(s+a)^2}$	$\xi=1$	
	$H(s)=\dfrac{k\omega_n^2}{s^2+2\xi\omega_n s+\omega_n^2}$	$0<\xi<1$	
PT_3	$H(s)=\dfrac{k}{(s+a)(s+b)(s+c)}$		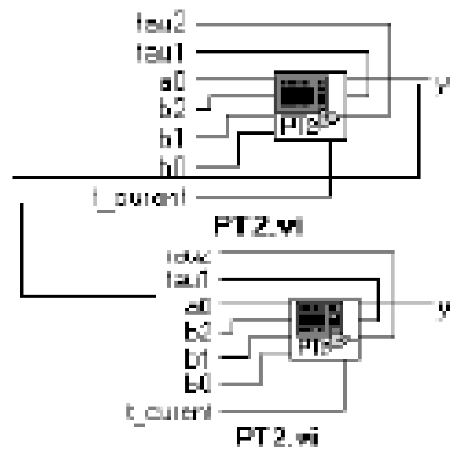
PT_4	$H(s)=\dfrac{k}{(s+a)(s+b)(s+c)(s+d)}$		

Table contents: type of the transfer function; Mathematical model; virtual LabVIEW instrumentation

I	$H(s) = \frac{k}{s}$	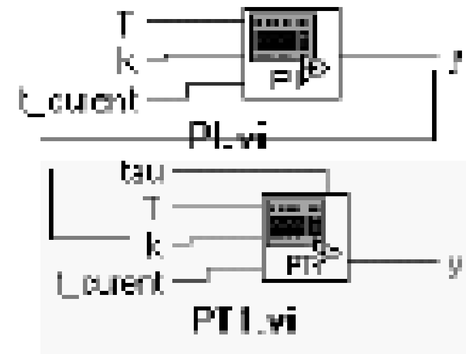
IT_1	$H(s) = \frac{k}{s} \cdot \frac{1}{T_i s + 1}$	
PDT_1	$H(s) = \frac{k(T_d s + 1)}{T_i s + 1}$	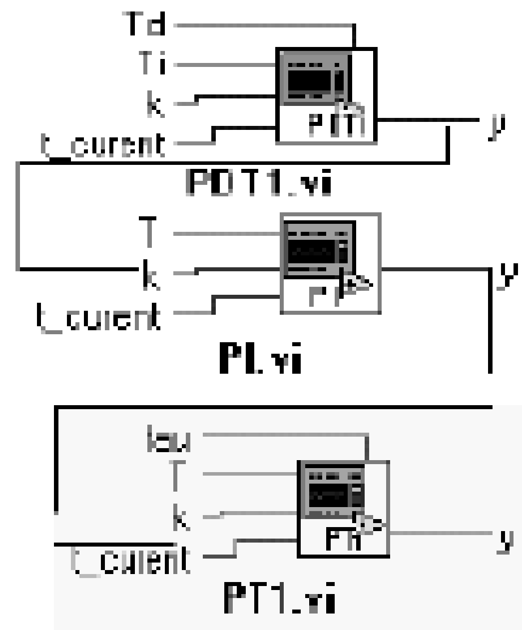
DT_1	$H(s) = \frac{T_d s}{Ts + 1_i}$	
PID	$H(s) = k(1 + T_d s + \frac{1}{T s_i})$	
PID T1	$H(s) = k(1 + T_d s + \frac{1}{T s_i}) \cdot \frac{1}{T_I s + 1}$	

Table 2
Some models of transfer functions and his characteristics, mathematical and physical models

P	$H(s)=K$	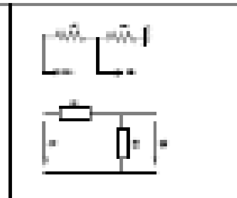	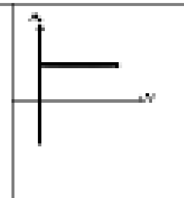	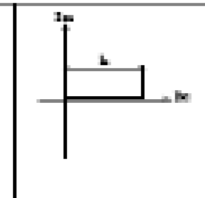	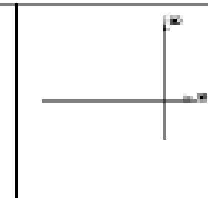	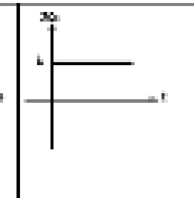
PT1	$H(s)=\dfrac{K}{T_i s+1}$	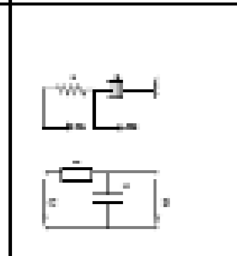	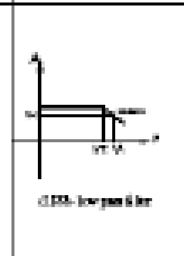	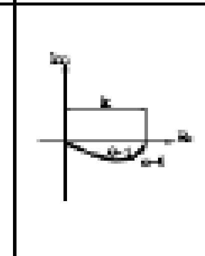	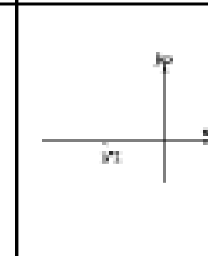	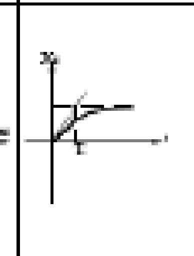
PT2	$H(s)=\dfrac{K}{(T_{i_1} s+1)(T_{i_2} s+1)}$	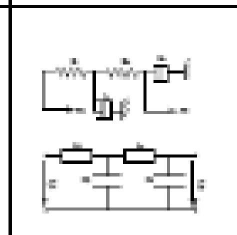	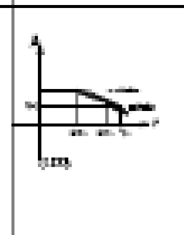	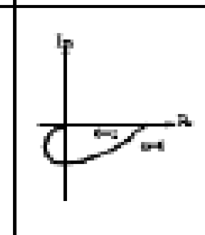	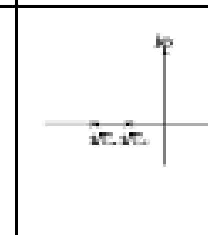	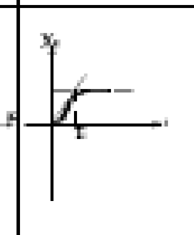
	$H(s)=\dfrac{K}{(T_{i_1} s+1)(T_{i_2} s+1)}$	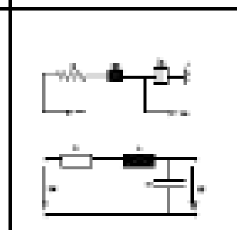	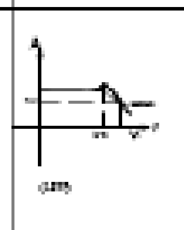	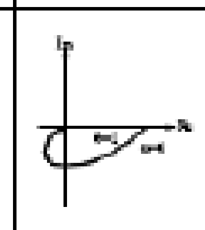	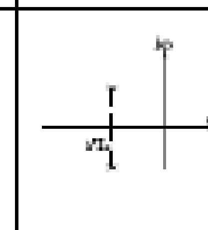	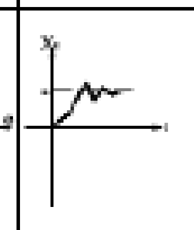

Table contents: Type of the transfer function; Mathematical model in Laplace plane; Physical electrical or mechanical model; Bode characteristic *A* vs.*f*; Nyquist characteristic; plane poles-zeros; real characteristic.

PT3	$H(s)=\dfrac{K}{(T_{i_1}s+1)(T_{i_2}s+1)(T_{i_3}s+1)}$	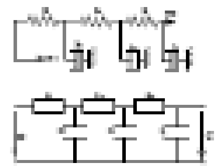	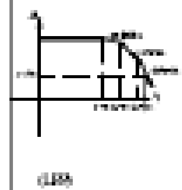	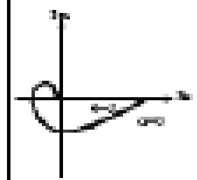	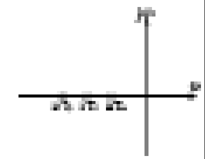	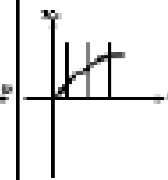
	$H(s)=\dfrac{K}{(T_{i_1}s+1)(T_{i_2}s^2+T_{i_3}s+1)}$	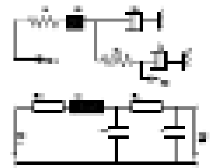	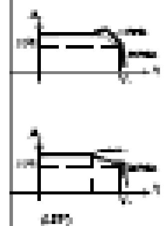	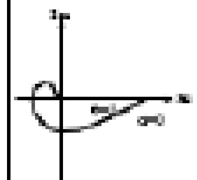	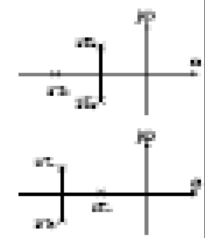	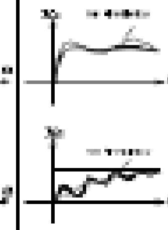
PT4	$H(s)=\dfrac{K}{(T_{i_1}s+1)(T_{i_2}s+1)(T_{i_3}s+1)(T_{i_4}s+1)}$	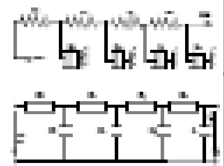	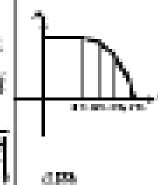	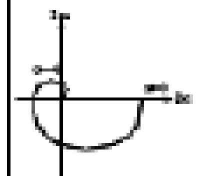	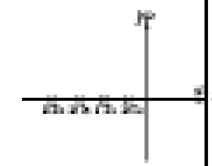	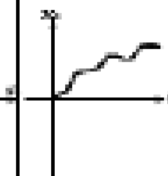
	$H(s)=\dfrac{K}{(T_{i_1}s+1)(T_{i_2}s+1)(T_{i_3}s^2+T_{i_4}s+1)}$	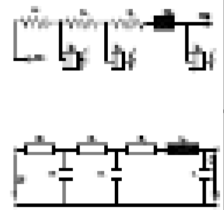	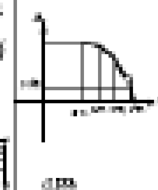	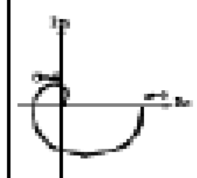	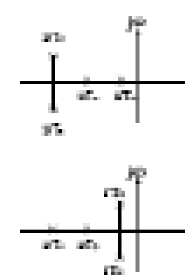	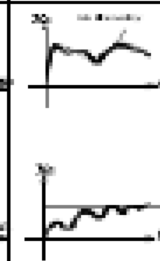
	$H(s)=\dfrac{K}{(T_{i_2}s^2+T_{i_1}s+1)(T_{i_3}s^2+T_{i_4}s+1)}$	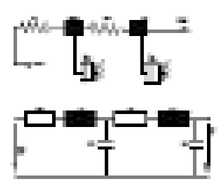	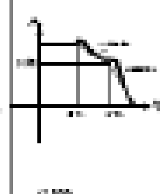		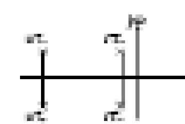	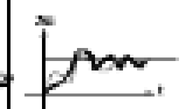

I	$H(s)=\frac{K}{s}$	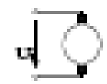	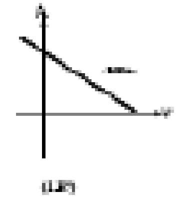	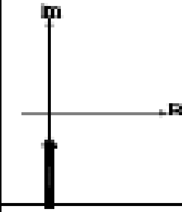	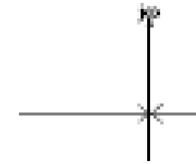	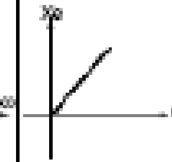
IT1	$H(s)=\frac{K}{s}\frac{1}{T_i s+1}$	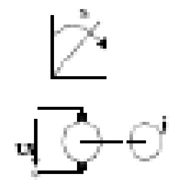	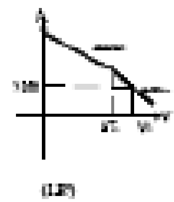	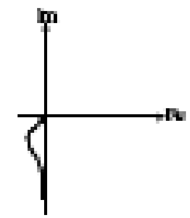	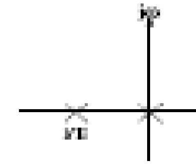	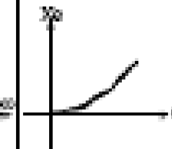
IT2	$H(s)=\frac{K}{s}\frac{1}{T_{i_2}s^2+T_{i_1}s+1}$	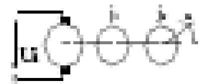	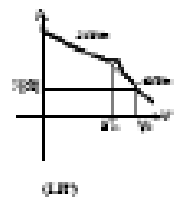	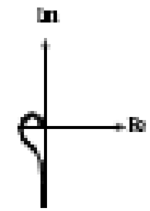	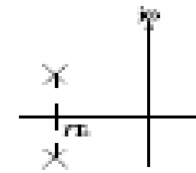	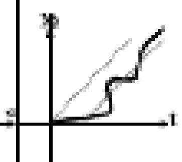
IT3	$H(s)=\frac{K}{s}\frac{1}{(T_i s+1)(T_{i_2}s^2+T_{i_1}s+1)}$	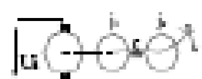	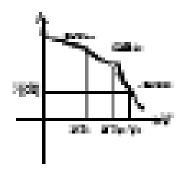	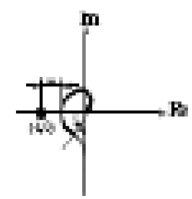	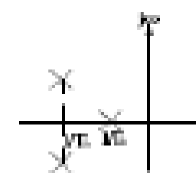	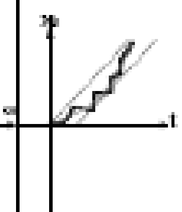

D	$H(s)=T_D s$	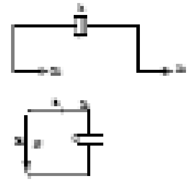	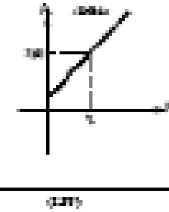	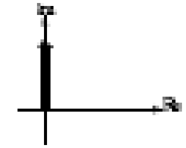	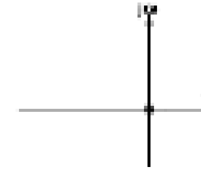	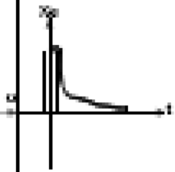
DT1	$H(s)=\dfrac{T_D s}{T_i s+1}$	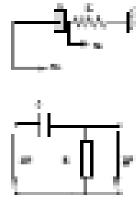	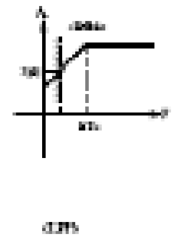	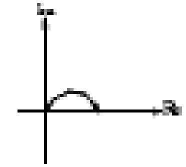	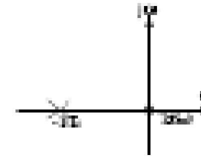	
D2T2	$H(s)=\dfrac{T_{D_2} s^2+T_{D_1} s}{T_{i_2} s^2+T_{i_1} s+1}$	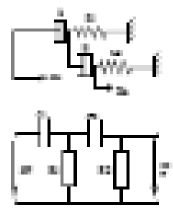	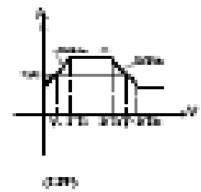	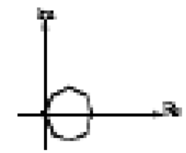	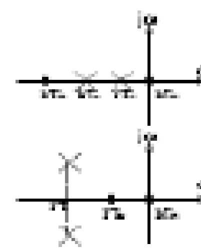	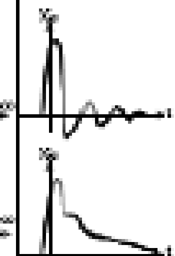
PDT	$H(s)=\dfrac{K(T_D s+1)}{T_i s+1}$ $T_D > T_i$	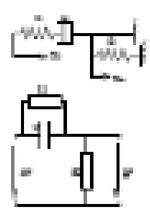	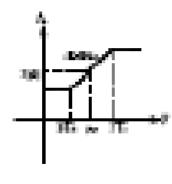	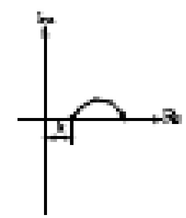	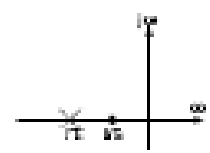	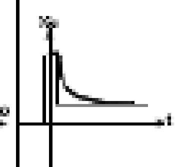

PDT1	$H(s)=\dfrac{K(T_D s+1)}{T_i s+1}$ $T_D < T_i$	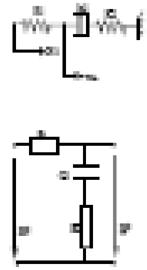	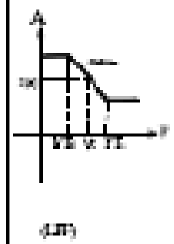	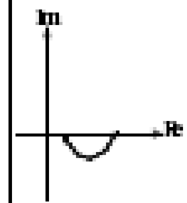	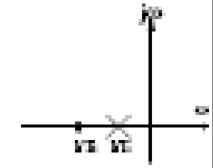	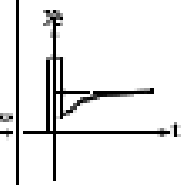
PD2T2	$H(s)=\dfrac{s^2+(a_1+b_2)s+a_1b_2}{s^2+(a_2+b_1)s+a_2b1}$ $a_1b_2=a_2b_1;\ (a_1+b_2)>(a_2+b_1)$	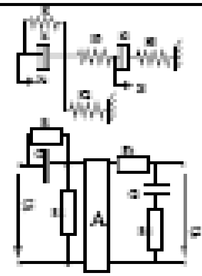	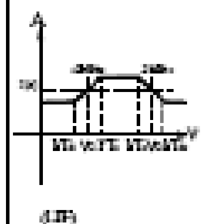	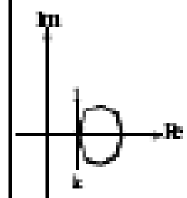	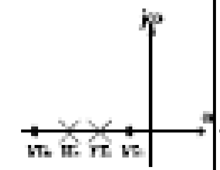	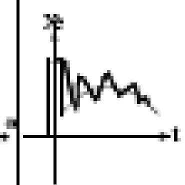
PD2T2	$H(s)=\dfrac{s^2+(a_1+b_2)s+a_1b_2}{s^2+(a_2+b_1)s+a_2b1}$ $a_1b_2=a_2b_1;\ (a_1+b_2)<(a_2+b_1)$	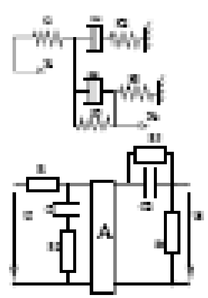	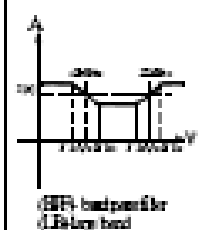	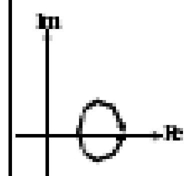	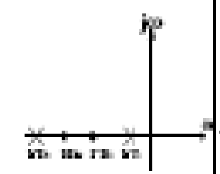	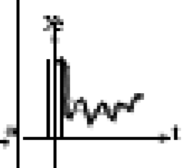
PD2T2	$H(s)=\dfrac{s^2+(a_1+b_2)s+a_1b_2}{s^2+(a_2+b_1)s+a_2b1}$ $a_1b_2=a_2b_1;\ (a_1+b_2)>(a_2+b_1)$ $a>b$	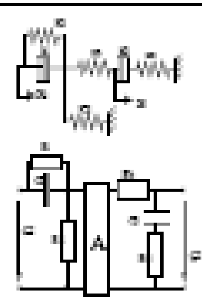	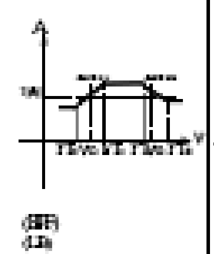	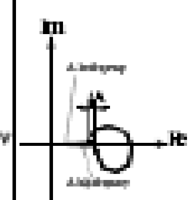	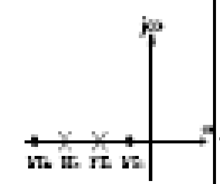	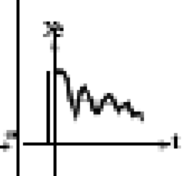

	$a > b$					
PD2T2	$H(s)=\dfrac{s^2+(a_1+b_2)s+a_1b_2}{s^2+(a_2+b_1)s+a_2b_1}$ $a_1b_2=a_2b_1;\ (a_1+b_2)>(a_2+b_1)$ $a<b$	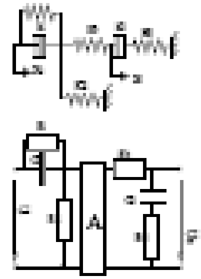	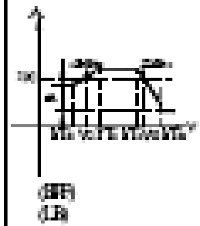	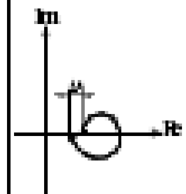	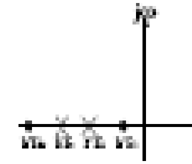	
PID	$H(s)=\left(1+T_D s+\dfrac{1}{T_i s}\right)K$ $4Td > T$	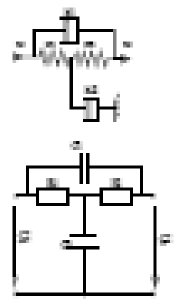	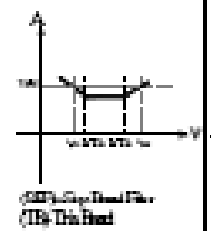	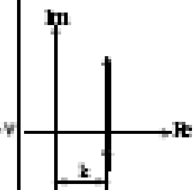	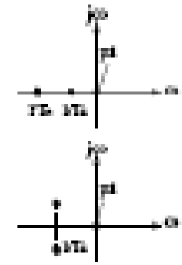	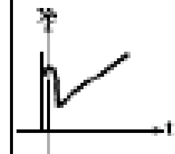
PIDT1	$H(s)=K\left(1+T_d s+\dfrac{1}{T_i s}\right)\dfrac{1}{T_1 s+1}$	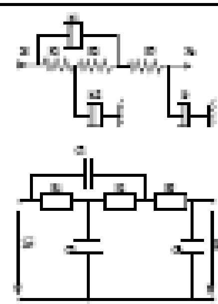	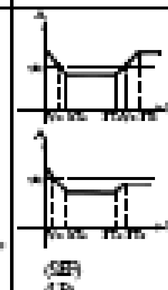	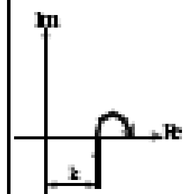	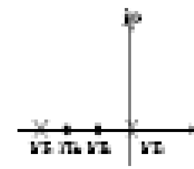	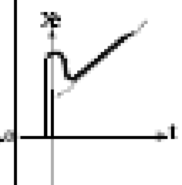
		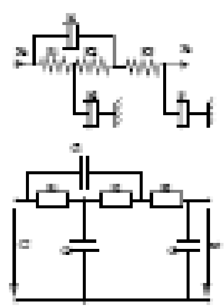	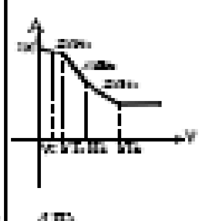	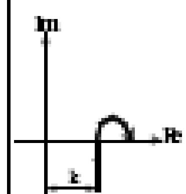	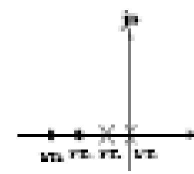	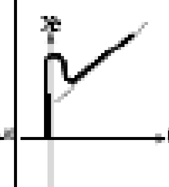

		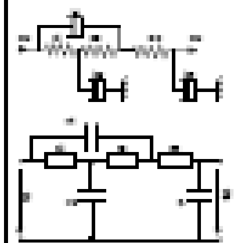	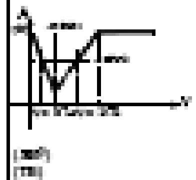	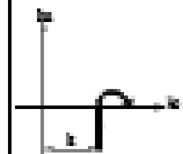	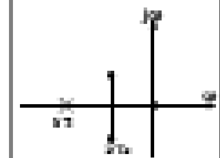	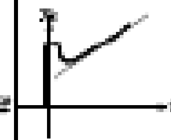
		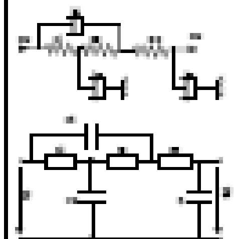	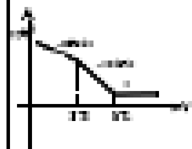	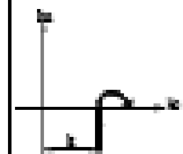	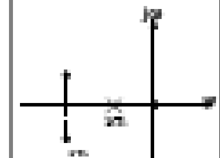	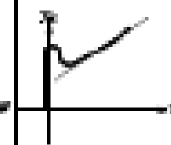
PIDT2	$H(s)=K\left(1+T_d s+\frac{1}{T_i s}\right)\frac{1}{T_2 s^2+T_1 s+1}$	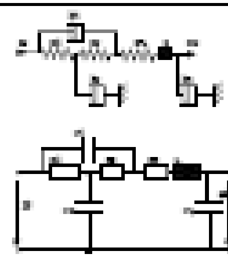	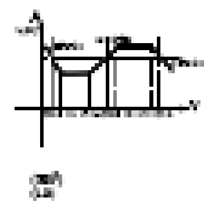	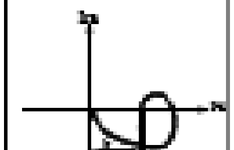	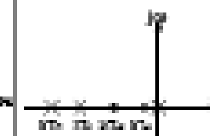	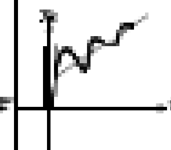

Case study of the Linear Hydraulic Motor (LHM)-optimizing the dynamic behavior of '' drivers

$$[H(s)] = \frac{\begin{bmatrix} x_{e1}(s) \\ x_{e2}(s) \end{bmatrix}}{\begin{bmatrix} x_{i1}(s) \\ x_{i2}(s) \end{bmatrix}} = \begin{bmatrix} H_{11} & H_{12} \\ H_{21} & H_{22} \end{bmatrix}$$

$$T_1 T_2 \frac{dx_e^2}{dt^2} + h(T_1 + T_2)\frac{dx_e}{dt} + x_e = kU$$

$$\begin{pmatrix} x_1' \\ x_2' \end{pmatrix} = \begin{bmatrix} 0 & 1 \\ -\frac{1}{T_1 T_2} & -\frac{h(T_1 + T_2)}{T_1 T_2} \end{bmatrix} \begin{pmatrix} x_1 \\ x_2 \end{pmatrix} + \begin{pmatrix} 0 \\ \frac{k}{T_1 T_2} \end{pmatrix} U(t)$$

$$Y = \begin{pmatrix} 1 & 0 \end{pmatrix} \begin{pmatrix} x_1 \\ x_2 \end{pmatrix}$$

The frequency of the system will be done by the element with the smaller frequency of the system aproximatelly determined by:

$$\nu = \frac{\prod \nu_i}{\sum \nu_i}$$

$$\left(x'(t)\right) = [A]\left(x(t)\right) + [B]\left(u(t)\right)$$
$$\left(y(t)\right) = [C]\left(x(t)\right) + [D]\left(u(t)\right)$$

$$Y(s) = C^T[sI - A]^{-1}x_0 + C^T[sI - A]^{-1}BU(s) + DU(s)$$

where:

$$T_1T_2 = \frac{m\dfrac{A_1c}{2E}}{A_1^2(1 - c_{fu}) + a_mb_m};\ h(T_1 + T_2) = \frac{ma_m + \dfrac{A_1c}{2E}b_m}{A_1^2(1 - c_{fu}) + a_mb_m};$$

$$kU = \frac{A_1(1 - c_{fu})Q}{A_1^2(1 - c_{fu}) + a_mb_m}.$$

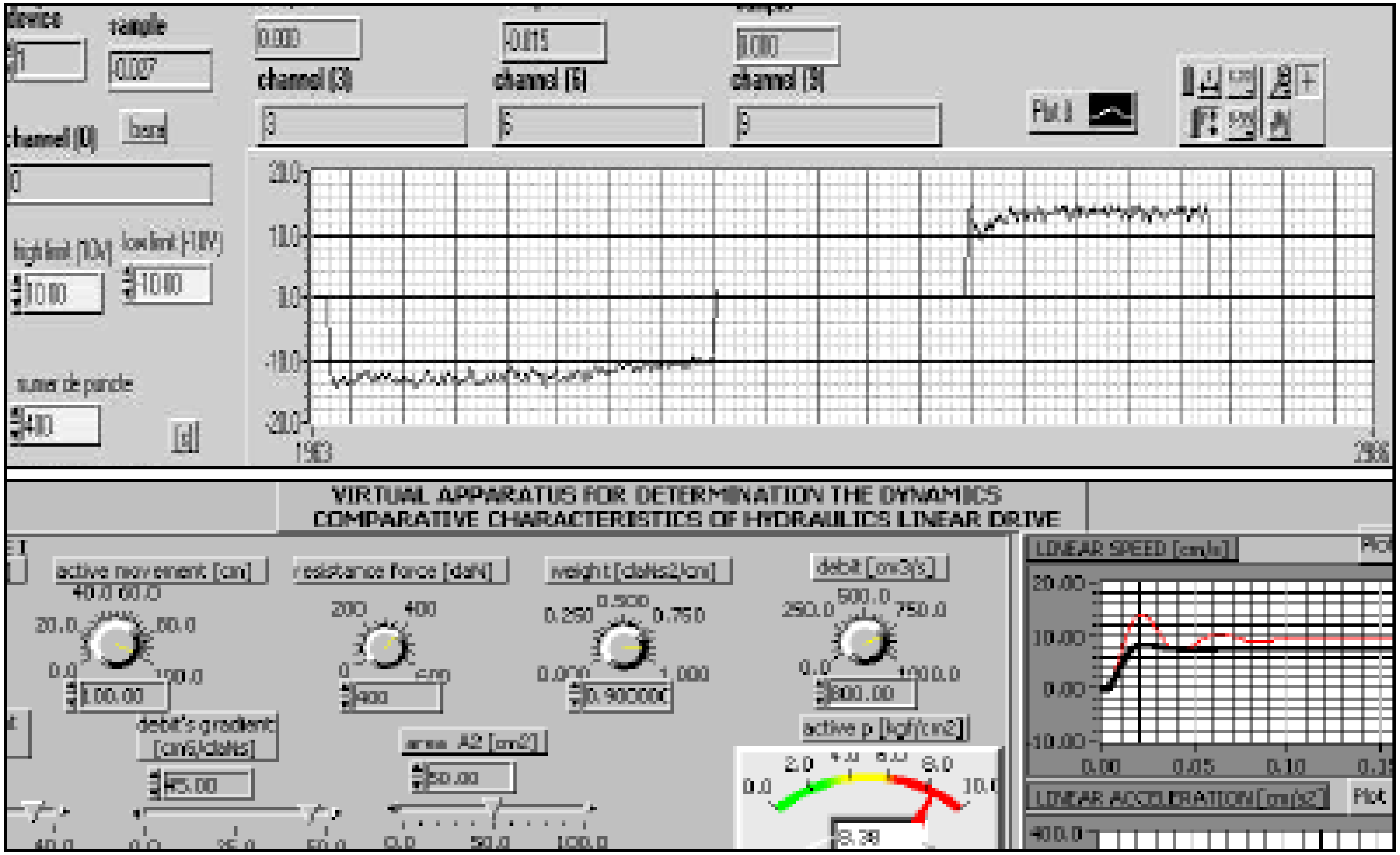

Fig.1: The front panel of the acquisition and theoretical virtual LabVIEW instruments: validation of the LHM mathematical model

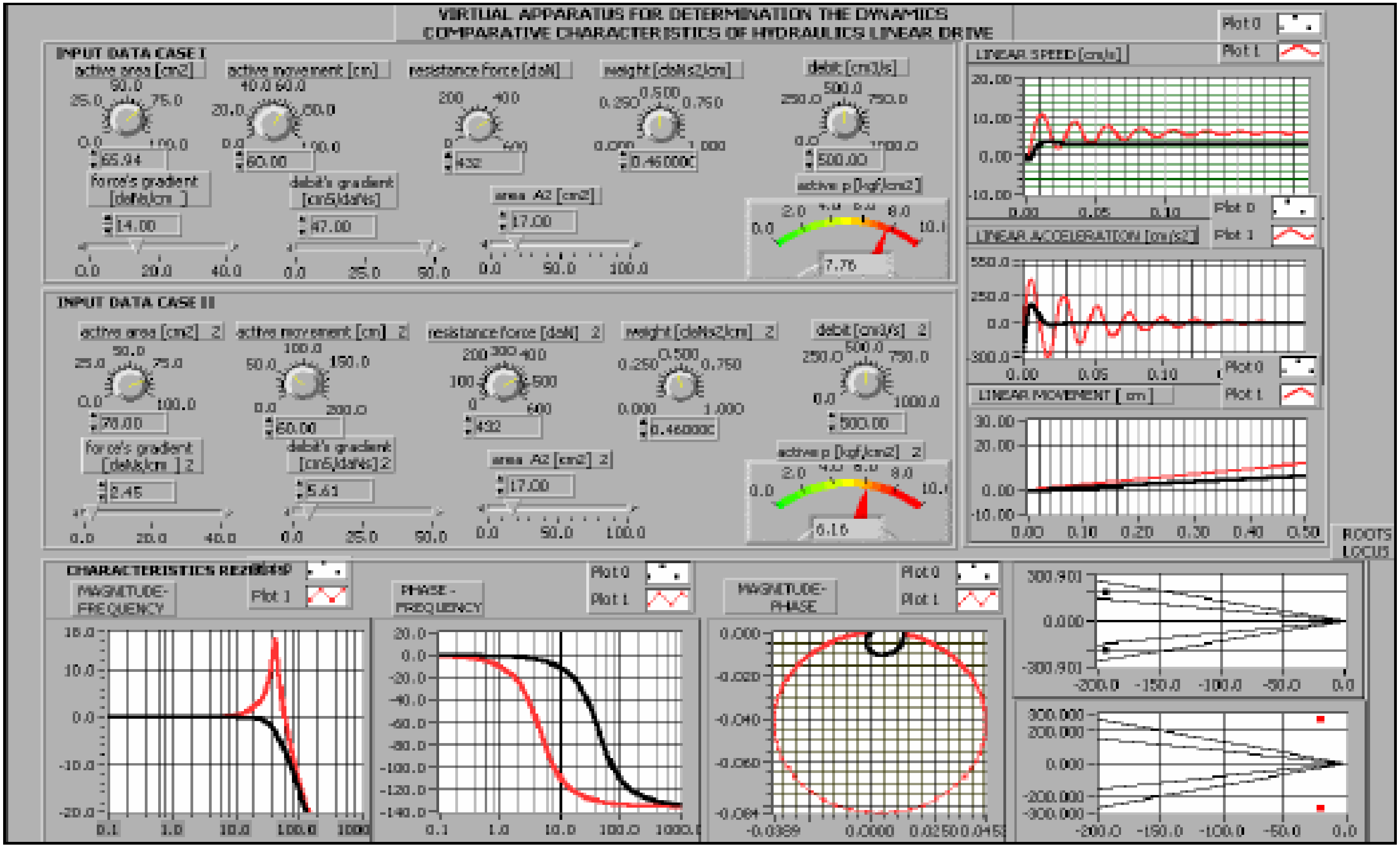
VIRTUAL APPARATUS FOR DETERMINATION THE DYNAMICS
COMPARATIVE CHARACTERISTICS OF HYDRAULICS LINEAR DRIVE
INPUT DATA CASE I
active area [cm2]
active movement [cm]
resistance force [daN]
weight [daNs2/cm]
debit [cm3/s]
force's gradient [daN/cm]
debit's gradient [cm5/daNs]
area A2 [cm2]
active p [kgf/cm2]
INPUT DATA CASE II
LINEAR SPEED [cm/s]
LINEAR ACCELERATION [cm/s2]
LINEAR MOVEMENT [cm]
ROOTS LOCUS
CHARACTERISTICS REZ
MAGNITUDE-FREQUENCY
PHASE-FREQUENCY
MAGNITUDE-PHASE
Plot 0
Plot 1

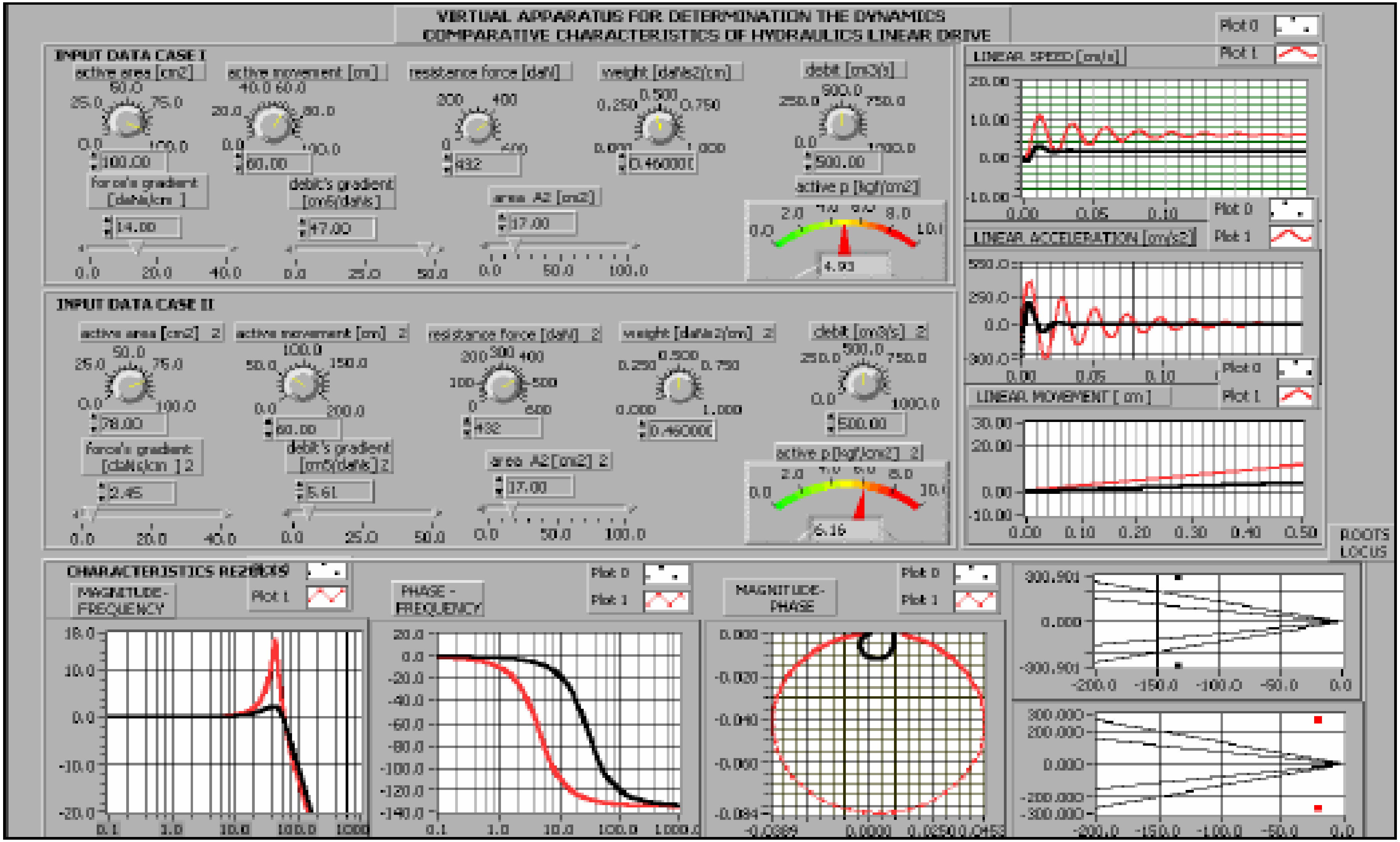

Fig.3: Front panel of the virtual LabVIEW LHM instrument for the comparative analyze, when was been changed the active area, A_1

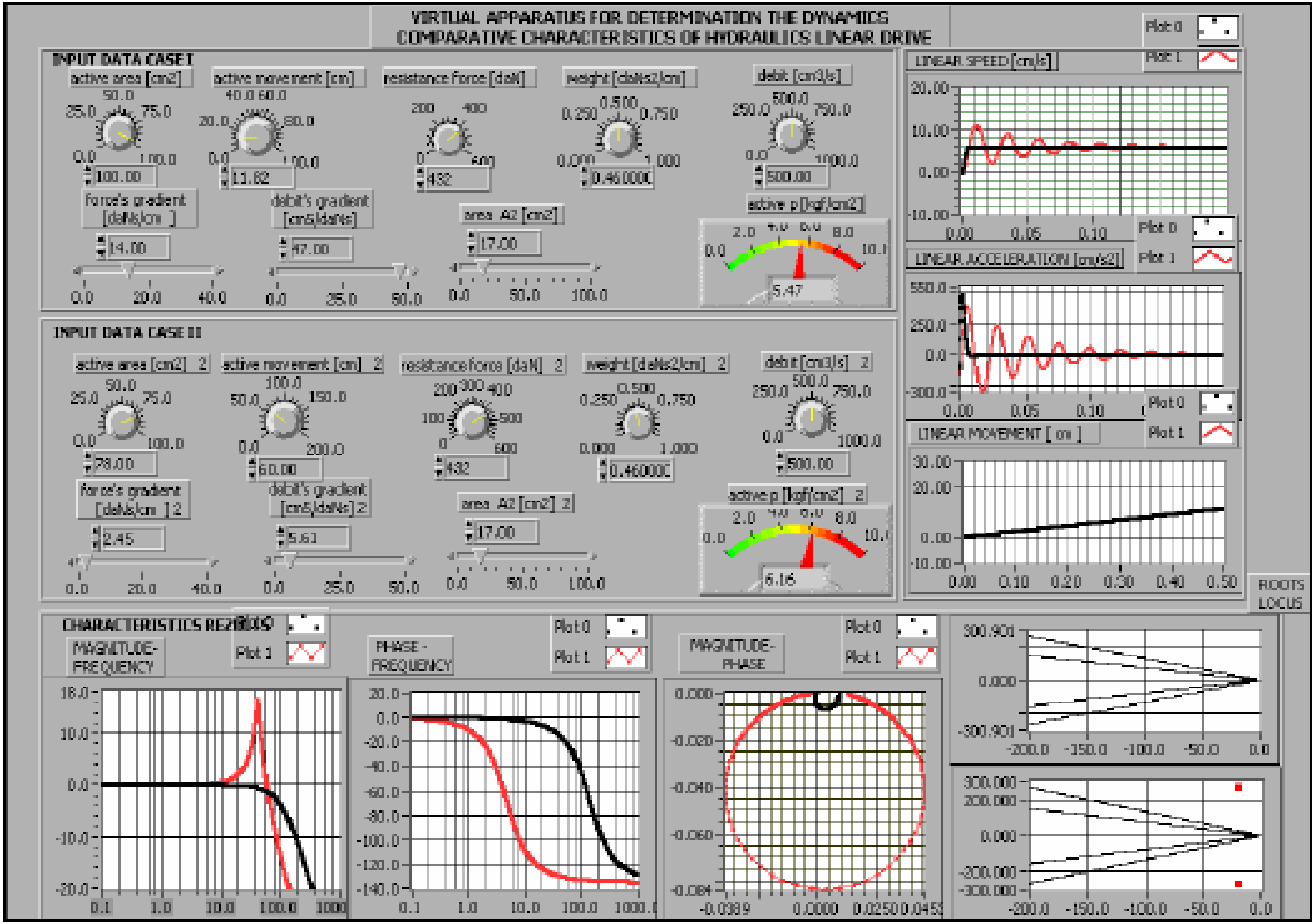

Fig.4: Front panel of the virtual LabVIEW LHM instrument for the comparative analyze, when was changed the active area and the movements of motor steam, A_1, c

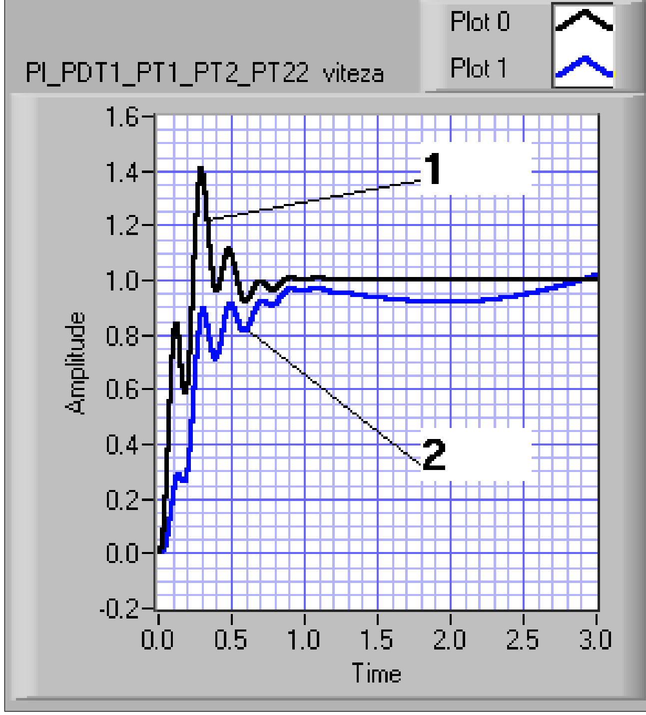
PI_PDT1_PT1_PT2_PT22 viteza
Plot 0
Plot 1
Amplitude
Time
1
2
1.6
1.4
1.2
1.0
0.8
0.6
0.4
0.2
0.0
-0.2
0.0 0.5 1.0 1.5 2.0 2.5 3.0

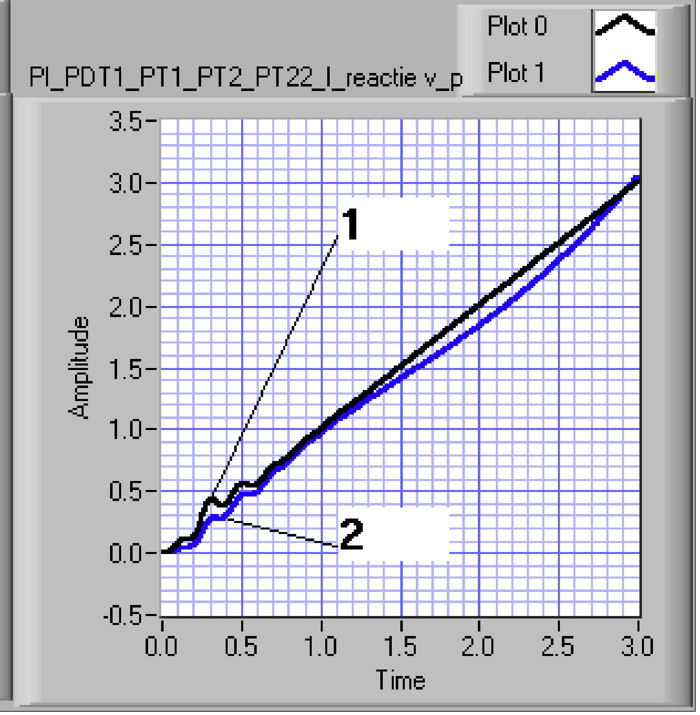
PI_PDT1_PT1_PT2_PT22_I_reactie v_p
Plot 0
Plot 1
Amplitude
Time
1
2
3.5
3.0
2.5
2.0
1.5
1.0
0.5
0.0
-0.5
0.0 0.5 1.0 1.5 2.0 2.5 3.0

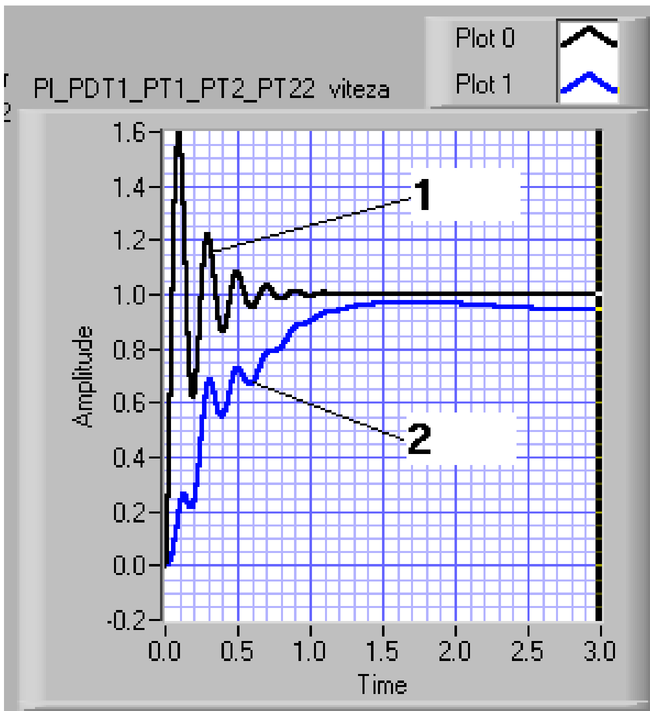
PI_PDT1_PT1_PT2_PT22 viteza
Plot 0
Plot 1
Amplitude
Time
1
2
1.6
1.4
1.2
1.0
0.8
0.6
0.4
0.2
0.0
-0.2
0.0 0.5 1.0 1.5 2.0 2.5 3.0

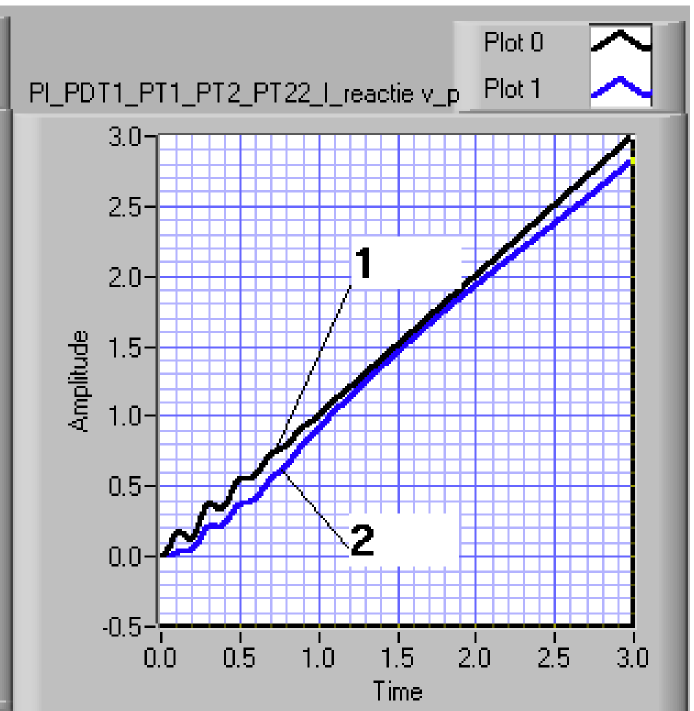
PI_PDT1_PT1_PT2_PT22_I_reactie v_p
Plot 0
Plot 1
Amplitude
Time
1
2
3.0
2.5
2.0
1.5
1.0
0.5
0.0
-0.5
0.0 0.5 1.0 1.5 2.0 2.5 3.0

	A	V	Fr	m	Q	bm	am	t	N	p
0	60.00000	500.0000	2.000000	0.200000	100.0000	0.800000	0.200000	1.000000	1000.000	4.000000
0	60.00000	500.0000	2.000000	0.400000	100.0000	0.800000	0.200000	1.000000	1000.000	4.000000
0	60.00000	500.0000	2.000000	0.600000	100.0000	0.800000	0.200000	1.000000	1000.000	4.000000

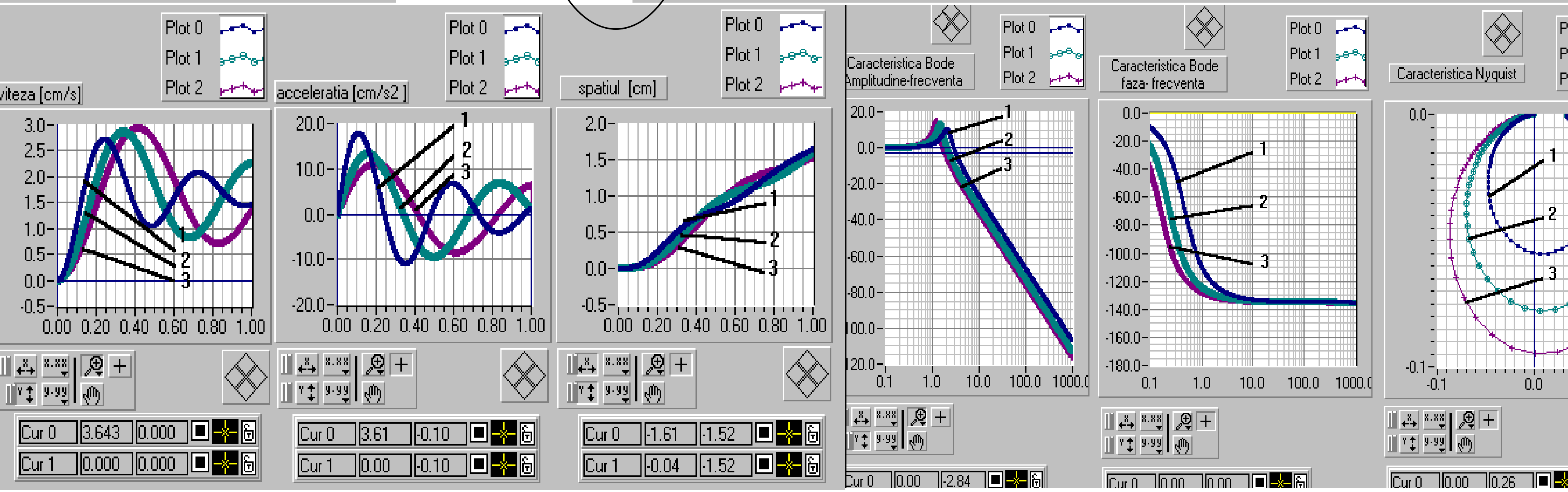

	A	V	Fr	m	Q	bm	am	t	N	p
0	60.00000	500.0000	2.000000	0.200000	100.0000	0.800000	0.200000	1.000000	1000.000	4.000000
0	60.00000	500.0000	2.000000	0.200000	100.0000	0.800000	0.200000	1.000000	1000.000	6.000000
0	60.00000	500.0000	2.000000	0.200000	100.0000	0.800000	0.200000	1.000000	1000.000	7.000000

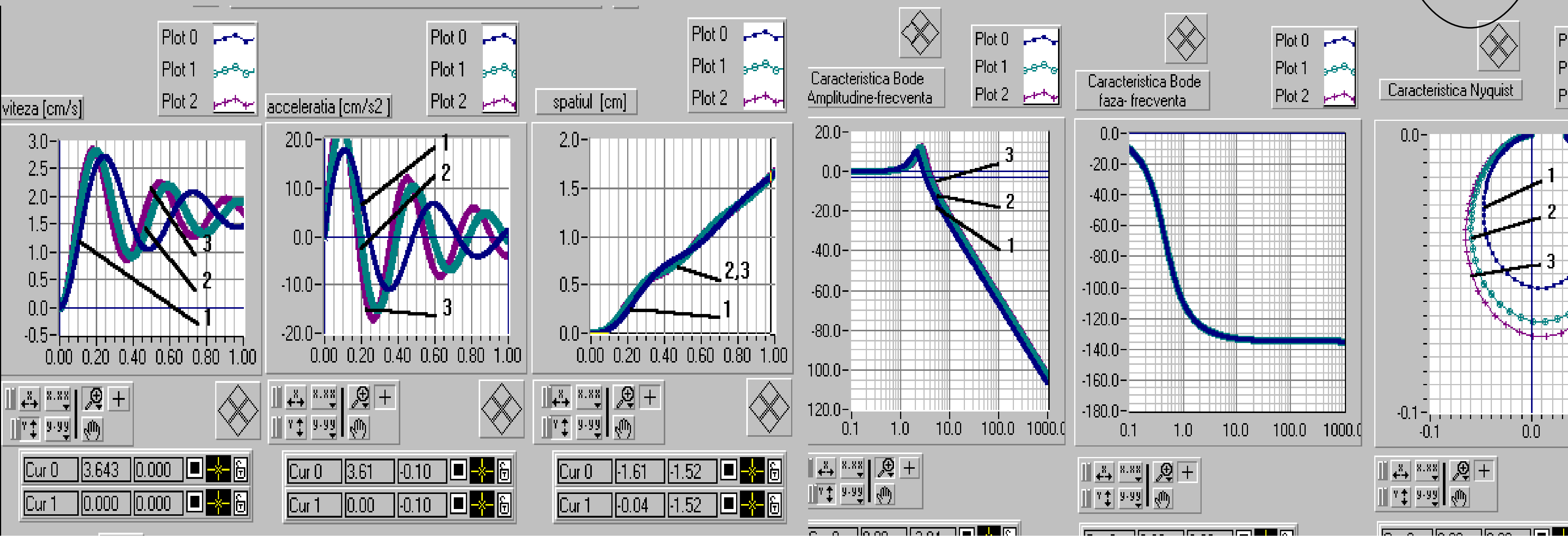

Analyzing the optimization applied LHM LabVIEW proper *VI* results the following remarks:

- By increase the **flow loss vs.force gradients** were obtained some transfer of the poles in the poles- zeros plane to the stability field, velocity were obtained without any vibrations, fig.2;
- By increase the **active area** was obtained the displacement of the poles outside of the precision – stability field, but one magnification of the answer with decrease of the acceleration time with the effect in to the increase of the movement precision, fig.3;
- By decrease of the **active movement** of the LHM steam was obtained one magnification of the velocity output with the same acceleration time with the second example, but without any vibrations of the velocity output,fig.4. By this method is possible **to choose the constructive or functional values** of the LHM to obtain one good dynamic behavior answer to obtain one good precision, or stability, or better solving the compromise precision- stability problem.
- **Without on-line work** of the proper LabVIEW *VI*-s is not possible to obtain these results.

Assisted optimisation of the hydraulic systems with many closed loops and different control laws

- In the paper were simulated the system CFP- LHM (constant flow pump- linear hydraulic motor) [15-18], VFP- RHM with regulator (variable flow pump- rotate hydraulic motor);
-
- CFP- PD- LHM (constant flow pump- proportional distribution- linear hydraulic motor);

- LHM-OHM (linear and oscillate hydraulic motor). For the control of the command signals were used some proper sub*VI*-s by manually, automat or using the intelligent systems with some neural networks, to control the electrical command signals [18-30].

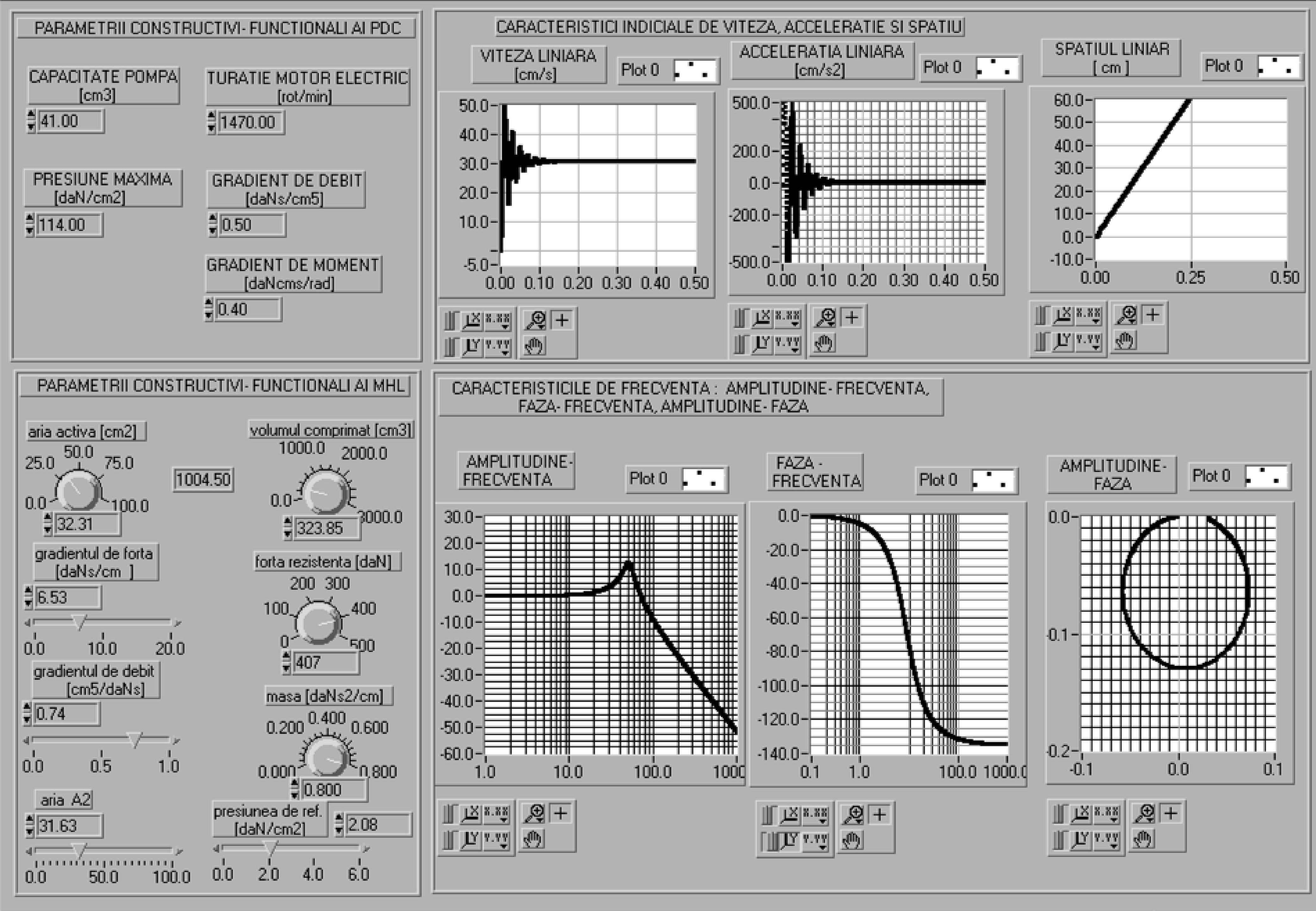
PARAMETRII CONSTRUCTIVI- FUNCTIONALI AI PDC
CAPACITATE POMPA [cm3]
41.00
TURATIE MOTOR ELECTRIC [rot/min]
1470.00
PRESIUNE MAXIMA [daN/cm2]
114.00
GRADIENT DE DEBIT [daNs/cm5]
0.50
GRADIENT DE MOMENT [daNcms/rad]
0.40
CARACTERISTICI INDICIALE DE VITEZA, ACCELERATIE SI SPATIU
VITEZA LINIARA [cm/s]
Plot 0
ACCELERATIA LINIARA [cm/s2]
Plot 0
SPATIUL LINIAR [cm]
Plot 0
PARAMETRII CONSTRUCTIVI- FUNCTIONALI AI MHL
aria activa [cm2]
32.31
1004.50
volumul comprimat [cm3]
323.85
gradientul de forta [daNs/cm]
6.53
forta rezistenta [daN]
407
gradientul de debit [cm5/daNs]
0.74
masa [daNs2/cm]
0.800
aria A2
31.63
presiunea de ref. [daN/cm2]
2.08
CARACTERISTICILE DE FRECVENTA : AMPLITUDINE- FRECVENTA, FAZA- FRECVENTA, AMPLITUDINE- FAZA
AMPLITUDINE- FRECVENTA
Plot 0
FAZA - FRECVENTA
Plot 0
AMPLITUDINE- FAZA
Plot 0

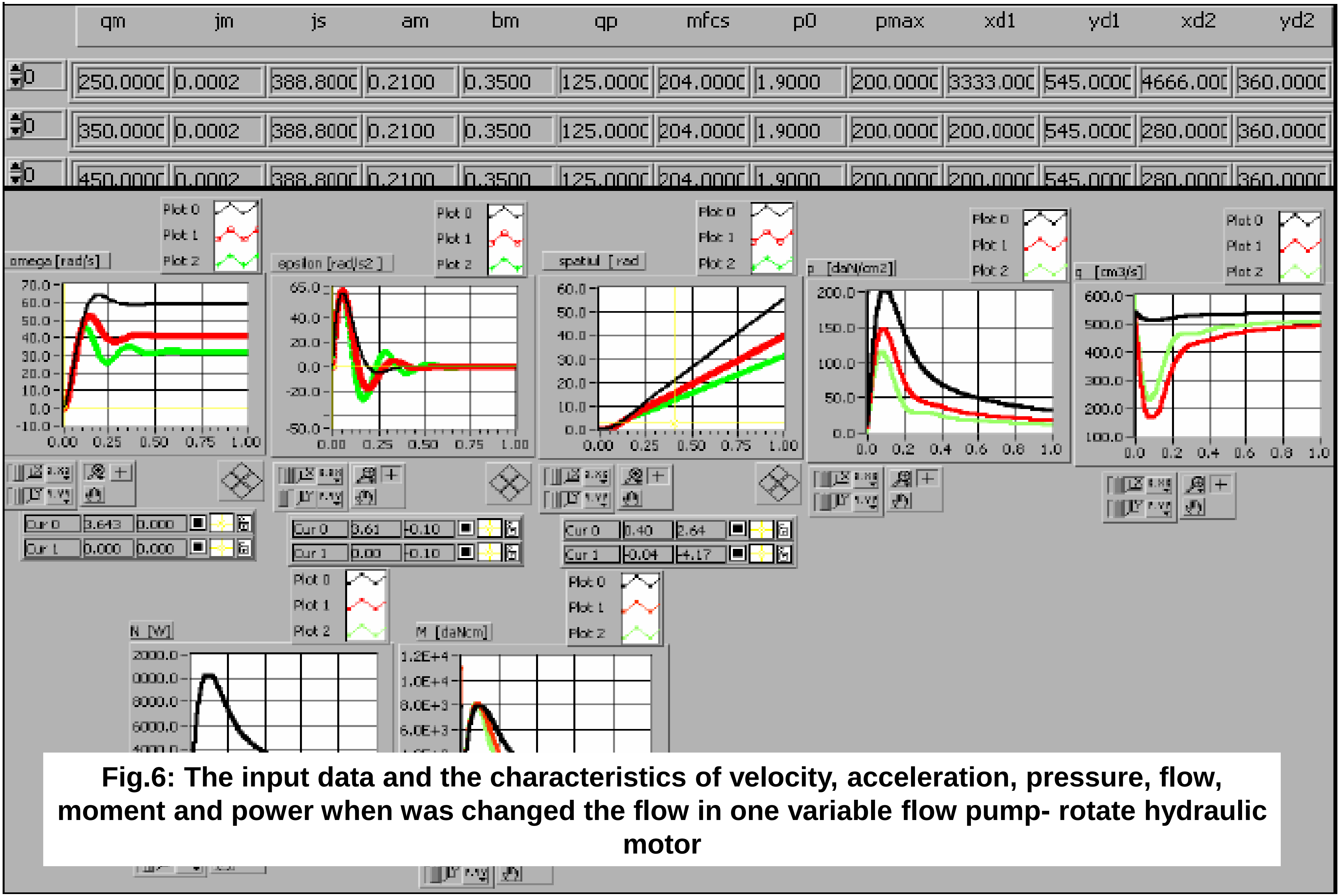

Fig.6: The input data and the characteristics of velocity, acceleration, pressure, flow, moment and power when was changed the flow in one variable flow pump- rotate hydraulic motor

250	0,0002	388,8	0,21	0,35	125	204	1,9	200	200	545	280	360
350	0,0002	388,8	0,21	0,35	125	204	1,9	200	200	545	280	360
450	0,0002	388,8	0,21	0,35	125	204	1,9	200	200	545	280	360

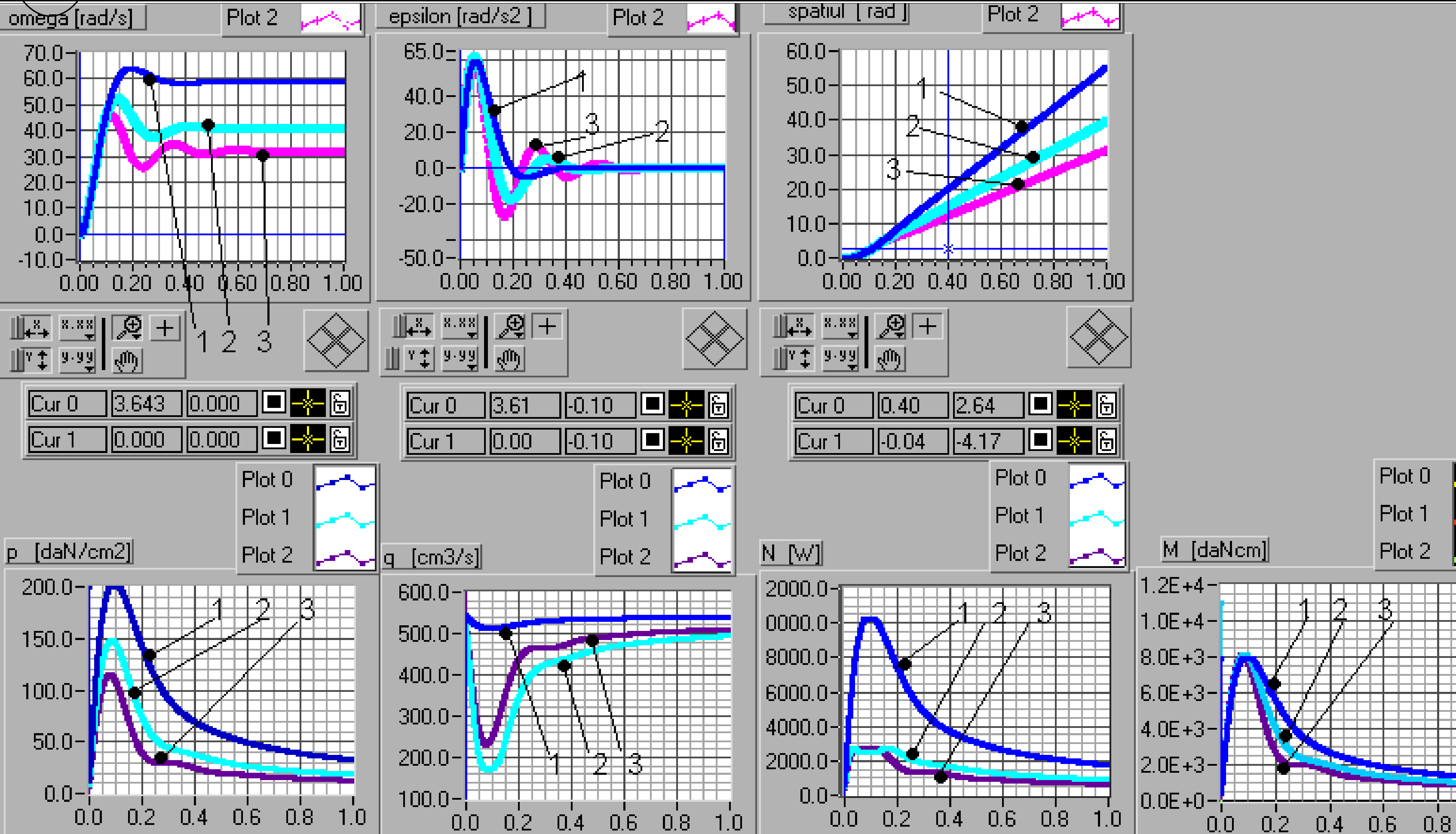

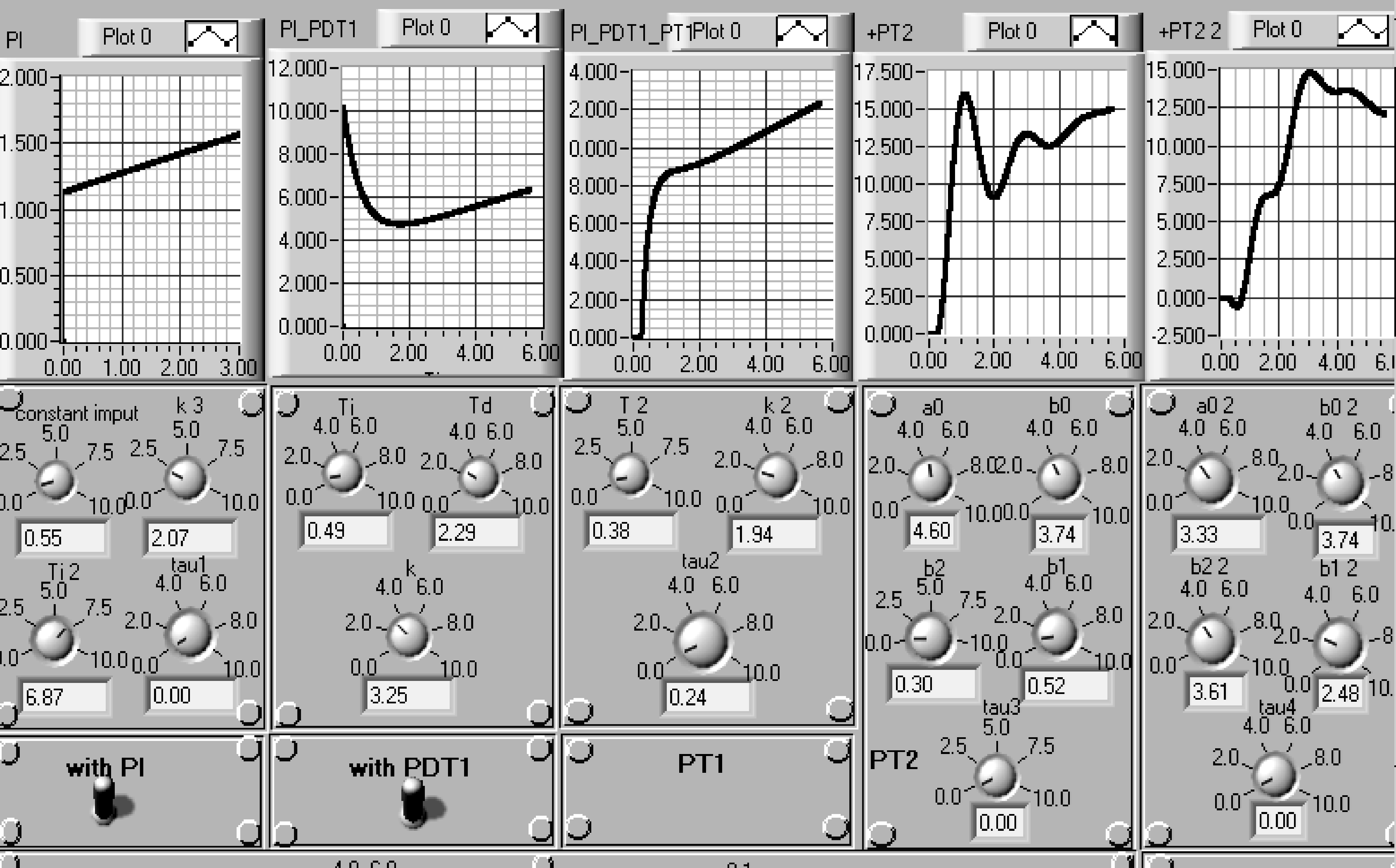

Fig.7: The indicial characteristics for the applied control low to the electrical command signals

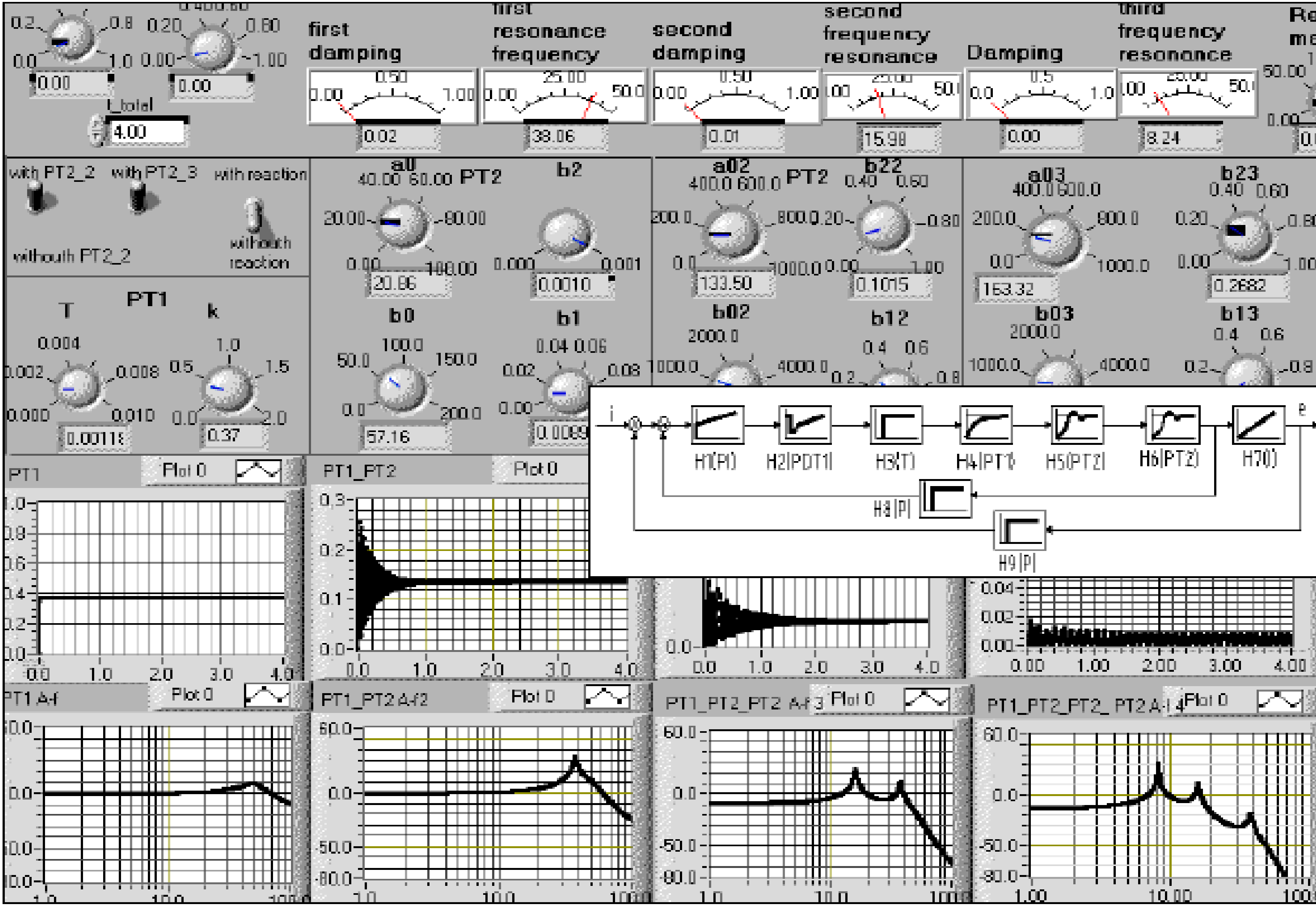

first damping
first resonance frequency
second damping
second frequency resonance
Damping
third frequency resonance
t_total
4.00
0.02
38.06
0.01
15.98
0.00
8.24
with PT2_2
with PT2_3
with reaction
withouth PT2_2
withouth reaction
a0
PT2
b2
a02
b22
a03
b23
20.86
0.0010
133.50
0.1015
163.32
0.2682
b0
b1
b02
b12
b03
b13
PT1
T
k
57.16
0.37
H1(P)
H2(PDT1)
H3(T)
H4(PT1)
H5(PT2)
H6(PT2)
H7()
H8(P)
H9(P)
PT1
Plot 0
PT1_PT2
PT1 A-f
PT1_PT2 A-f 2
PT1_PT2_PT2 A-f 3
PT1_PT2_PT2_ PT2 A-f 4

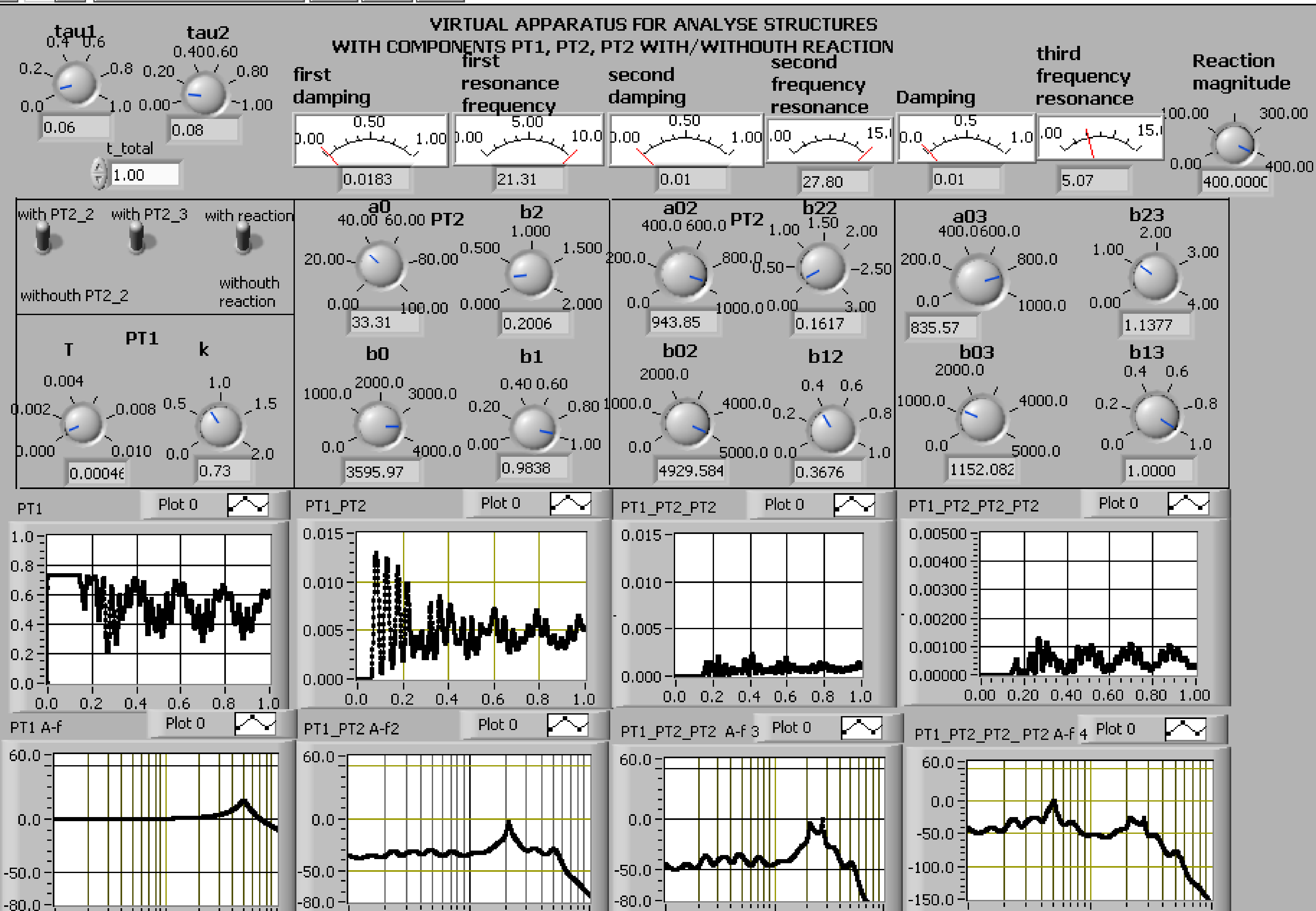
VIRTUAL APPARATUS FOR ANALYSE STRUCTURES
WITH COMPONENTS PT1, PT2, PT2 WITH/WITHOUTH REACTION
tau1
0.06
tau2
0.08
t_total
1.00
first damping
0.0183
first resonance frequency
21.31
second damping
0.01
second frequency resonance
27.80
Damping
0.01
third frequency resonance
5.07
Reaction magnitude
400.0000
with PT2_2
with PT2_3
with reaction
withouth PT2_2
withouth reaction
PT1
T
0.00046
k
0.73
a0
PT2
33.31
b2
0.2006
b0
3595.97
b1
0.9838
a02
PT2
943.85
b22
0.1617
b02
4929.584
b12
0.3676
a03
835.57
b23
1.1377
b03
1152.082
b13
1.0000
PT1
Plot 0
PT1_PT2
Plot 0
PT1_PT2_PT2
Plot 0
PT1_PT2_PT2_PT2
Plot 0
PT1 A-f
Plot 0
PT1_PT2 A-f2
Plot 0
PT1_PT2_PT2 A-f 3
Plot 0
PT1_PT2_PT2_ PT2 A-f 4
Plot 0

Conclusions

- The designed proper virtual LabVIEW instrumentation we can use **in many other application** and the research of many electrical, hydraulic or complex systems.
- The transfer function method and the used mathematical model for the LHM or for some other showed systems **we can apply in many future researches**.
- The virtual LabVIEW **library** what contents many hydraulic, electric elements and many servo systems we **can use in the theoretical and experimental research to optimize** the dynamic behaviour answer, to decrease the research time activities and to obtain some good results in to the developing and implementing in the future the intelligent systems.
- By applying the virtual LabVIEW instrumentation is open the way **to optimize choose** of all these **parameters**.

- By using the artificial intelligence, proper neuronal network and direct and inverse kinematics results;

Optimization of the space trajectory by using the neural network and inverse kinematics- application in SUM Toyama motor

Prof.univ.Ph.D.Eng.Shigeki Toyama
Tokyo Univ. A&T,Japon
Prof.univ.Ph.D.Eng.Adrian OLARU
senior member of IACSIT (Singapore)
International
Association of Computer Sciences and Information Technology
University Politehnica of Bucharest, ROMANIA
Assoc.prof.univ.Ph.D.Eng.Liviu Ciupitu
University Politehnica of Bucharest, ROMANIA
Ph.D.Eng.Şerban OLARU
Romsys Company, Bucharest, ROMANIA

GENERALITY OF NEURAL NETWORK AND INVERSE KINEMATICS

- **The inverse kinematics was used to control** the end-effector's trajectory in the space.

- **The inverse kinematics solutions** obtained by geometrical method **are more difficult to find**, when the degree of freedom increase.

- **In the paper was proposed assisted optimization of the trajectory error, after apply the inverse kinematics control,** one new method with proper neural network what used three layers, many time delay blocks and recurrent links.

- **The used neural network are 3-8-3-3 type**, justified by the input and output data.

What are news in the paper and description of the proposed research method

- Determination of the direct cinematic coordinates
- Study of some more important neural network with proper created LabVIEW instruments
- Proposed, designed and study one new proper neural network with LabVIEW proper virtual instrument
- Created one new mathematical model for proposed neural network
- Researched some parameters from mathematical model what have more important influence to the target with the important goal to reduce the errors

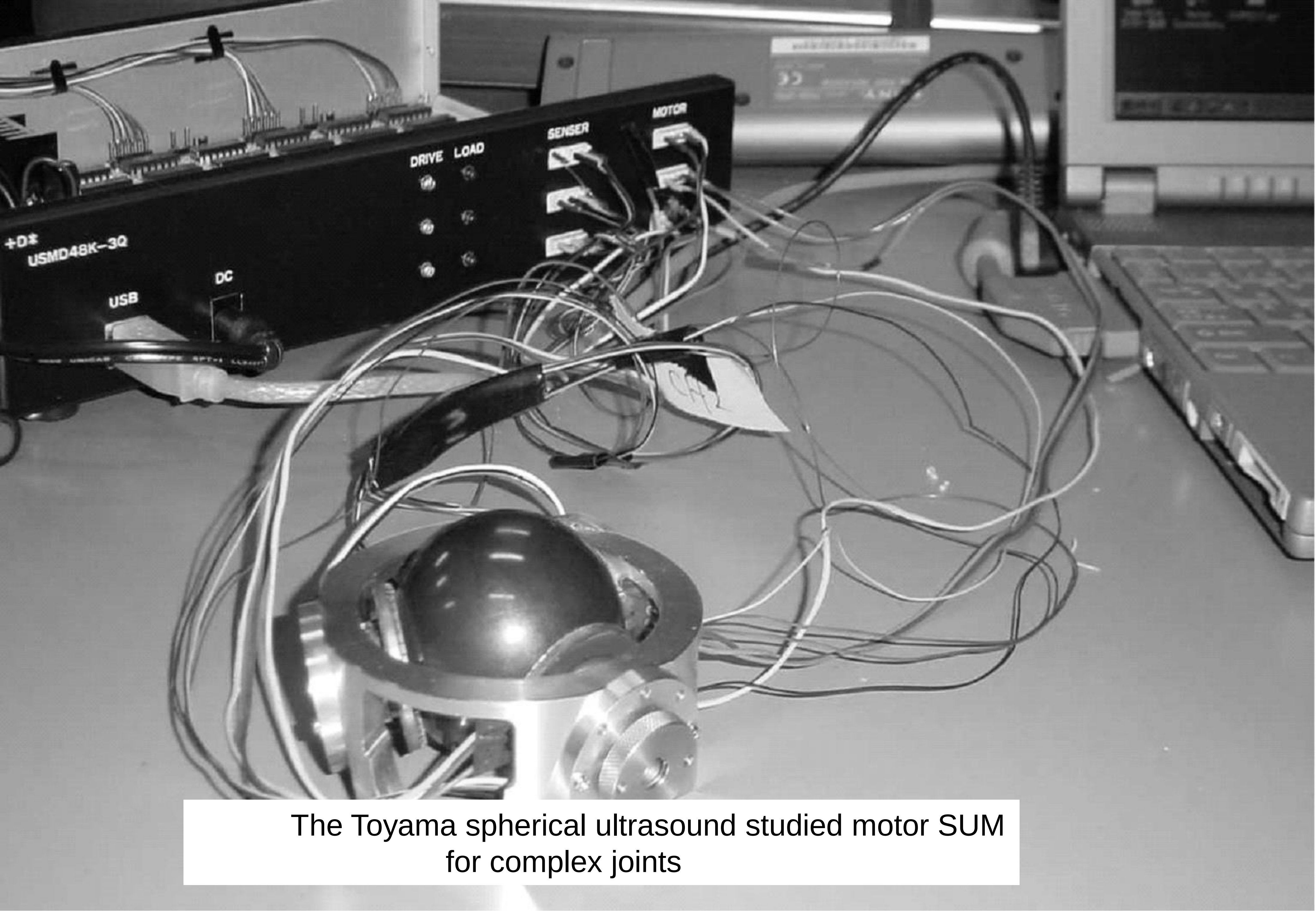

The Toyama spherical ultrasound studied motor SUM
for complex joints

Direct kinematics problem of SUM motor

- **P**stop = **T**(φ1, φ2, φ3) **P**start $\Leftrightarrow$
- **P**stop = **T**1(φ1) **T**2(φ2) **T**3(φ3) **P**start
- **T**1(φ1) = $\mathbf{R}_Z(-\beta)\,\mathbf{R}_Y(\alpha')\,\mathbf{R}_Z(\varphi 1)\,\mathbf{R}_Y(-\alpha')\,\mathbf{R}_Z(\beta)$
- **T**2(φ2) = $\mathbf{R}_Y(\alpha')\,\mathbf{R}_Z(\varphi 2)\,\mathbf{R}_Y(-\alpha')$
- **T**3(φ3) = $\mathbf{R}_Z(\beta)\,\mathbf{R}_Y(\alpha')\,\mathbf{R}_Z(\varphi 3)\,\mathbf{R}_Y(-\alpha')\,\mathbf{R}_Z(-\beta)$

$$\mathbf{R}_{Y(\theta)} = \begin{pmatrix} \cos\theta & 0 & \sin\theta \\ 0 & 1 & 0 \\ -\sin\theta & 0 & \cos\theta \end{pmatrix}$$

$$\text{and } \mathbf{R}_{Z(\theta)} = \begin{pmatrix} \cos\theta & -\sin\theta & 0 \\ \sin\theta & \cos\theta & 0 \\ 0 & 0 & 1 \end{pmatrix}$$

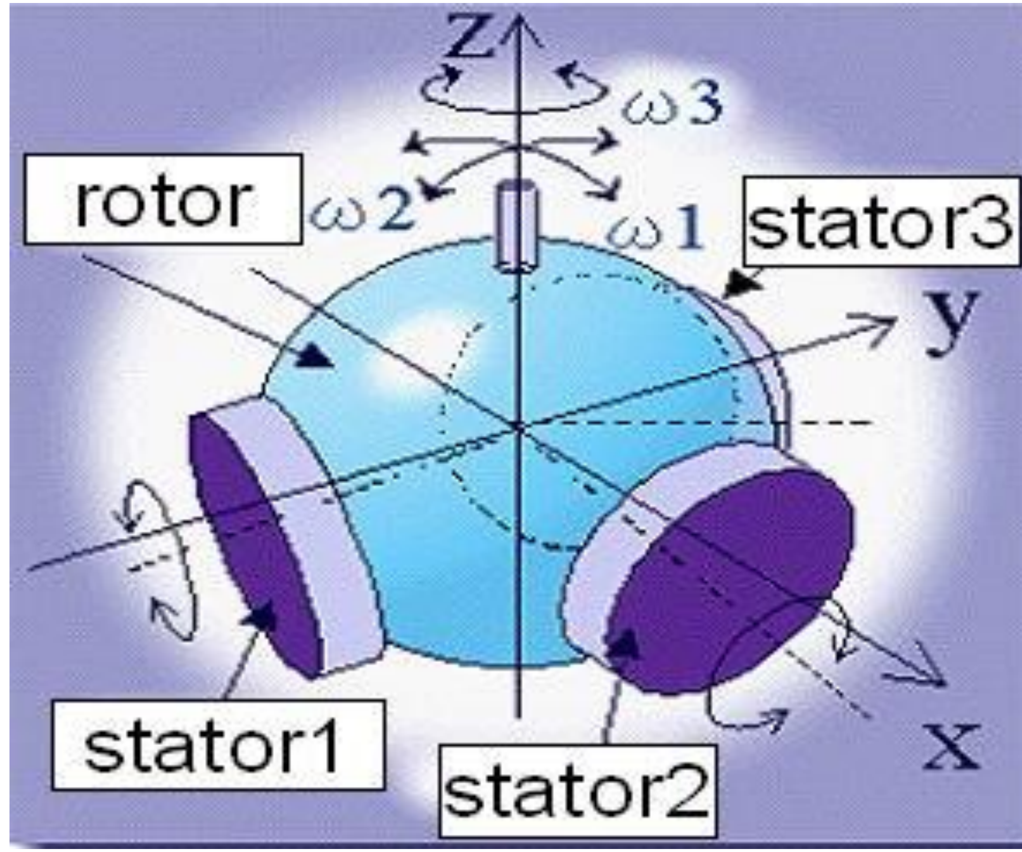

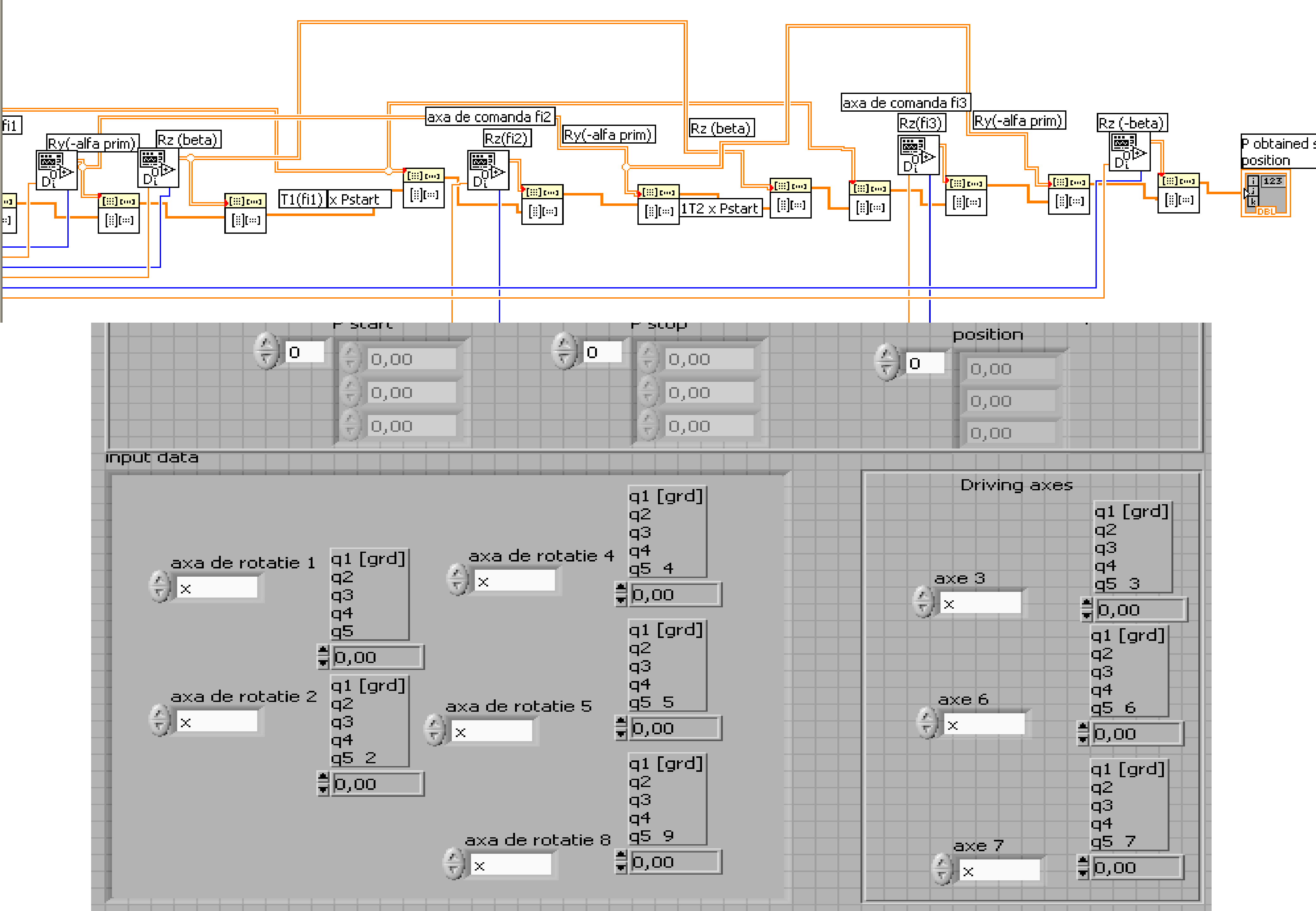
fi1
Ry(-alfa prim)
Rz (beta)
T1(fi1)
x Pstart
axa de comanda fi2
Rz(fi2)
Ry(-alfa prim)
Rz (beta)
1T2 x Pstart
axa de comanda fi3
Rz(fi3)
Ry(-alfa prim)
Rz (-beta)
P obtained
position
P start
P stop
position
input data
axa de rotatie 1
axa de rotatie 2
axa de rotatie 4
axa de rotatie 5
axa de rotatie 8
q1 [grd]
q2
q3
q4
q5
Driving axes
axe 3
axe 6
axe 7

Generality of the Neural Networks, Studied Robot and Choose the Proper Neural Network for inverse kinematics problem

- **Neural network are composed of simple elements** operating in parallel, **like a biological nervous systems**.
- **All neural network work in parallel** and we can training them to touch quickly the imposed target.
- **The back propagation algorithm work by changing on-line** the biases and weights matrices.
- **For the proper research we used one proper teaching method** by transfer the target to the hidden layers and change on-line the hidden layer target.

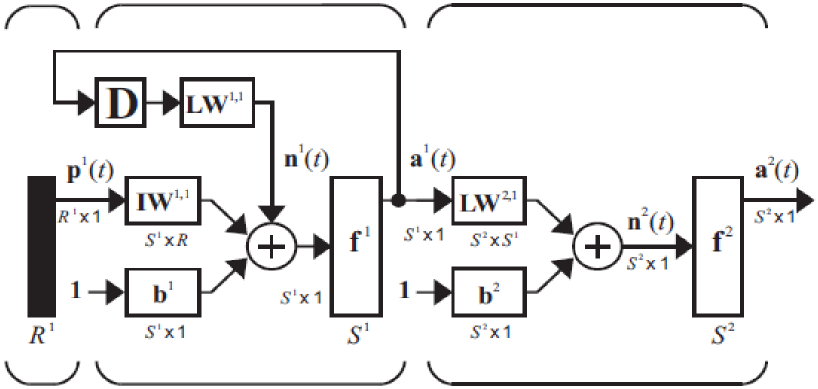

Fig.2: The Layer Neural Network (LNN)

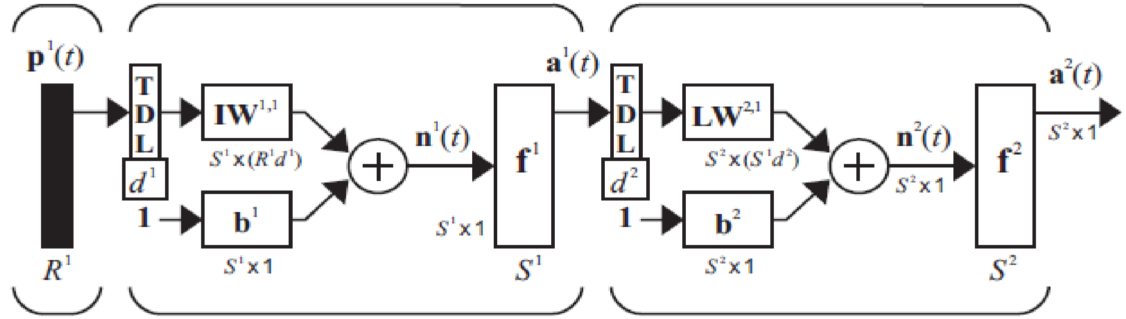

Fig.3: Focused Time-Delay Neural Network (FTDNN)

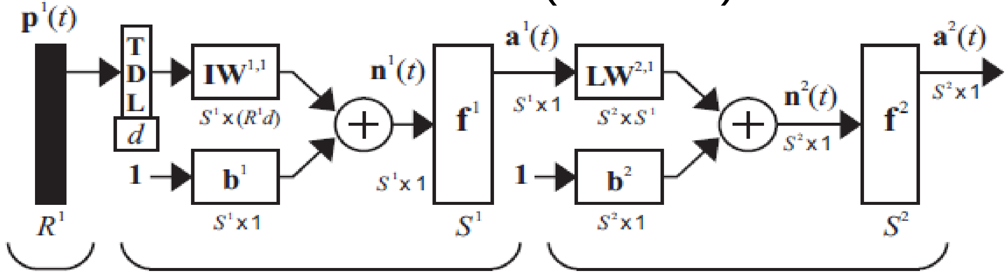

Fig.4: Distributed Time-Delay Neural Network (DTDNN)

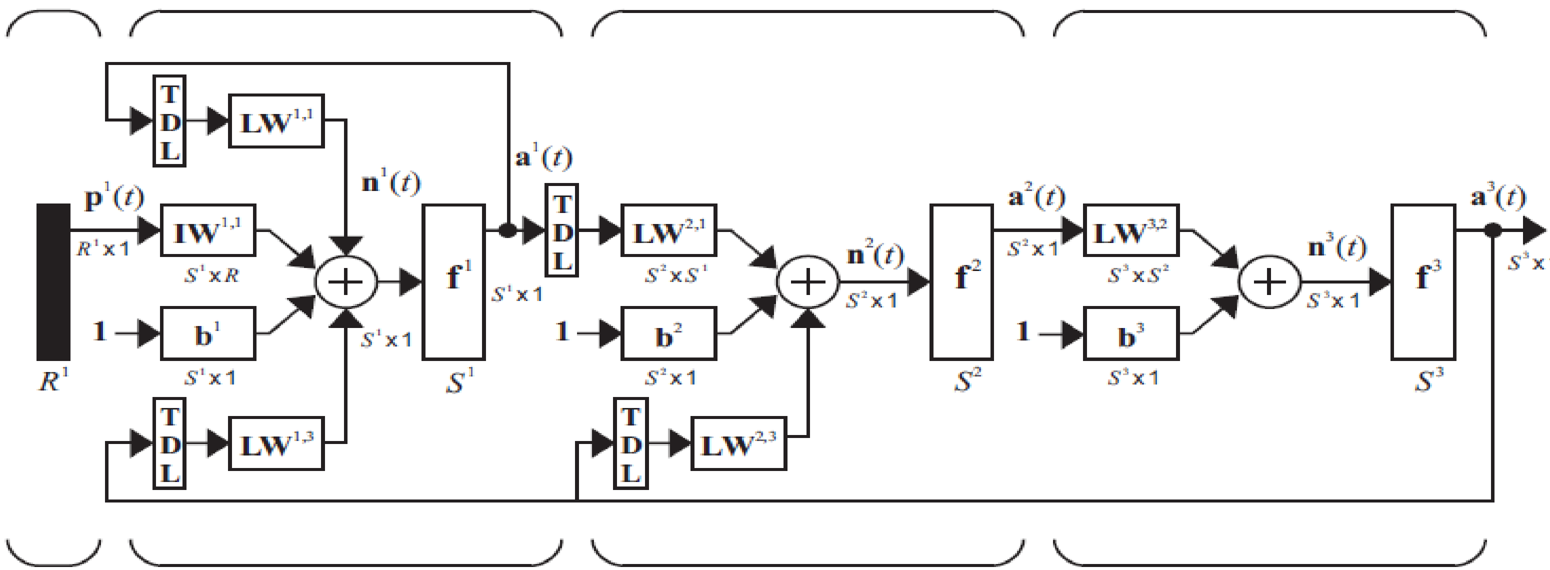

Fig.5: Layered Digital Dynamic Network (LDDN)

Justify the choose of the BSHTNN-TDRL type with 3-8-3-3 neurons

- **After the numerical simulation** of some more important neural networks used solving the inverse kinematics problem we find that the error are more than **80%.**
- **To reduce these errors** was proposed one new proper neural network type- Bipolar Sigmoid Hyperbolic Tangent with many Time Delay and Recurrent Links- **BSHTNN(TDRL).**

- For the assisted **solving the inverse cinematic** problem was used one neural network with three layers with the following configuration:

  3-8-3-3 with bipolar sigmoid hyperbolic tangent neural network type.

- **This configuration was choose** because the input must be 3 to control three internal coordinates (relative angles), 8 because more neurons in hidden layer not influence positive the target errors like you can see in the presented research, 3 because must be used the direct kinematics to obtain the output, 3 because the output must be the same number with target (target are the space position of the end-effector).

The neural network algorithm used for the control of the P point space position

- will be imposed the final point P_{stop} knowing the start position $P_{start}(x,y,z)$; the target of the command with neural network will be the difference between the stop and start points;
- the input data will be the normalized Hall sensors data;
- using the neural network will be find the angular movement around of each stators axes φ_i in the normalized form [-1,1] (**inverse kinematics);**
- by using the maximum value of the angular relative movement φ_{max} will be obtained **the real movement in each stator axes**;
- by using the **direct kinematics** and **the determined angular relative real position** φ_i will be obtained the real movement of P;
- by the difference between the obtained absolute movement (calculated) and the target movement (programmed) **will be obtained the errors;**
- with the errors will be adjusted all neural network parameters like: biases, weight matrices, teaching gain in each layers, **intermediate targets data**, amplifier gains, amplifier gain of the recurrent links, step of the time delay.

Mathematical Model and LabVIEW Instrument of the used Neural Network

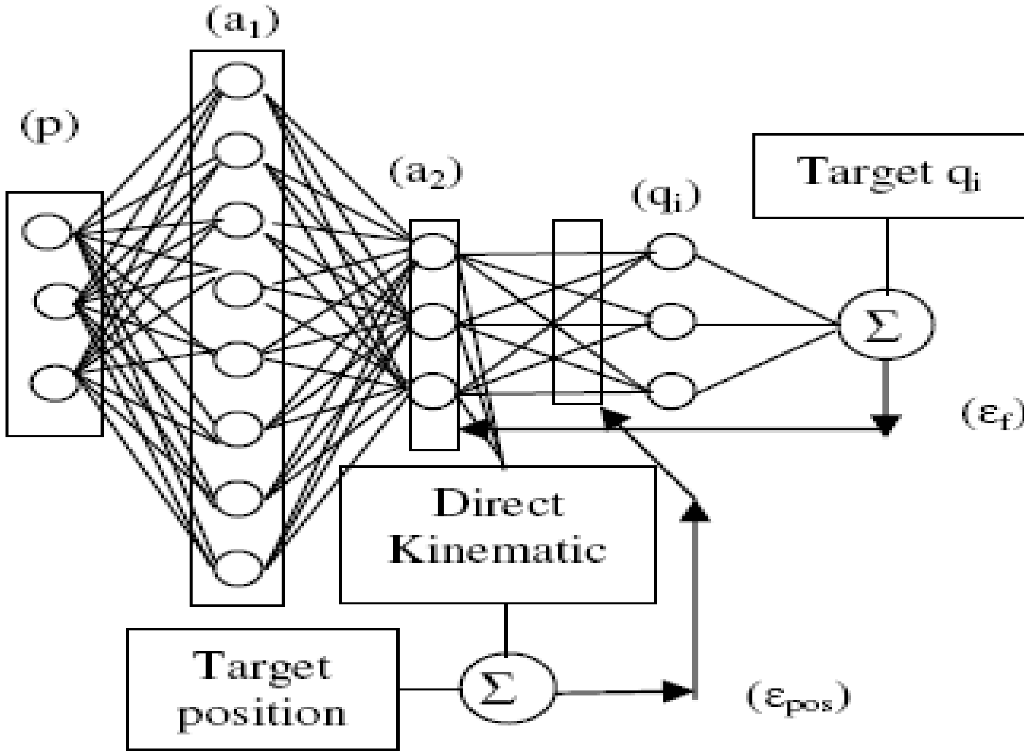

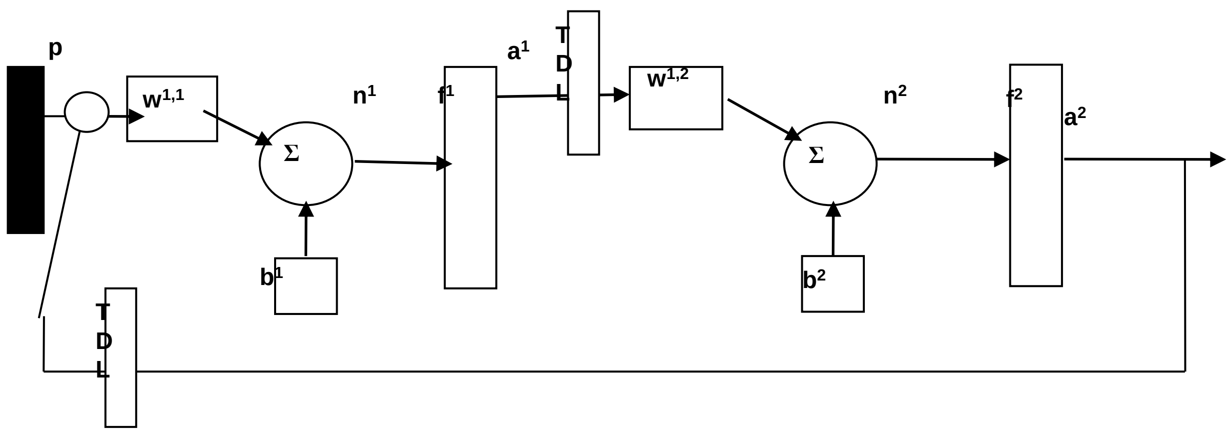

retea layer intrare2_gauss.vi

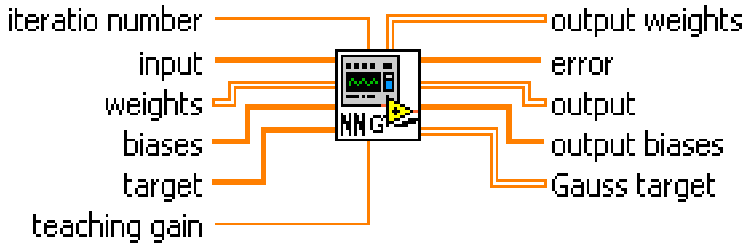

retea layer intrare2_perceptron.vi

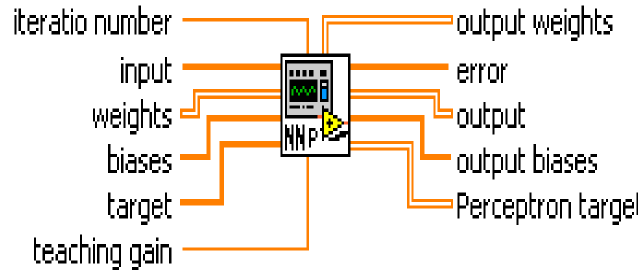

retea layer intrare2_linear.vi

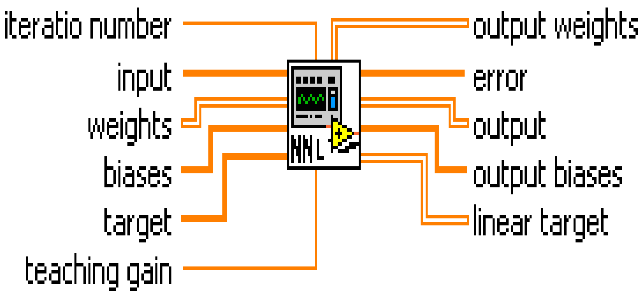

retea layer intrare2_sigmoid bipolar.vi

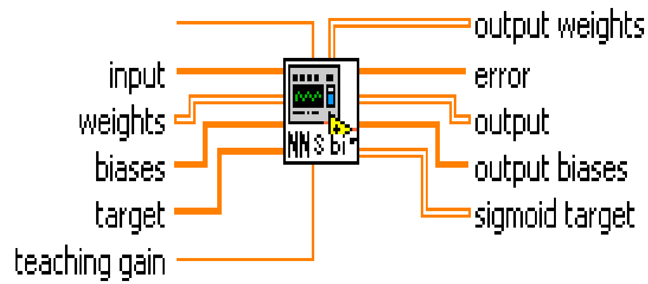

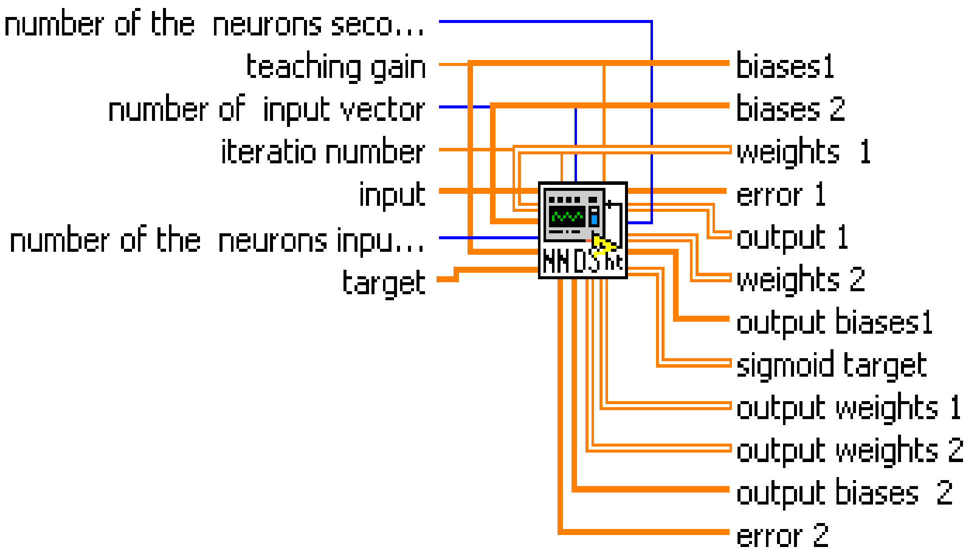

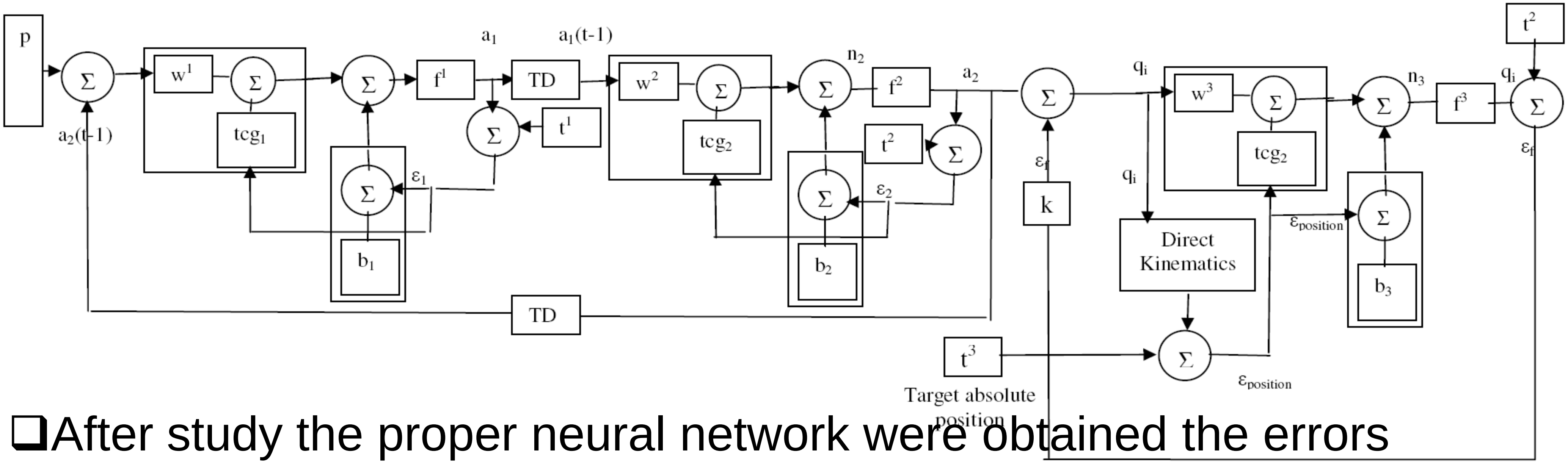

- After study the proper neural network were obtained the errors between the target and the obtained absolute coordinates in limits of 20%.

- The network work by apply the internal coordinate q_i obtained in the output 3-8-3 to the Direct Kinematics new layer with 3 neurons.

- **To reduce these errors** were researched all proper neural network parameters with more important influences to the target- see **parameters p_1-p_9** from the mathematical model and **the configuration of the network.**

$$n_1 = [\underbrace{w^1}_{p_1} + \underbrace{tcg_1}_{p_2} \cdot \varepsilon_1](p - a_2(t - p_3 + 1)) + (b_1 + \varepsilon_1)$$

$$a_1 = \frac{p_4(1 - e^{-n_1})}{1 + e^{-n_1}}$$

$$\varepsilon_1 = t_1 - a_1$$

$$n_2 = [w^2 + \underbrace{tcg_2}_{p5} \cdot \varepsilon_2](a_1(t - p_6 + 1)) + (b_2 + \varepsilon_2)$$

$$a_2 = \frac{p_7(1 - e^{-n_2})}{1 + e^{-n_2}}$$

$$\varepsilon_2 = t_2 - a_2$$

$$q_i = p_8(a_2 - \varepsilon_f)$$

$$r_i = \begin{pmatrix} c_1 s_2 l_3 + (c_1 c_2 s_3 + c_1 s_2 c_3) l_4 \\ s_1 s_2 l_3 + (s_1 c_2 s_3 + s_1 s_2 c_3) l_4 \\ l_1 + l_2 + c_2 l_3 + (-s_2 s_3 + c_2 c_3) l_4 \end{pmatrix}$$

$$\varepsilon_{pos} = t_3 - r_i$$

$$n_3 = [w^3 + \underbrace{tcg_2}_{p_5} \cdot \varepsilon_{pos}](q_i) + (b_3 + \varepsilon_{pos})$$

$$a_3 = \frac{p_9(1 - e^{-n_3})}{1 + e^{-n_3}}$$

$$\varepsilon_f = t_2 - a_3$$

The study parameters are: p_{i} are:

- p_1- the number of neurons;
- p_2 – the first teaching gain;
- p_3- step of the first time delay;
- p_4- the first sensitive function gain;
- p_5- the second teaching gain;
- p_6- the step of the second time delay;
- p_7- the second sensitive function gain;
- p_8- the magnify gain of the proportional error control;
- p_9- the third sensitive function gain.

Assisted Research of some Parameters of proposed Neural Network and some results

The assisted research shown in [3-9] studied the influences to the errors between the neural network output and the target (the space position of the end-effector) of the following neural network parameters:

- ❑ number of neurons in each layers;
- ❑ the sensitive function and the configuration of the complex network like: SBHTNN, SBHTNN-TD, SBHTNN-TD+TD, SBHTNN-TDRL
- ❑ the magnifier factor of the trajectory error;
- ❑ the variable step of the time delay and the position of these blocks;
- ❑ the different cases of hidden layer target data;
- ❑ the case when the hidden target data were on-line adjusted.

- Some of the studied cases are shown in the figs. of the citated papers for same different parameters. The synthetic results are shown in the table 1.

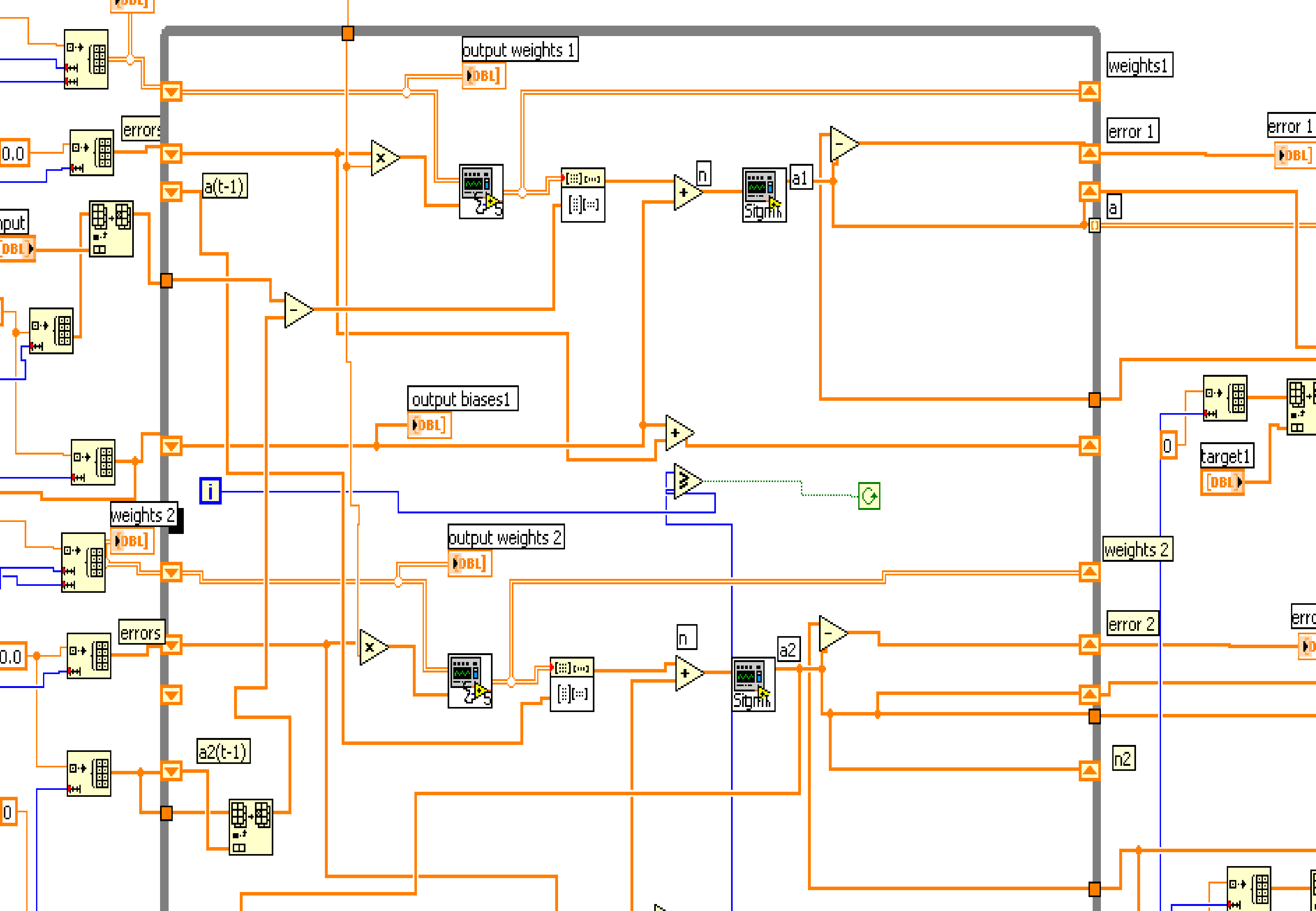

output weights 1
weights1
errors
error 1
error 1
a(t-1)
a1
a
n
output biases1
i
target1
weights 2
output weights 2
weights 2
errors
error 2
n
a2
n2
a2(t-1)

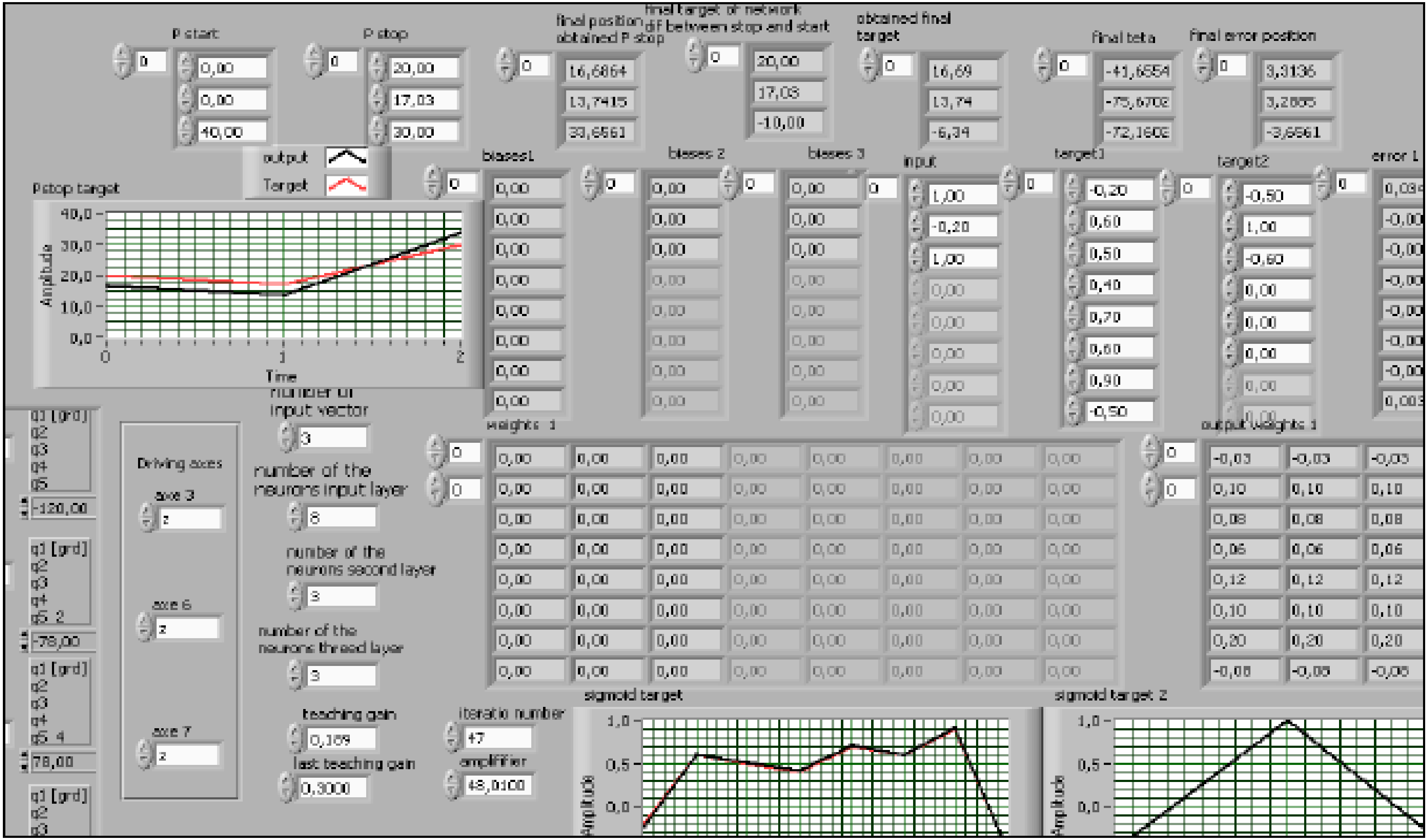

Fig.17: The front panel of the SUM neural network type BSHTNN with TDRL

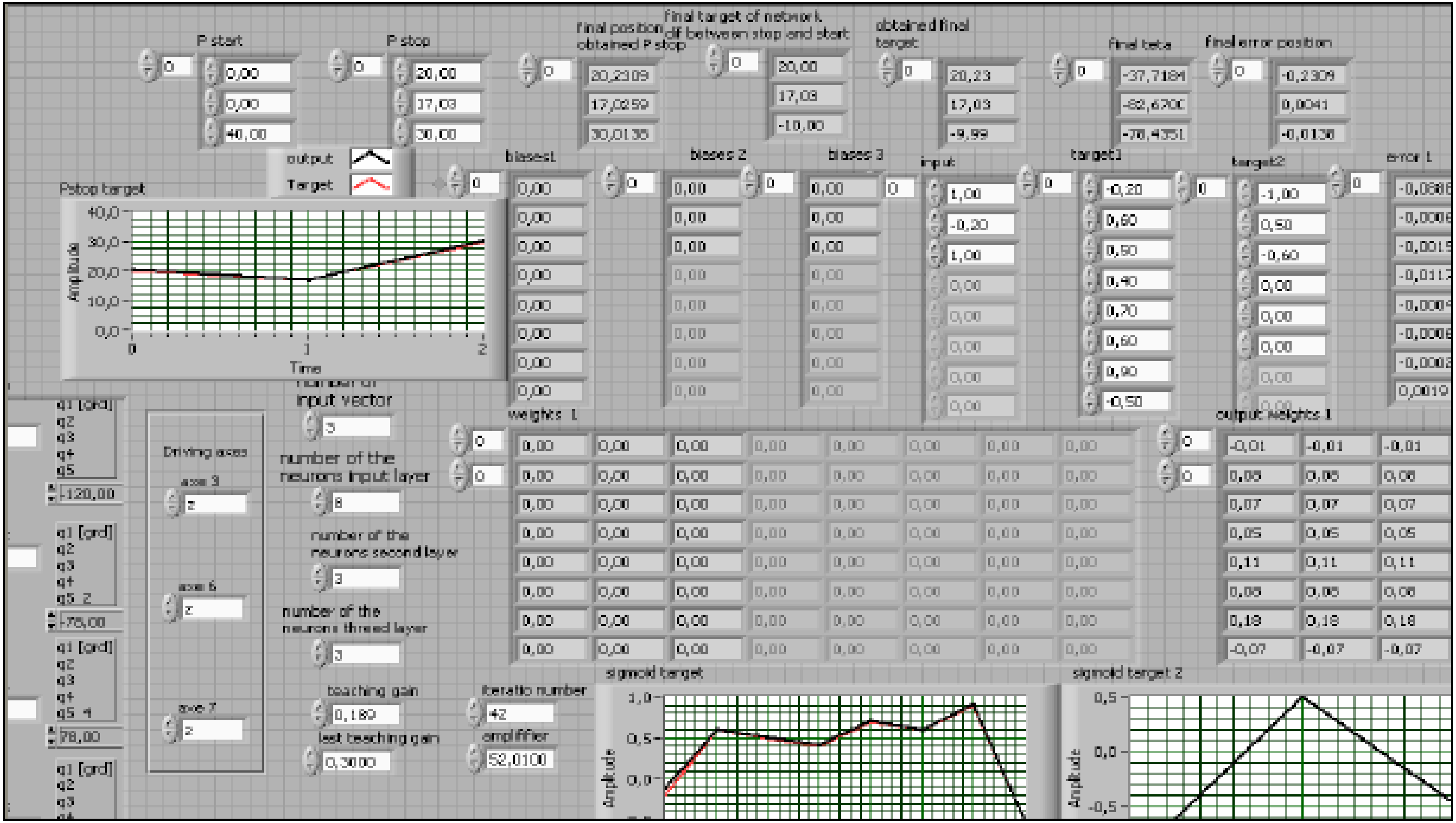

Fig.18: The front panel of the SUM neural network type BSHTNN with TDRL when the amplifier gain and the iteration number were changed

Table 1

The synthetic results of the assisted research of the proposed neural network

Ex. number	Config.	Comp. NN	Amplif. gain	Teach gain	Target data	Obt. Pos.	Obtained φ_i	Target hidden	Iteration number	Rel err.
1	3-8-3-3	BSHTNN TDRL	52.01	0.189	20 17.3 -10	20.239 17.0259 30.0138	-37.7184 -82.67 -78.435	-1 0.5 -0.6	42	1%
2	3-7-3-3	BSHTNN	52.01	0.189	-"-	12.30 29.32 24.23	-38.23 -112 -85	-1 0.5 -0.6	132	30%
3	3-8-3-3	BSHTNN TD	52.01	0.189	-"-	15.1764 24.9820 27.3053	67.5955 21.7510 26.0883	-1 0.5 -0.6	132	20%
4	3-8-3-3	BSHTNN TD+TD	52.01	0.189	-"-	19.8665 16.650 30.4646	-38.7591 -82.6825 -78.5155	-1 0.5 -0.6	132	10%
5	3-8-3-3	BSHTNN TDRL	48	0.189	-"-	19.397 15.835 31.193	-34.8942 -76.2740 -72.4487	-1 0.5 -0.6	132	11%
6	3-8-3-3	BSHTNN TDRL	52.01	0.189	-"-	16.686 13.741 33.656	-45.40 22.213 26.2534	-0.5 1 -0.6	42	14%

Discussion and Conclusion

After analysing the obtained results after the assisted research, synthetic presented in the table 1, we can do the following remarks:

- **the change of the number of the neurons** in the first layer don't change the errors;
- **the change of the amplifier gain** and the teaching gain assured the decrease of the error from 18% to 4% for the 132 number of iteration;
- one substantial decreasing of the errors and the decreasing of the number of iteration was obtained by **on-line changing of the hidden layer target data**, 11% to 1% for 52 iteration.

With this method, by applying the control of the inverse kinematics and by using the proposed neural network type, will be possible to obtain one optimization of the robot or SUM motor end-effector position in the space.

The applying method, the proposed neural network, the assisted research with the virtual LabVIEW instrumentation opens the way to apply in the robot the SUM motors and the intelligent systems.

- **by using this sensitive function** is possible to obtain one very short iteration number and one optimal gradient error; the sigmoid gain determines, by increasing them, one acceleration convergence process, but the value is strictly limited;
- **the closed loop with time-delay of the output**, consecutive applied with time-delay in odd number in the first layer, determines one very short iteration process to the target;
- **applying the time-delay with the same pass delay**, determines the sum of the errors between the both side of the target curve with the instability convergence process.

The paper shown some of the more important neuron network types, proper mathematical models, how can teaching these network and what are the results after numerical simulation with proper virtual LabVIEW instrumentation.

All created virtual instruments work on-line and it is possible to see the influences of the input elements, weights, biases or of the number of the neurons in hidden layer or in the input data layer. It is possible to see on-line what was happened when was changed the target form of the curve, the components.

- By using the intelligent smart damper

Optimization of the dynamic behavior- by using the smart dampers

Prof.univ.Ph.D.Eng.Adrian OLARU
senior member of IACSIT (Singapore)
International
Association of Computer Sciences and Information Technology
University Politehnica of Bucharest, ROMANIA
Ph.D.Eng.Şerban OLARU
Romsys Company, Bucharest, ROMANIA

News presented in this research:

- ❑ The assisted research of one magnetorheological damper;
- ❑ Put in evidence the influences of this damper to the dynamic behavior of the industrial robots;
- ❑ The new mathematical model for one magnetorheological damper;
- ❑ The assisted theoretical simulation of the new model;
- ❑ The parameterization of the known characteristics of the magnetorheological damper;
- ❑ The theoretical research with LabVIEW instrumentation to establish the influences of the mathematical model coefficients to the characteristics parameters from the parameterization curves;
- ❑ The assisted experimental research were established the values of all coefficients of the proper mathematical model to assure the concordance between the experimental and the theoretical characteristics with the errors under the 1%;
- ❑ The assisted optimization of the dynamic parameters.

By knowing the real mathematical model of the damper will be possible to develop the new matrix -vector form of the force- moment torsor and to develop the next research of the **global dynamic behavior of the industrial robot with the intelligent damper.**

NEW MATHEMATICAL MODEL OF THE BOUC-WEN MODEL

model (Dyke et al., 1998) what was researched and for what was determined all values of the coefficients in concordance with the real characteristics

$$f(i) = c_0(x' - y') + k_0(x - y) + k_1(x - x_0) + \alpha z$$

$$y' = \frac{1}{c_0 + c_1}[\alpha z + c_0 x' + k_0(x - y)]$$

$$z' = -\gamma|x' - y'||z||z|^{n-1} - \beta(x' - y')|z|^n + \delta(x' - y')$$

$$\alpha(i) = \alpha_3 i^3 + \alpha_2 i^2 + \alpha_1 i + \alpha_0$$

$$c_0(i) = c_{03} i^3 + c_{02} i^2 + c_{01} i + c_{00}$$

$$c_1(i) = c_{13} i^3 + c_{12} i^2 + c_{11} i + c_{10}$$

$$k_0(i) = k_{03} i^3 + k_{02} i^2 + k_{01} i + k_{00}$$

$$\delta = \sum \delta_{0i} \sin(2\pi \upsilon_i + \varphi_i)$$

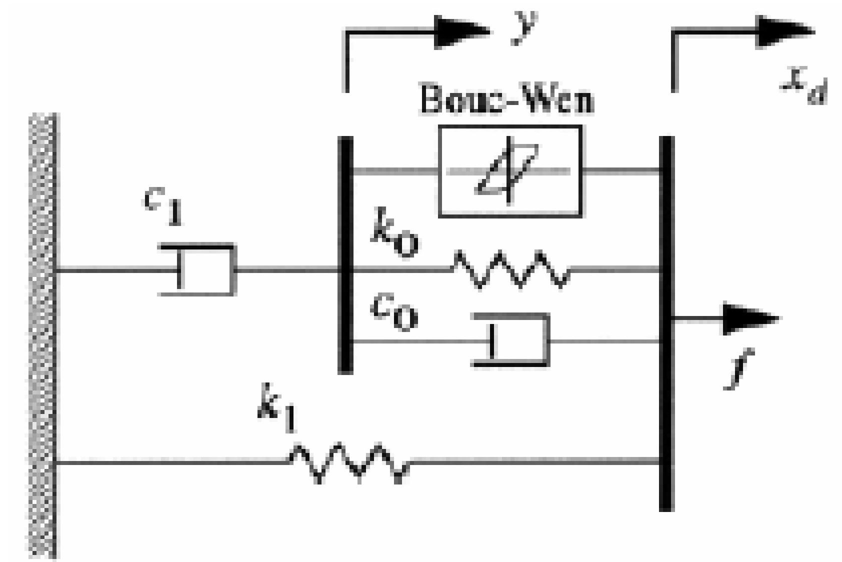

Damper force function of the current intensity of the input in a coils of the rheological damper

THE NEW MATHEMATICAL MODEL OF THE MAGNETORHEOLOGICAL DAMPER

$$f = c_0(x' - y') + k_0(x - y) + k_1(x - x_0) + \alpha z$$

$$y' = \frac{1}{c_0 + c_1}[\alpha z + c_0 x' + k_0(x - y)]$$

$$z' = -\gamma|x' - y'|z|z|^{n-1} - \beta(x' - y')|z|^n + \delta(x' - y')$$

$$\alpha(i) = \alpha_3 i^3 + \alpha_2 i^2 + \alpha_1 i + \alpha_0$$

$$c_0(i) = c_{03} i^3 + c_{02} i^2 + c_{01} i + c_{00}$$

$$c_1(i) = c_{13} i^3 + c_{12} i^2 + c_{11} i + c_{10}$$

$$k_0(i) = k_{03} i^3 + k_{02} i^2 + k_{01} i + k_{00}$$

$$\delta = \sum \delta_{0i} \sin(2\pi\upsilon_i + \varphi_i)$$

These equations contents the contributions to the new mathematical magnetorheological damper model, after the assisted theoretical and experimental research.

where $\boldsymbol{f}$ is the damping force [N]; $\boldsymbol{x}$ and $\boldsymbol{y}$ are the primary, respectively the secondary displacement variables [m]; $\boldsymbol{z}$ is the internal history dependency variable of the MRD [m]; $\boldsymbol{k_0}$, $\boldsymbol{k_1}$ are the non linear internal rigidity of the MRD, [N/m] depending of the current intensity $\boldsymbol{i}$ [A]; $\boldsymbol{c_0}$ and $\boldsymbol{c_1}$ are the internal viscous damping parameters of the MRD [Ns/m]; $\boldsymbol{\alpha}$ is the internal parameter what have non linear evolution and depend of the magnetic variable field (electrical intensity); parameter $\boldsymbol{\beta}$ characterize the gain of increasing of the damping force versus velocity; $\boldsymbol{x_0}$ is the perturbation displacement [m]; $\boldsymbol{\delta}$ is the histeresys parameter; $\boldsymbol{\delta_{0i}}$ is the histeresys parameter for each frequencies from the Fourier spectrum; $\boldsymbol{\upsilon_i}$ is the frequency from the Fourier spectrum; $\boldsymbol{\varphi_i}$ is the phase in each frequencies.

NEW MATRICEAL- VECTORIAL MATHEMATIC MODEL OF ONE ROBOTIZED STRUCTURE

Damper force of the magnetorheological damper function of the current intensity of the spools of the damper

$$\begin{pmatrix}F^{0}\\ M^{0}\end{pmatrix}=\begin{bmatrix} z_u & 0\\ 0 & z_u\end{bmatrix}\left(\begin{pmatrix} D_{0,i}(F_R^i+f(i))\\ D_{0,i}M_R^i\end{pmatrix}-diag\begin{bmatrix} sign\frac{v_u^i}{\left|v_u^i\right|}m_{u_i} & sign\frac{\omega_u^i}{\left|\omega_u^i\right|}J_{g_i}\end{bmatrix}\cdot\begin{pmatrix}\left(a_{i,0}^i\right)+\left[\widehat{\omega}_{i,0}^i\right]^2\left(r_{g_i}^i\right)\\ \left(\varepsilon_{i,i-1}^i\right)+\left[\omega_{i-1,0}^i\right]\left(\omega_{i,i-1}^i\right)\end{pmatrix}\right)+$$

$$+\begin{bmatrix} z_u & 0\\ 0 & z_u\end{bmatrix}\cdot\begin{pmatrix}(0)\\ \left[G_{i,k}\right]\left(\widehat{b}_{i,k}\right)\left(\left(D_{0,i}(F_R^i+f(i))\right)-diag\left[sign\frac{v_u^i}{\left|v_u^i\right|}m_{u_i}\right]\cdot\left[D_{0,i}\right]\left(\left(a_{i,0}^i\right)+\left[\widehat{\omega}_{i,0}^i\right]^2\left(r_{g_i}^i\right)\right)\right)\end{pmatrix},$$

Active torsor of the force- moment

Dual vector of the linear and angular accelerations

Resistance torsor of the force- moment

Moment matrix of the resistance forces

Matrix of the incidences joints- bodies

THE VIRTUAL PROPRE LABVIEW INSTRUMENTATION USED IN THE THEORETICAL AND EXPERIMENTAL RE4SEARCH

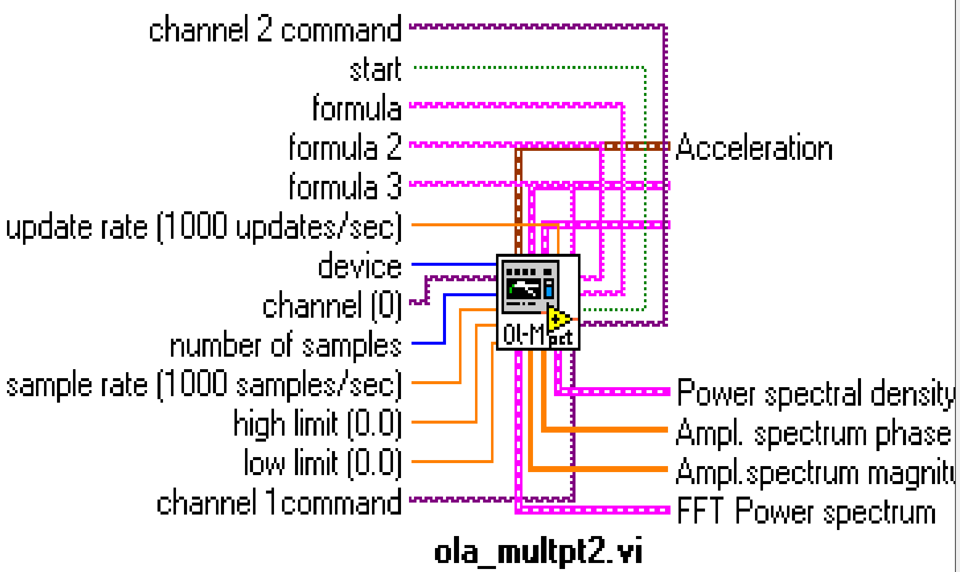

Virtual instrument *VI* for the assisted command and acquisition

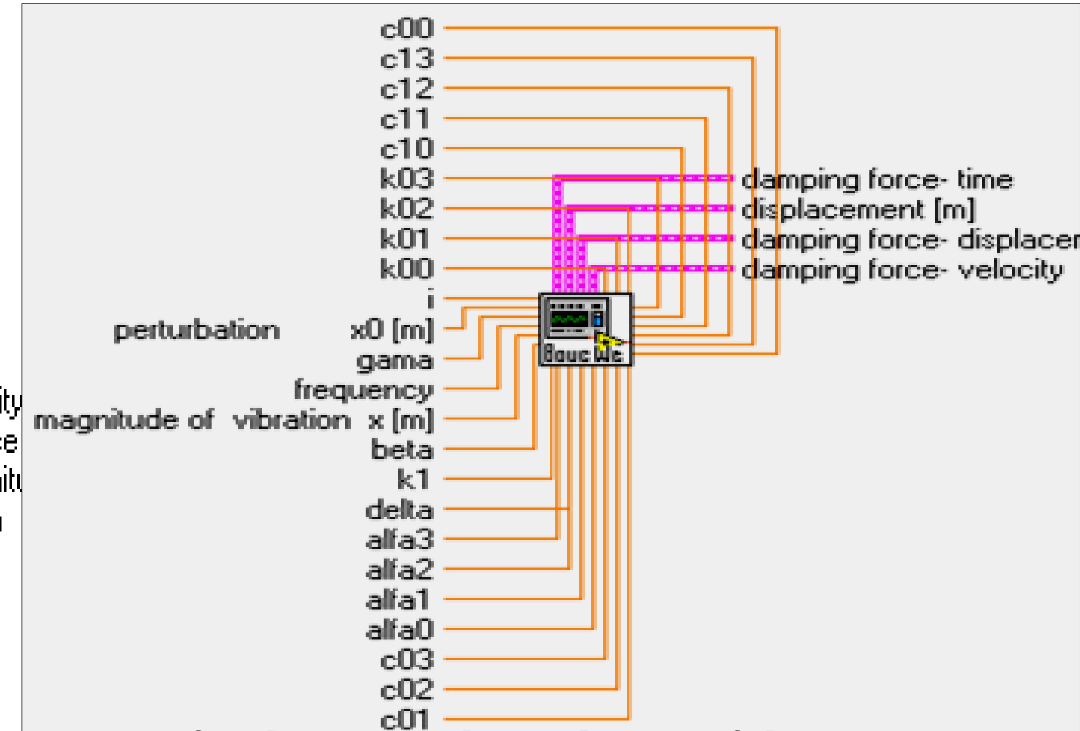

VI for the assisted simulation of the magnetorheological damper characteristics

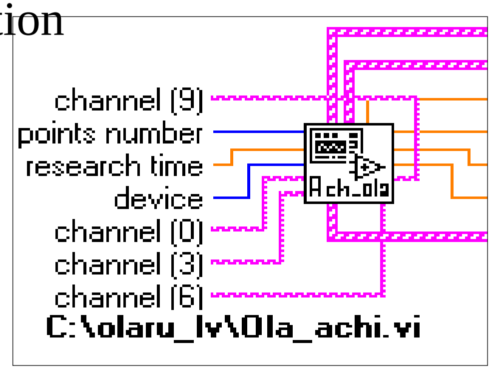

VI for the data acquisition to the five simultaneously channels

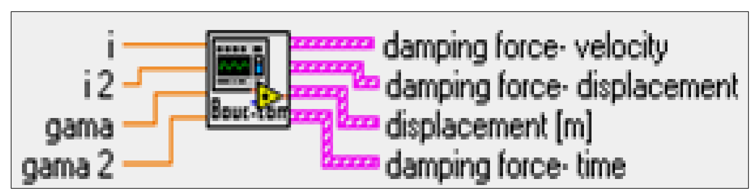

VI for comparative analyze of the damper characteristics

SOME REZULTS OF THE NUMERICAL SIMULATION

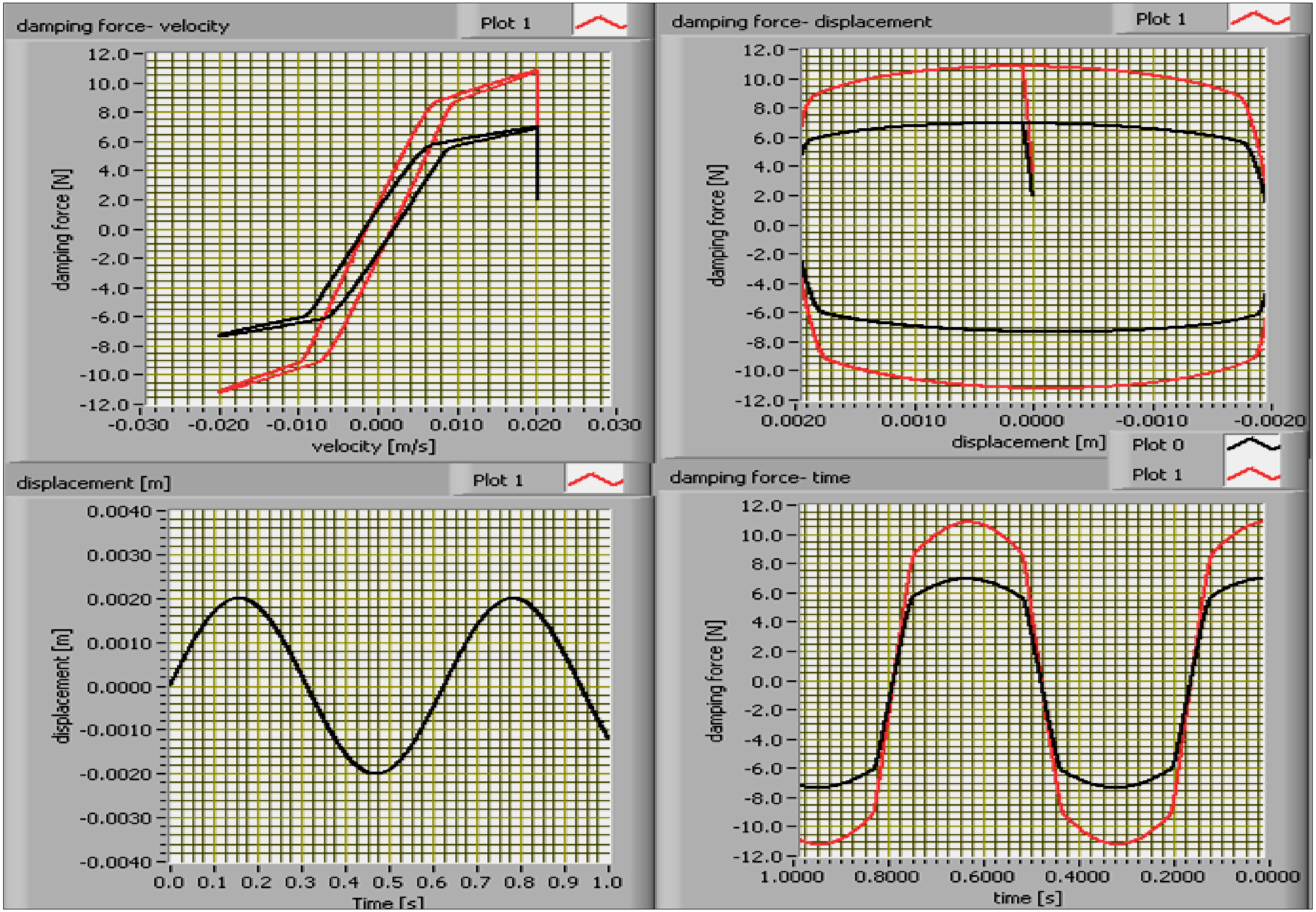

The MRD characteristics: damping force vs. velocity, damper force vs. displacement, damper force vs. time, velocity vs. time in the case when was changed the current intensity *i* from 1.2A to 1.5A.

Parameterization of the damper force vs. velocity characteristics

- Parameterization has the goal to introduce some parameters for each zone of the alure of the characteristics

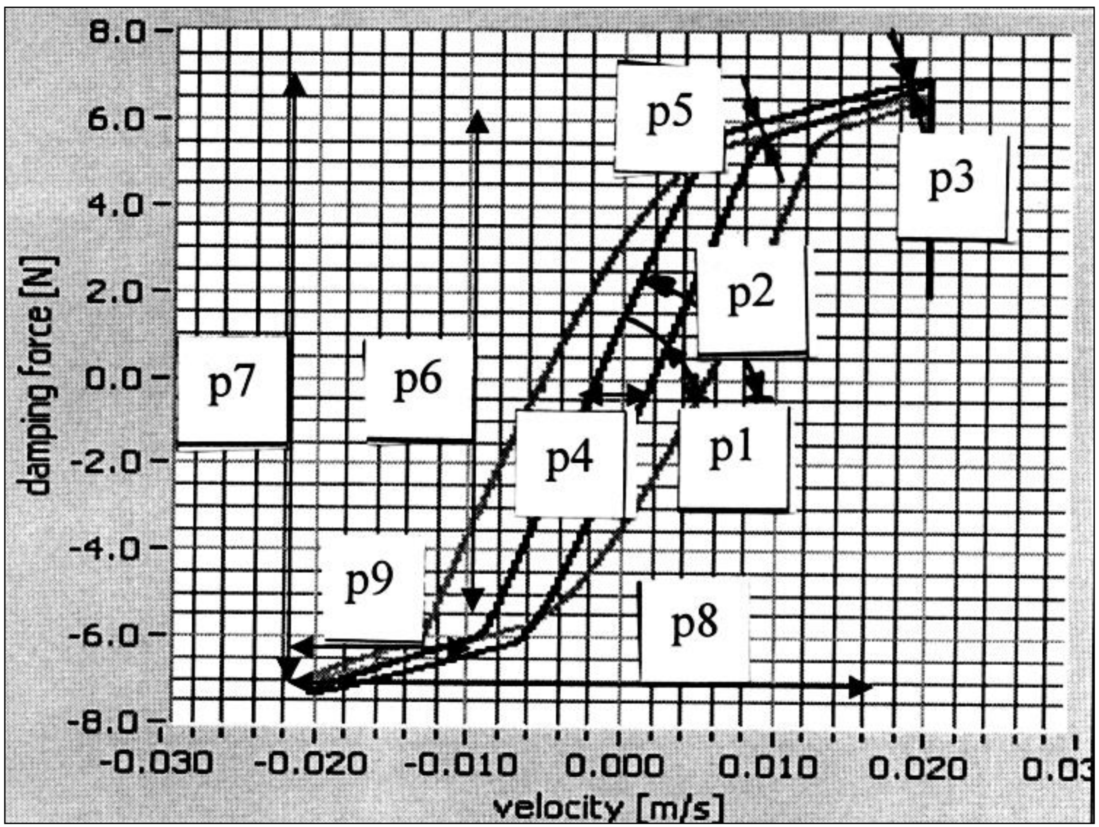

•parameter **p1** reprezent the inclination of the alure in spreading phase;
•**p2** inclination of the alure in a compress phase;
•**p3** inclination of the alure histerezis top;
•**p4** maximal histerezis value of the minimal velocity;
•**p5** magnitude of the histerezis at the maximal velocity;
•**p6** the second value of the cvasilineare alure of the charact.;
•**p7** the second maximal value of the charact.;
•**p8** the first maximal value aof the charact.;
•**p9** the first value of the histerezis top.

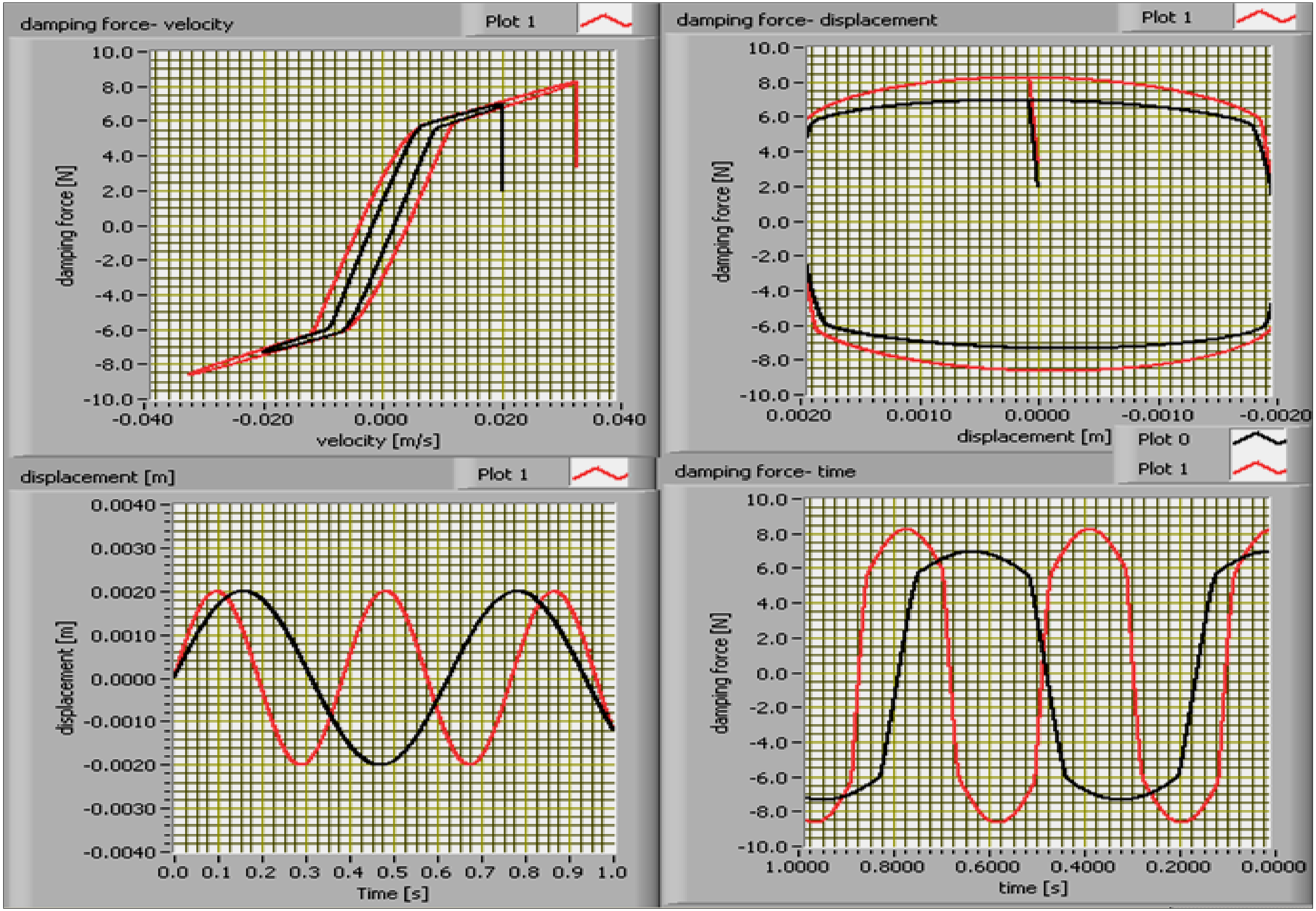

The MRD characteristics: damping force vs. velocity, damper force vs. displacement, damper force vs. time, velocity vs. time in the second case when was changed the frequency ν from to 1.6Hz to 2.6Hz

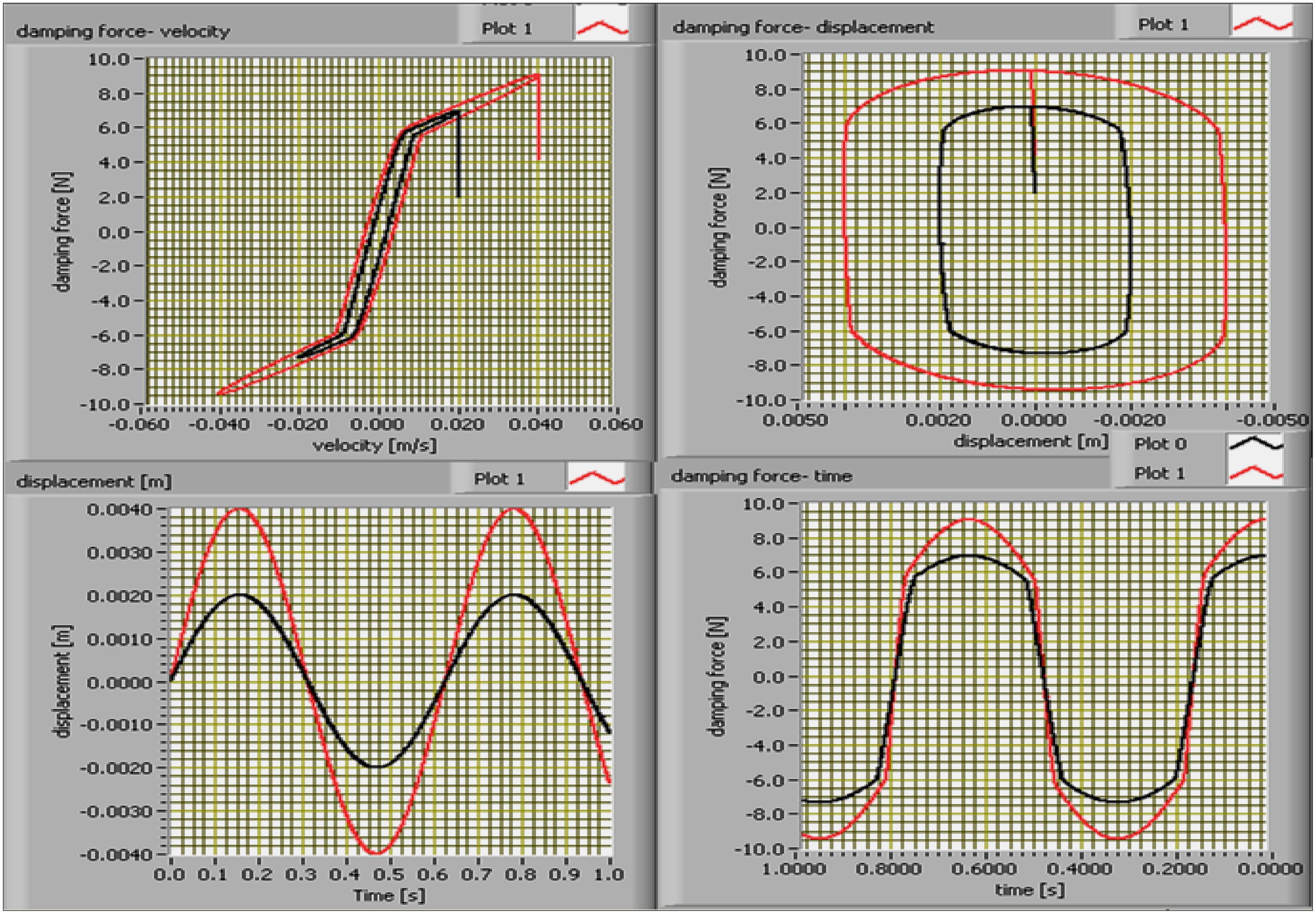

The MRD characteristics: damping force vs. velocity, damper force vs. displacement, damper force vs. time, velocity vs. time in the second case when was changed the magnitude of vibration x from 0.002m to 0.004m

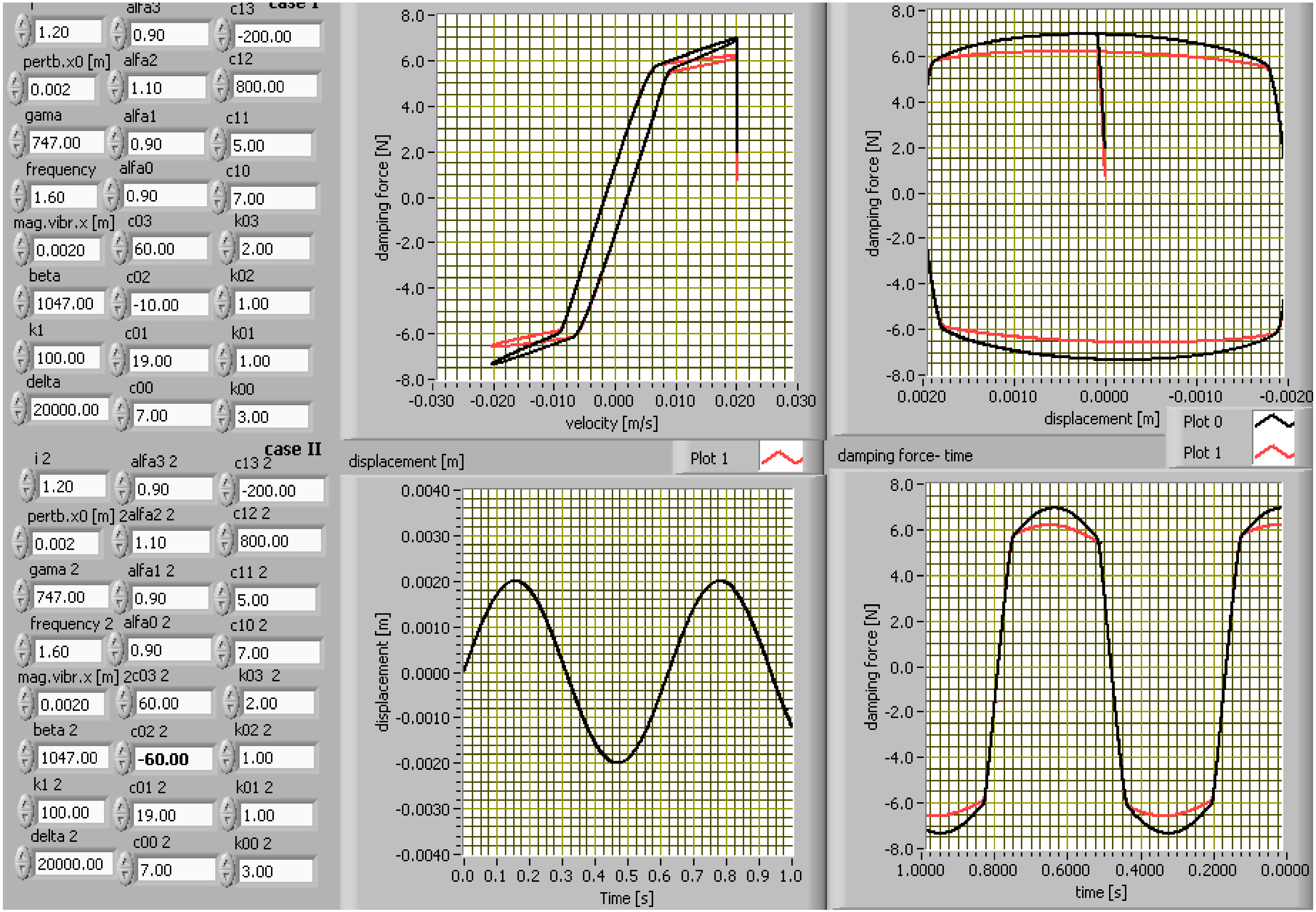

The MRD's characteristics: damper force vs.velocity, displacement, time, velocity vs. time in the case when was changed $c02$ from -10 to -60

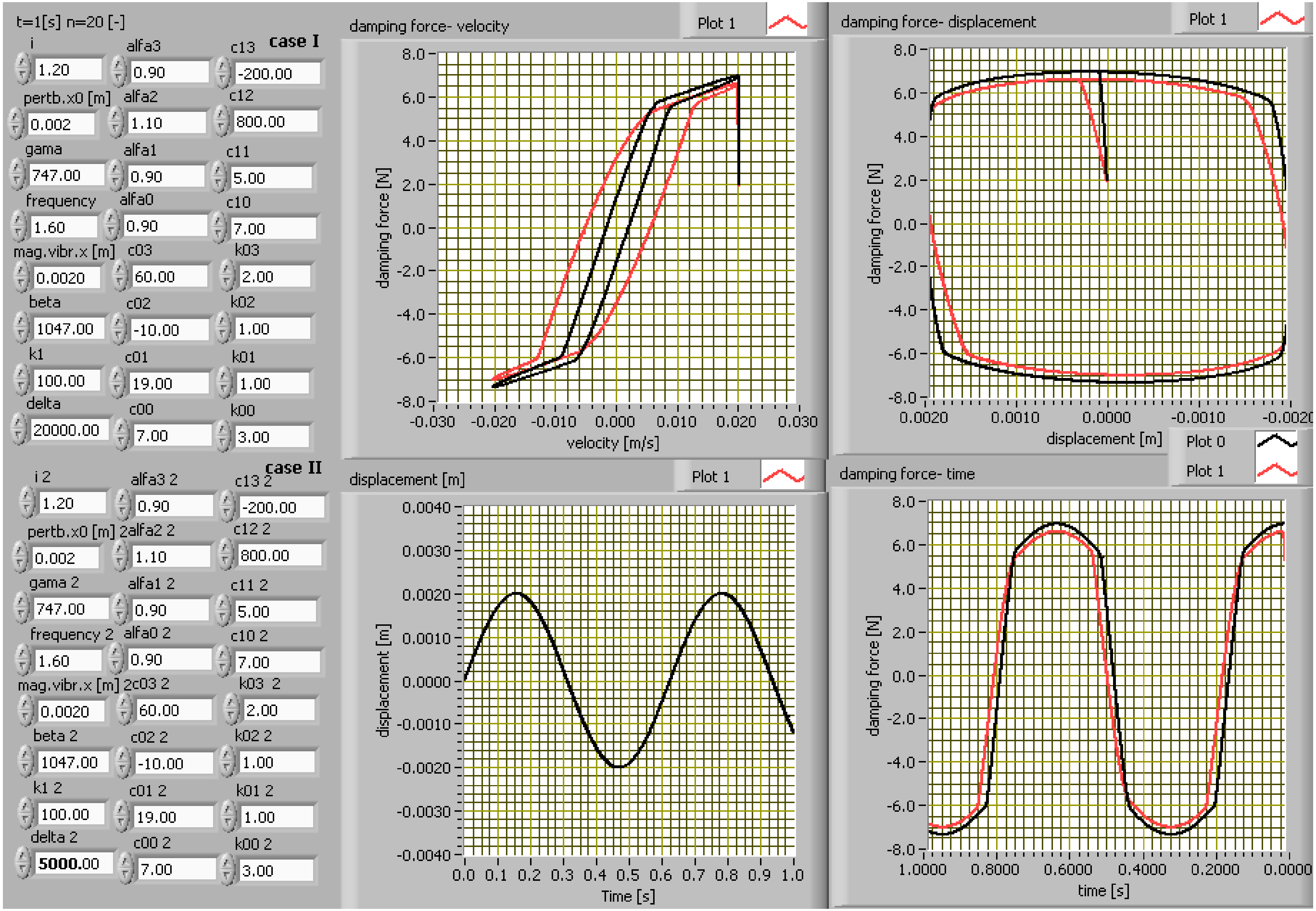

The MRD’s characteristics: damper force vs.velocity, displacement, time, velocity vs. time in the case when was changed δ from 20000 to 5000

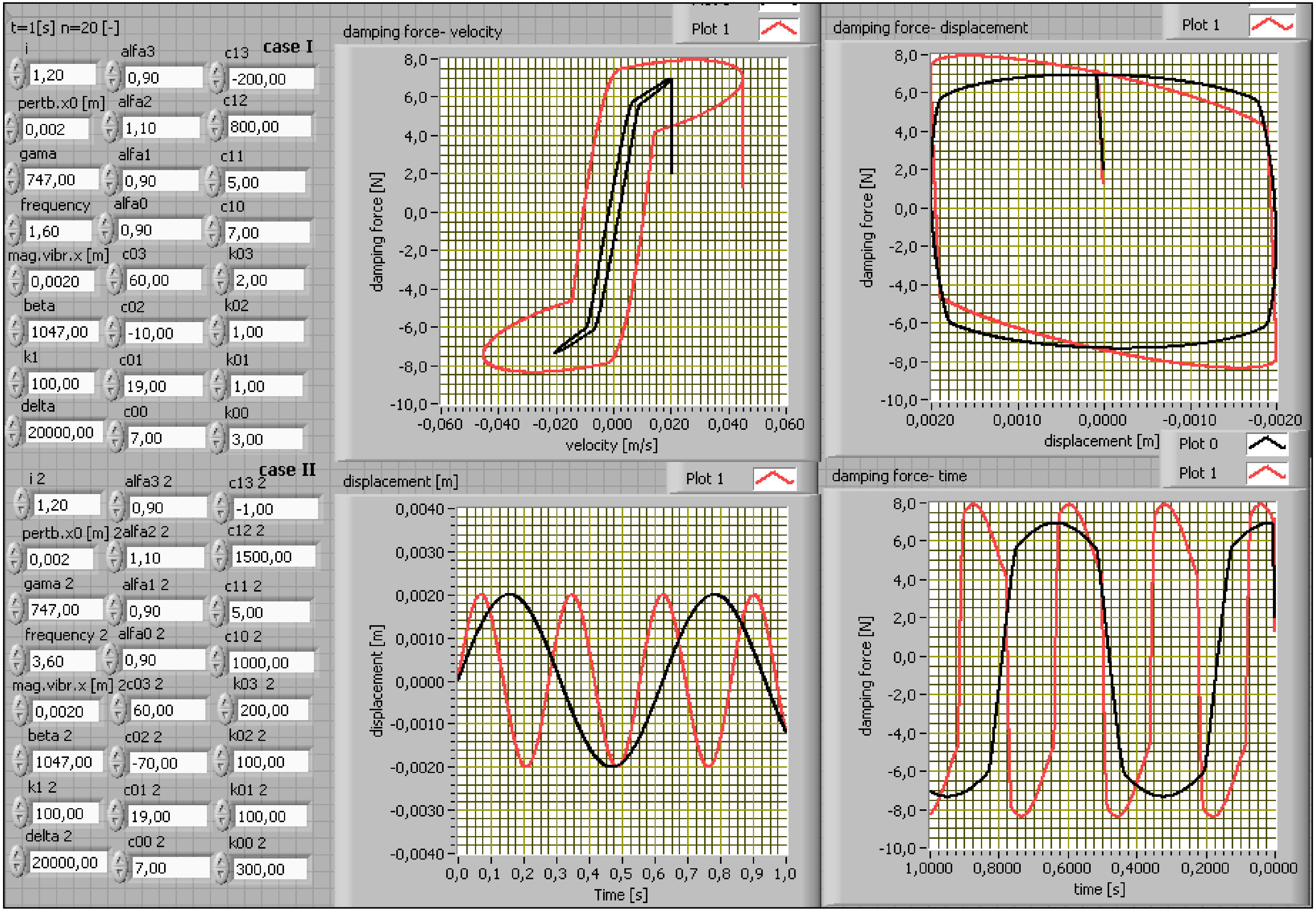

The MRD's characteristics: damper force vs.velocity, displacement, time, velocity vs. time in the case when was changed v , $k00$, $k01$, $k02$, $c02$, $c10$, $c12$, $c13$

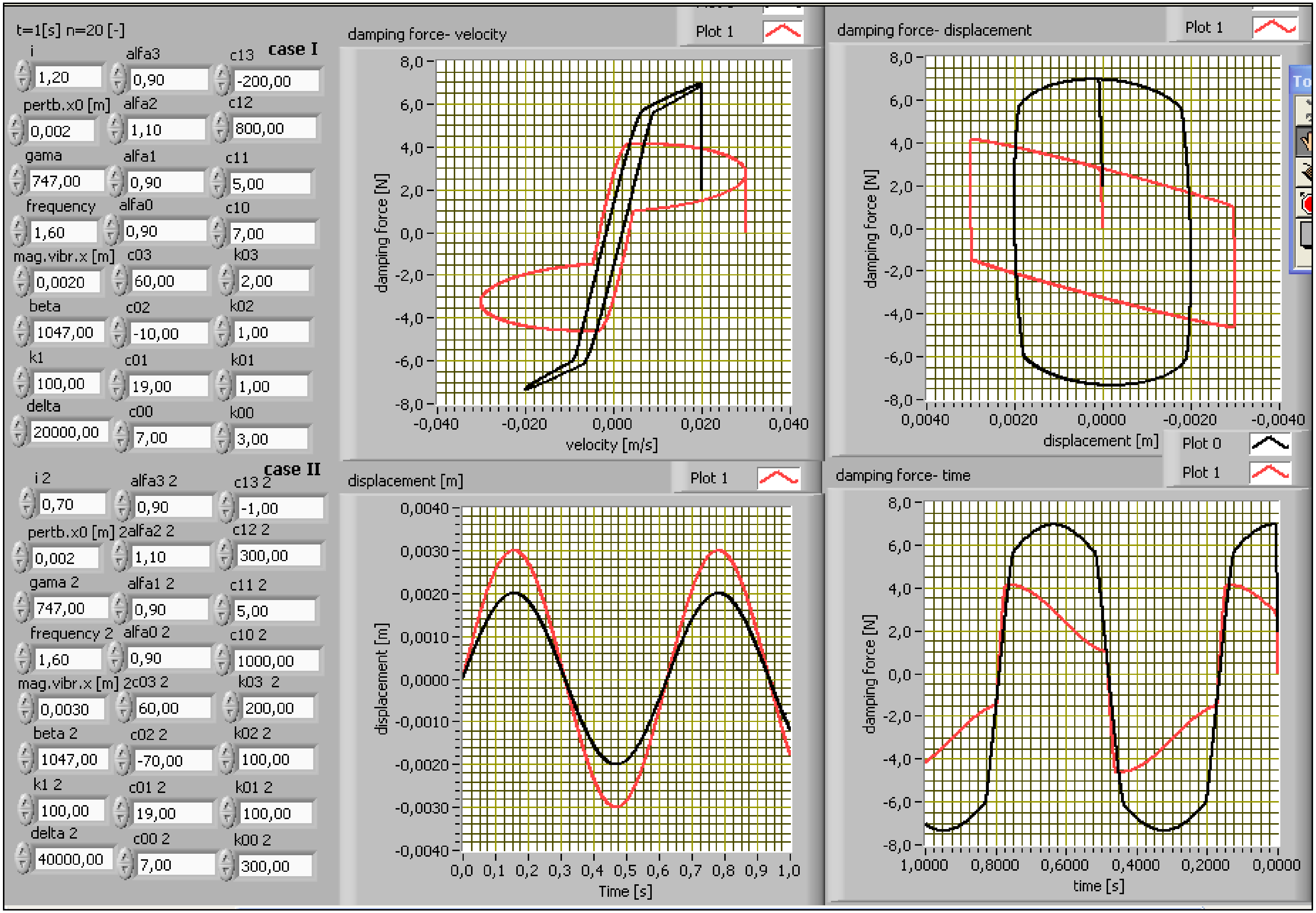

The MRD's characteristics: damper force vs.velocity, displacement, time, velocity vs. time in the case when was changed $k00$, $k01$, $k02$, $k03$, $c02$, $c10$, $c12$, $c13$, i , x , δ

Numerical simulation

Transpose the damper mathematical model in to the LabVIEW virtual instrument

Simulate some characteristics for the different model's coefficients

Observe how were changed the characteristics parameters p_i

Adjust the values of all mathematical coefficients to obtain the same F-v characteristic

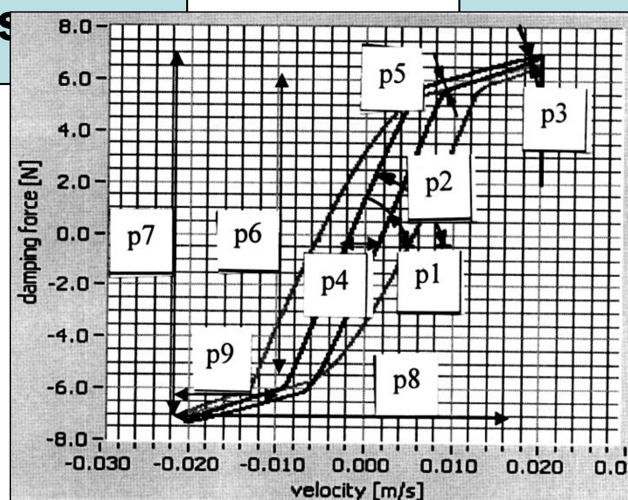

THE RESULTS AFTER THE NUMERICAL SIMULATION

After the analyze of the numerical simulation we can remark the followings:

- the change of the current intensity ***i*** determines the change of the parameters **p1, p2, p6, p7;**
- the change of the perturbation displacement x_a determines the change of the parameters **p3, p5**;
- the change of the internal coefficient ***γ*** determines the change of the parameters **p3, p5**;
- the change of the magnitude of the vibration ***x*** determines the change of the parameters **p7, p8, p9**;
- the change of the global rigidity ***k*1** determines the change of the parameters **p3, p4, p5, p7;**
- the change of the damping force gain ***β*** determines the change of the parameters **p3, p6, p7;**
- the change of the histheresis term ***δ*** determines the change of the parameters **p1, p2, p3, p4, p5, p9;**
- the change of the internal coefficient of the second order ***α*2** determines the change of the parameters **p3, p6, p7**;
- the change of the internal coefficient of the first order ***α*1** determines the change of the parameters **p3, p6, p7, p9**;
- the change of the viscose damping parameter of the second order ***c*02** determines the change of the parameters **p3.**

All the coefficients of the mathematical model were changed and were analyzed the influences to the parametrical force vs. velocity damper characteristic [1].

EXPERIMENTAL SETUP

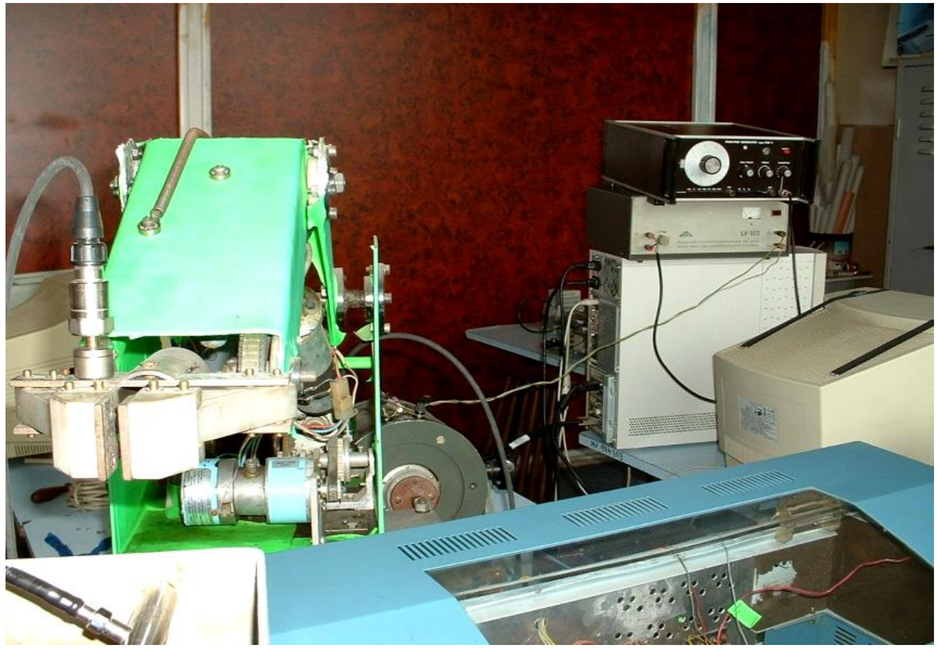

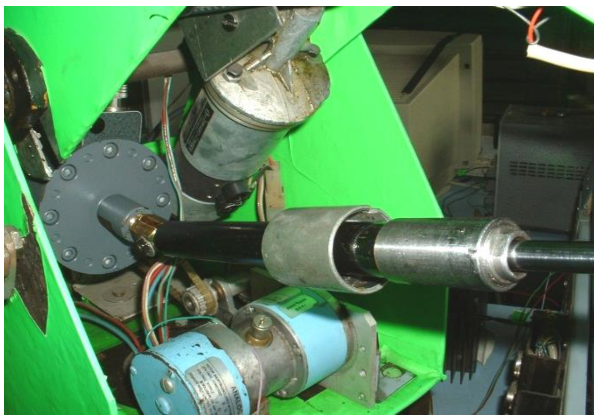

The experimental stand contains the following components:

- **didactical arm type robot;**
- **the electromagnetic exciter type 11075 from RFT Germany;**
- **connector type CB-68 LP from National Instruments USA; acquisition board type PCI 6224M from National Instruments USA;**
- **function generator type POF-1 from KABID Poland; amplifier type LV 102 from MMF Germany for the generator;**
- **personal computer from Taiwan;**
- **inductive displacement transducer type 16.1 IAUC Romania;**
- **Hottinger apparatus type KWS/T-5 from Germany;**
- **proper MRD.**

EXPERIMENTAL RESEARCH OF THE GLOBALE DYNAMIC COMPLIANCE WITH MAGNETORHEOLOGICAL DAMPER

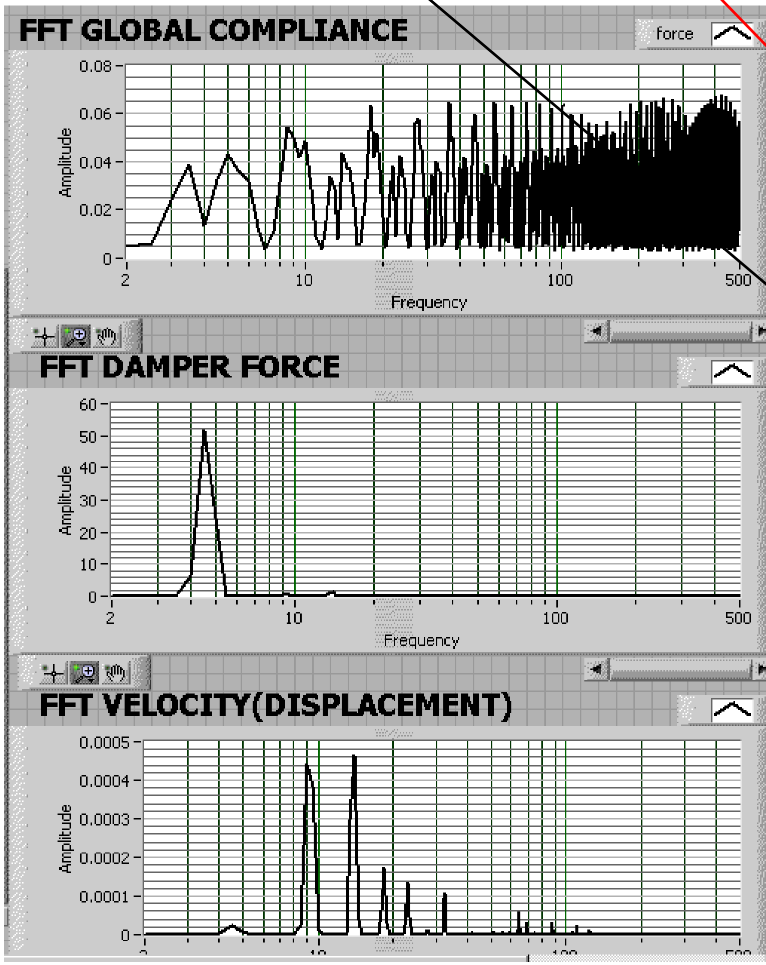

Fourier spectrum of the velocity, damper force, Global dynamic compliance

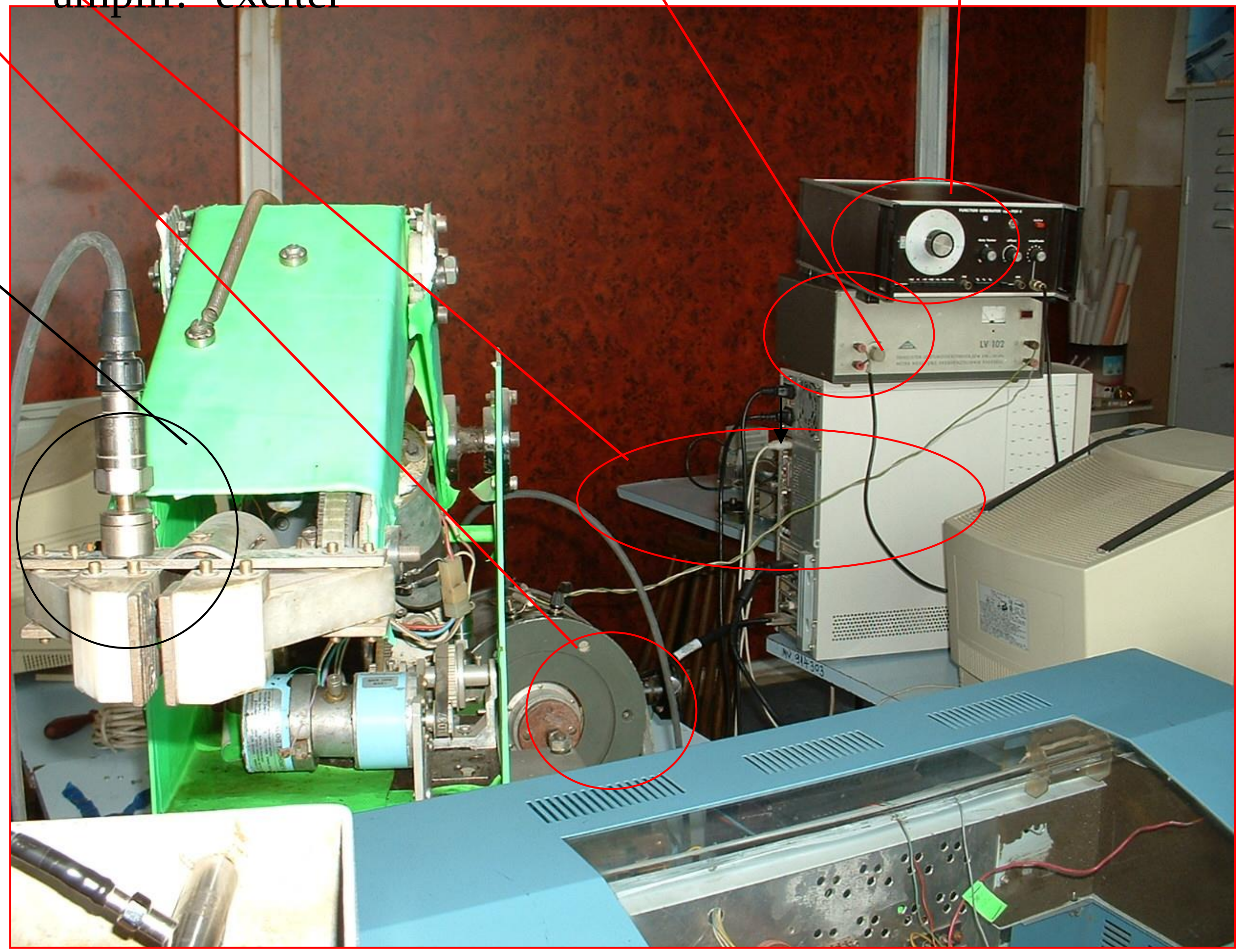

The experimental setup

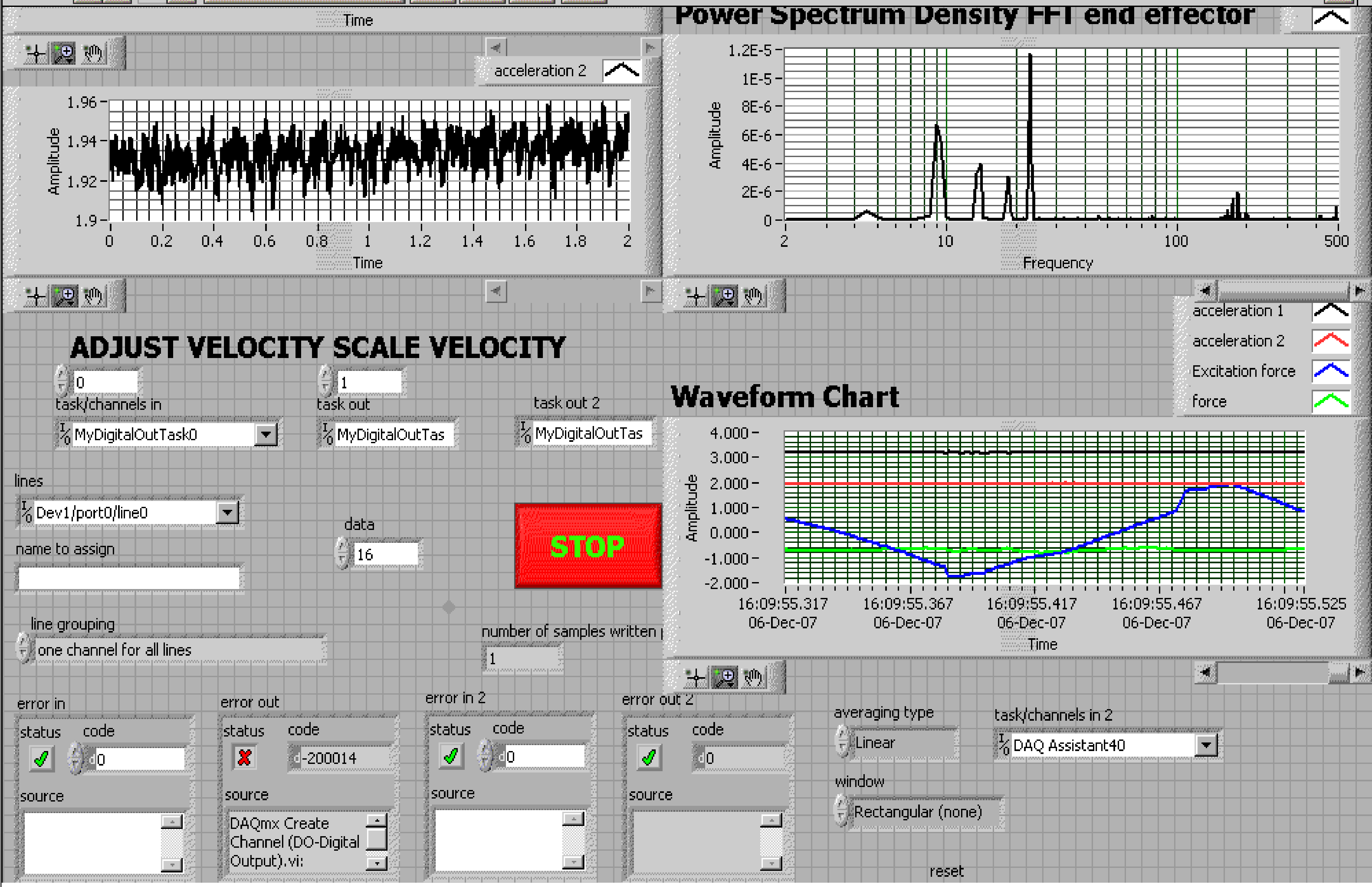

The front panel of the data acquisition *VI*

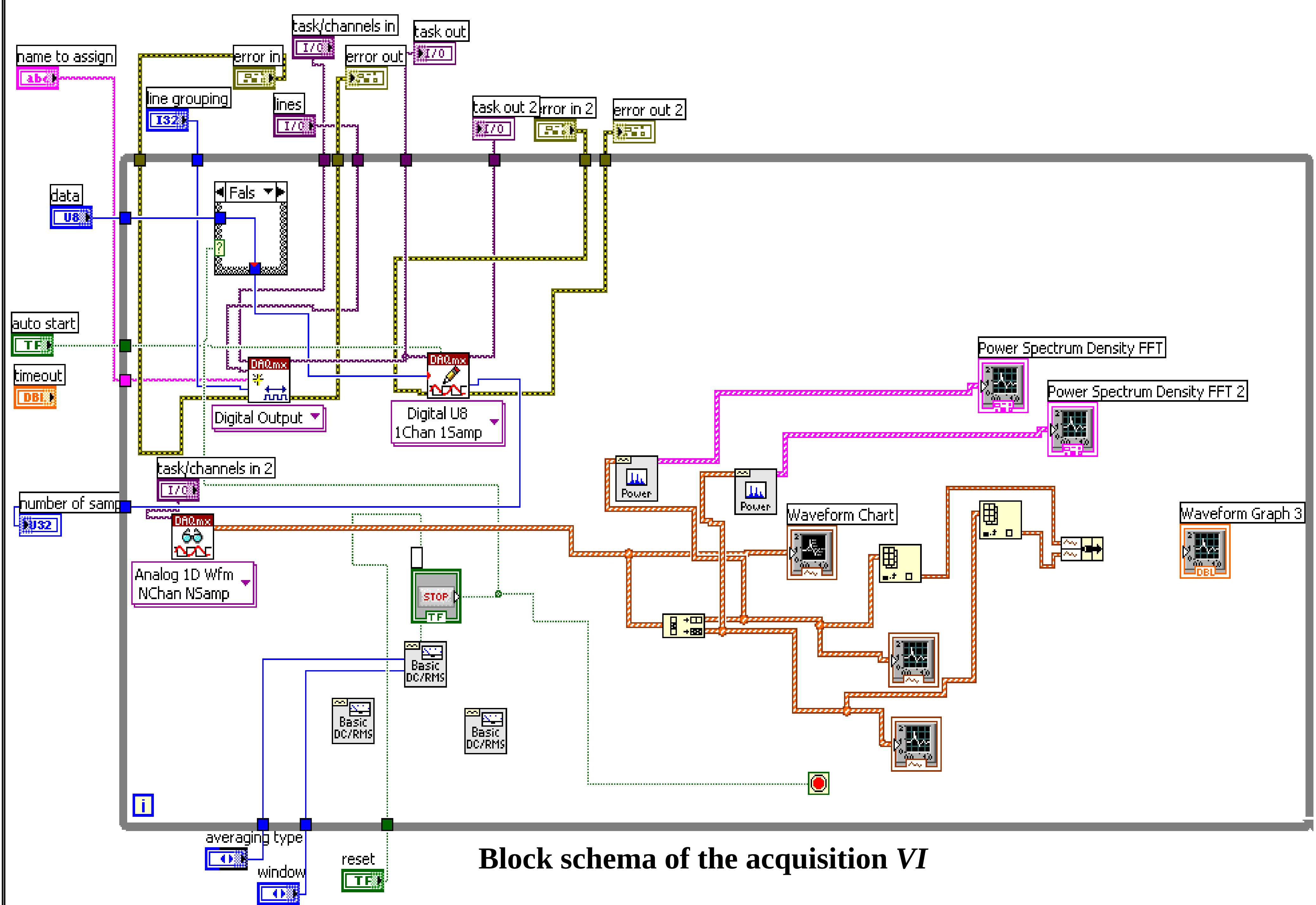

Block schema of the acquisition *VI*

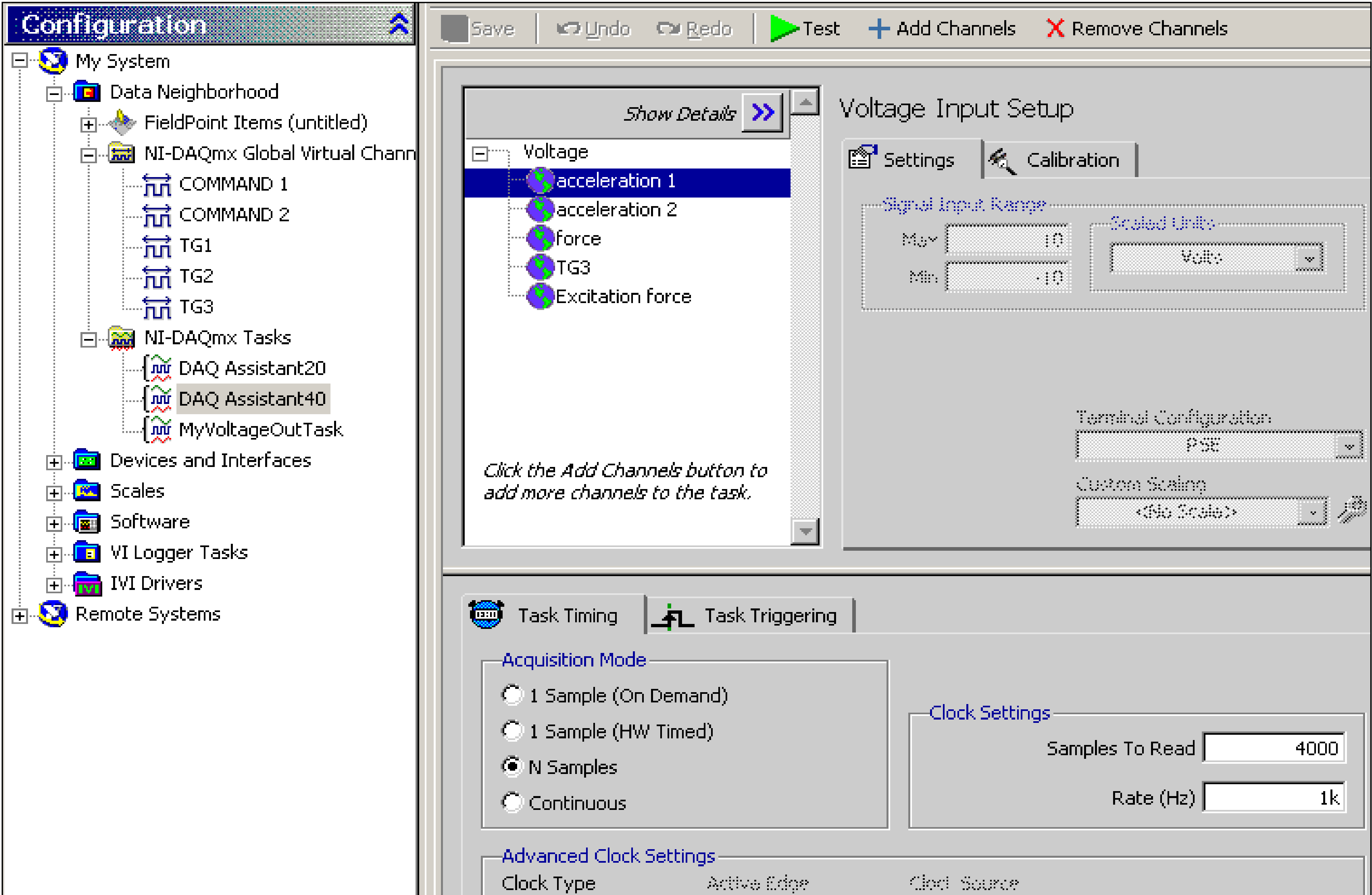

Proper acquisition task DAQ Assistant 40 used in the acquisition

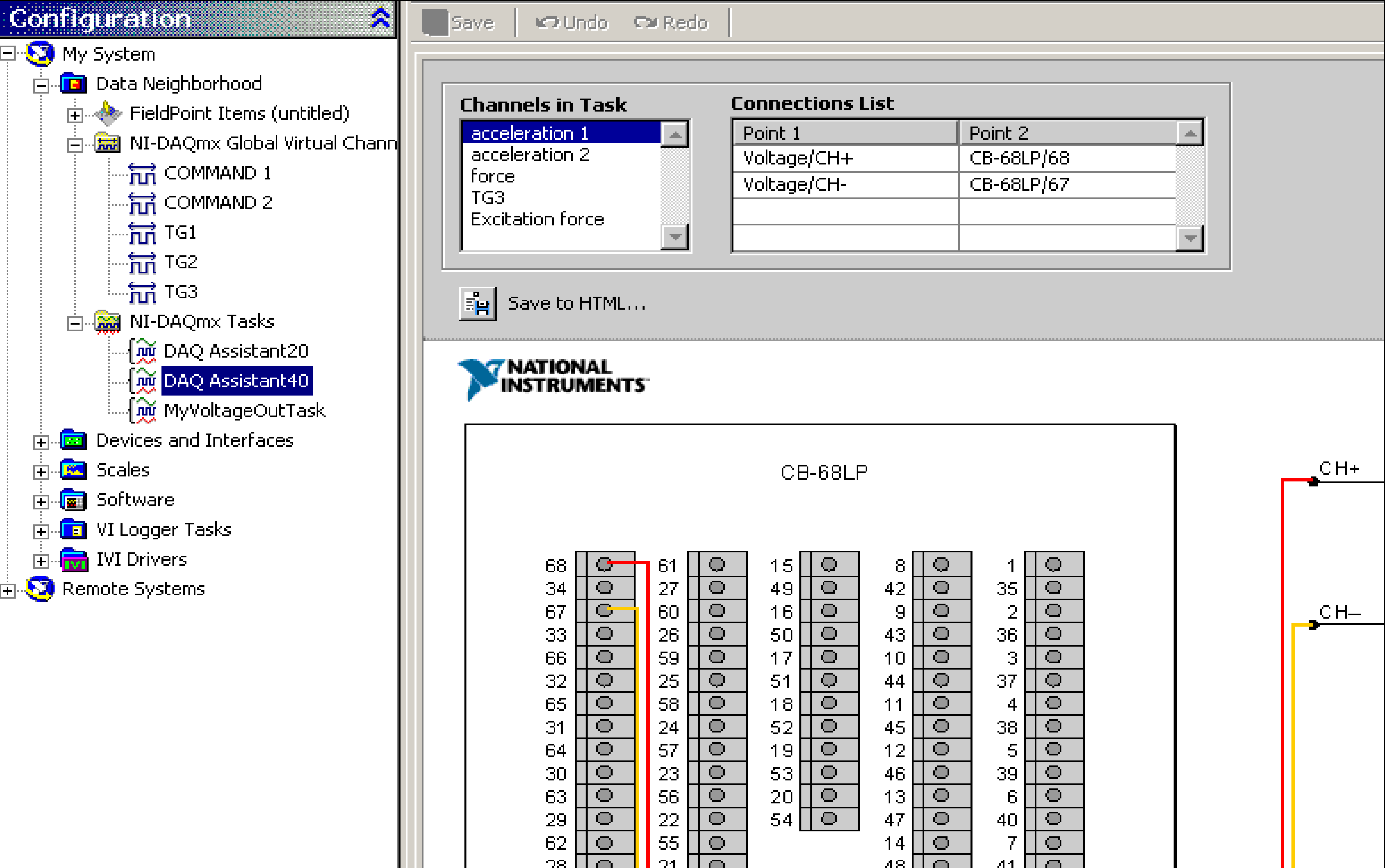

The links in the acquisition bord connector

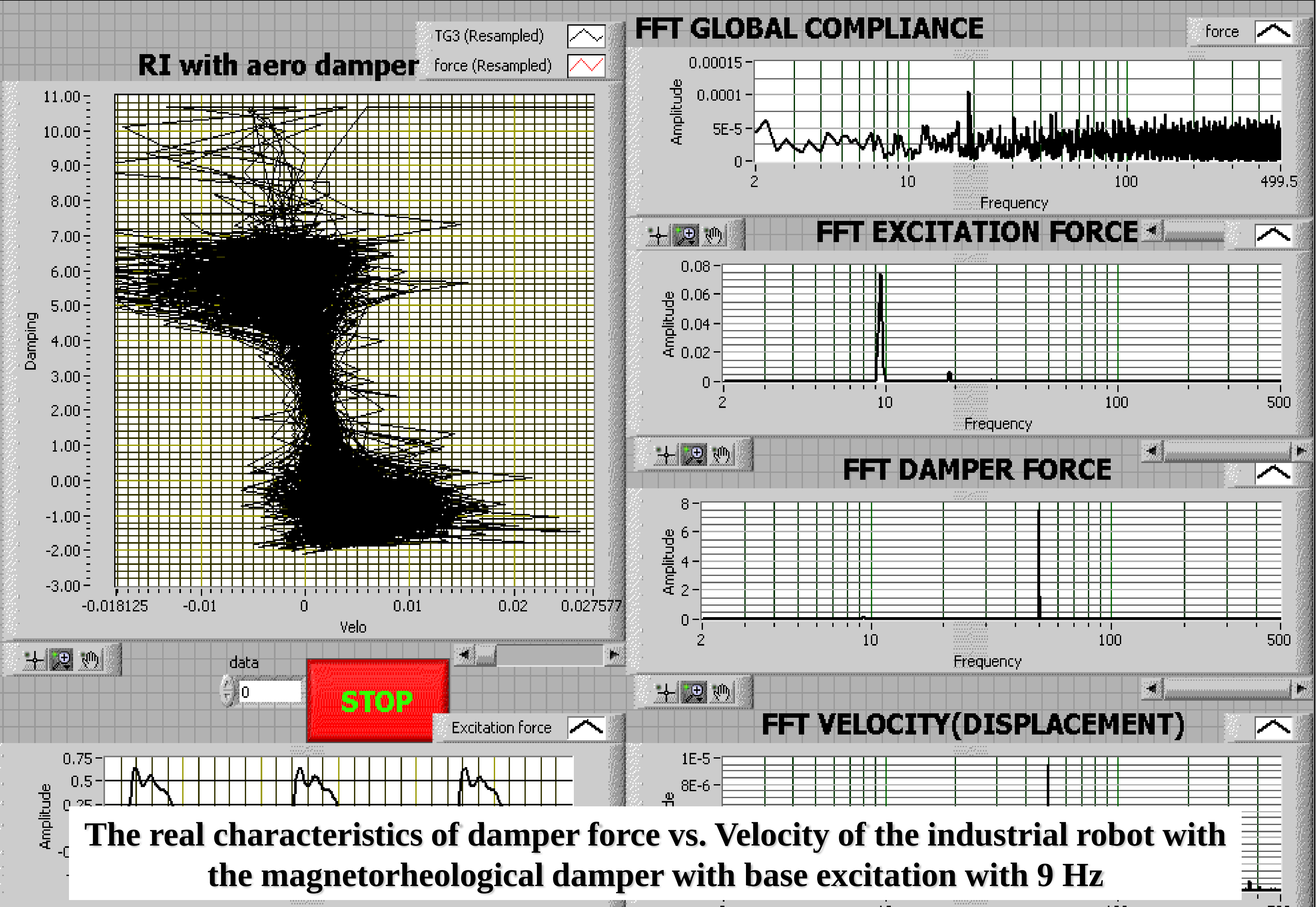

The real characteristics of damper force vs. Velocity of the industrial robot with the magnetorheological damper with base excitation with 9 Hz

Validation of the mathematical model and determine the exactly values of all coefficients

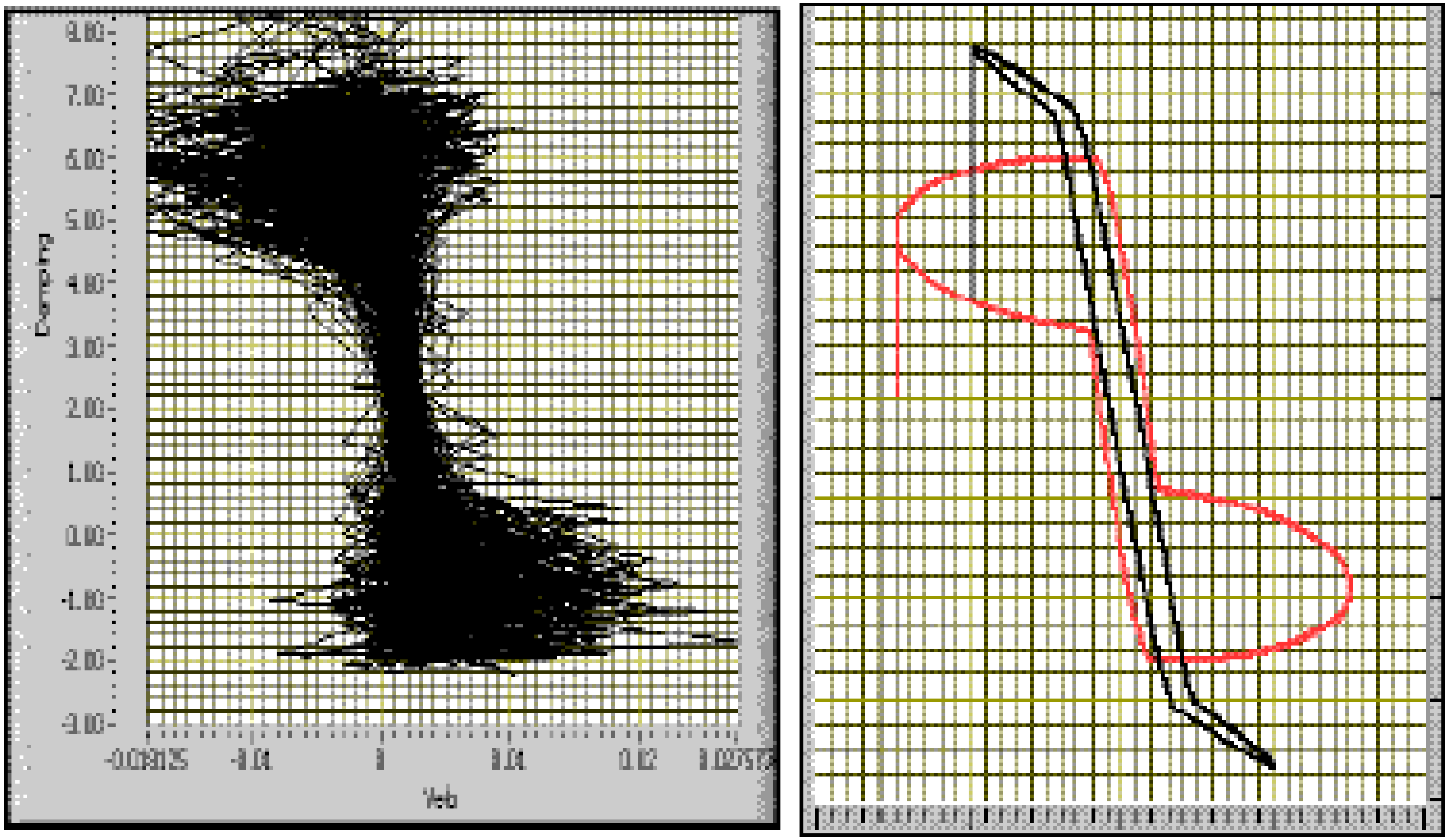

Comparative characteristics of the real with the simulate for the damper force vs. velocity when internsity of the current was i=0.8A

Validated mathematical model

$$f = c_0(x' - y') + k_0(0.003 - y) + 100(x - 0.002) + \alpha z$$

$$y' = \frac{1}{c_0 + c_1}[\alpha z + c_0 x' + k_0(0.003 - y)]$$

$$z' = -747|x' - y'|z|z|^{n-1} - 1047(x' - y')|z|^n + 40000(x' - y')$$

$$\alpha(i) = 0.9i^3 + 1.1i^2 + 0.9i + 0.9$$

$$c_0(i) = 60i^3 - 70i^2 + 19i + 7$$

$$c_1(i) = -i^3 + 300i^2 + 5i + 1000$$

$$k_0(i) = 200i^3 + 100i^2 + 100i + 300$$

$$\delta = 50\sin(10\pi + 0.21) + 1.1\sin(18\pi + 0.31) +$$

$$+ 1.4\sin(30\pi + 0.62)$$

All values of the coefficients were identified by compare the theoretical with experimental results by analyze of the coefficients influences to the parameters of the curves

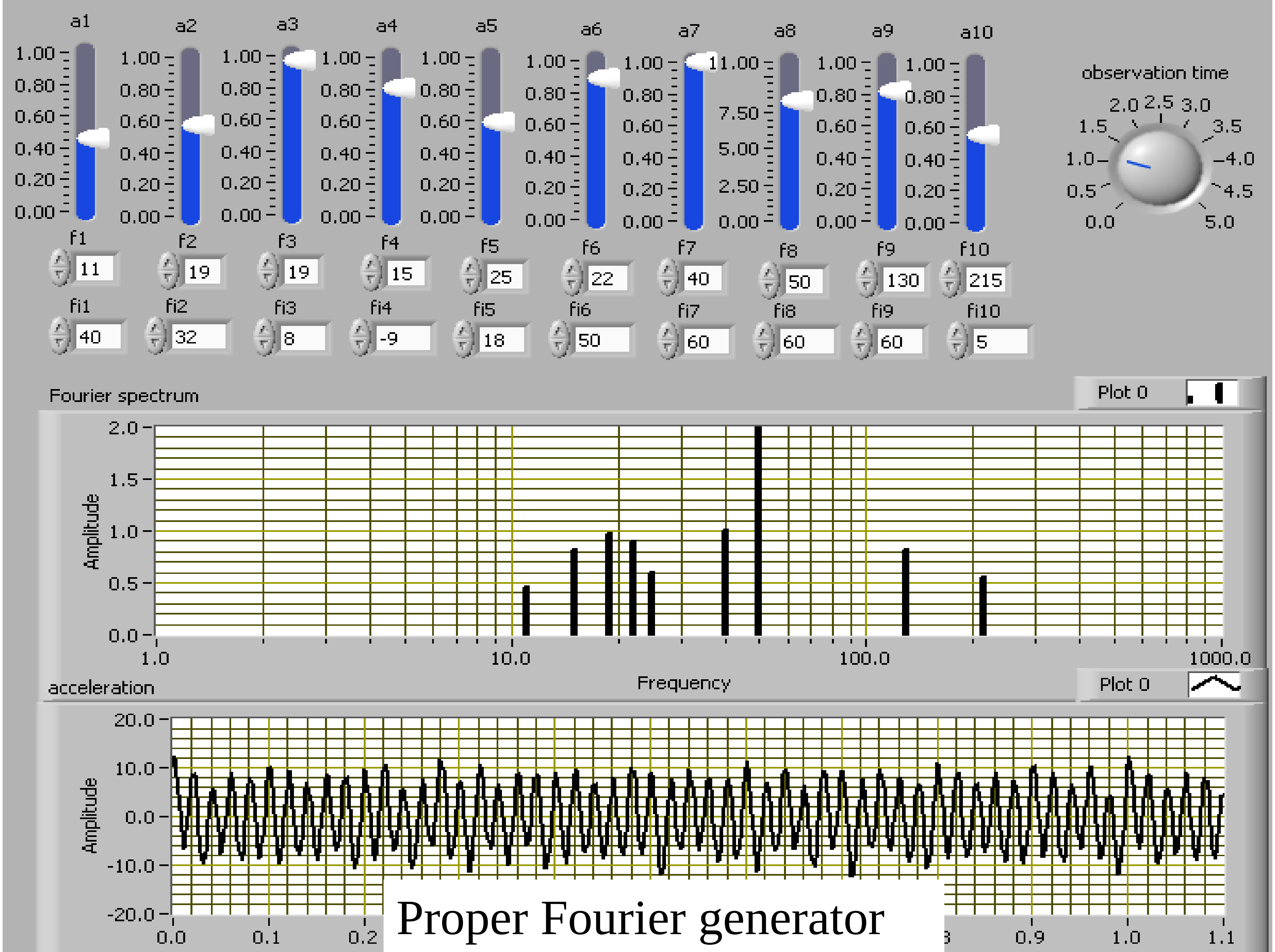

Proper Fourier generator

Intelligent damper schema

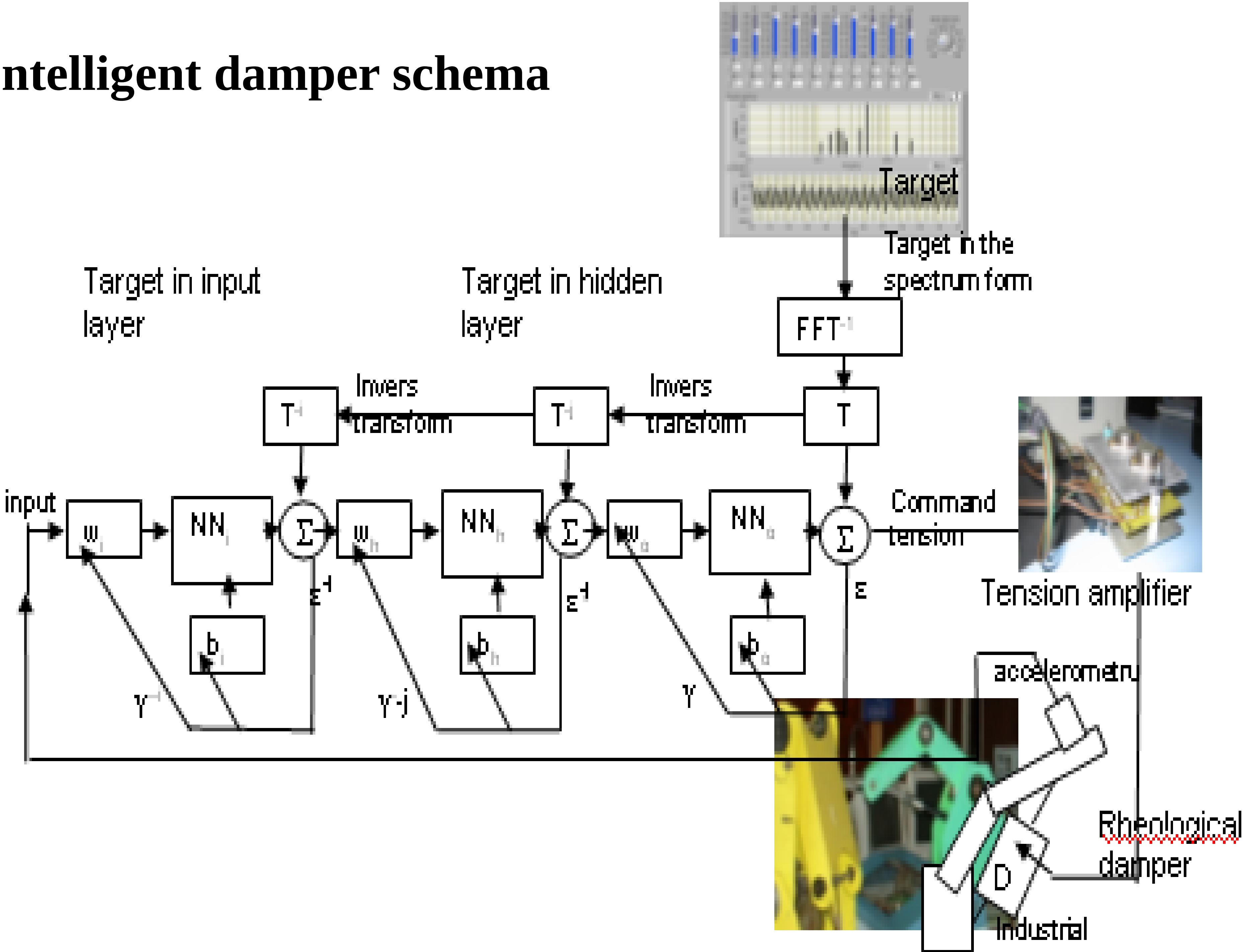

Fourier spectrum for one intelligent and for one conventional structure

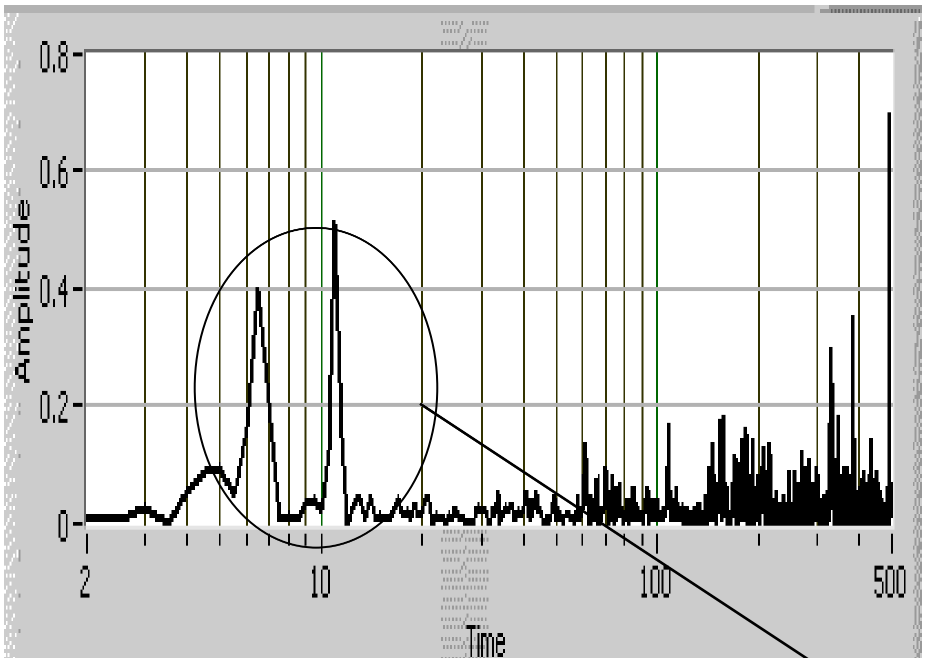

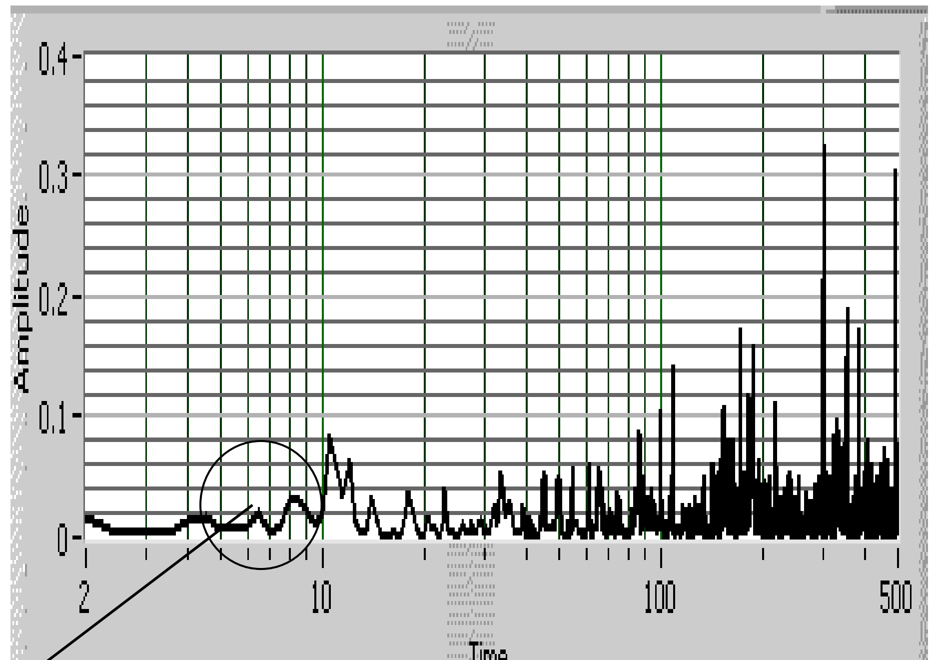

Atenuation of the magnitude at the slow frequencies by using the intelligent magnetorheological damper

conventional structure **intelligent structure**

Some results after application of the intelligent damper

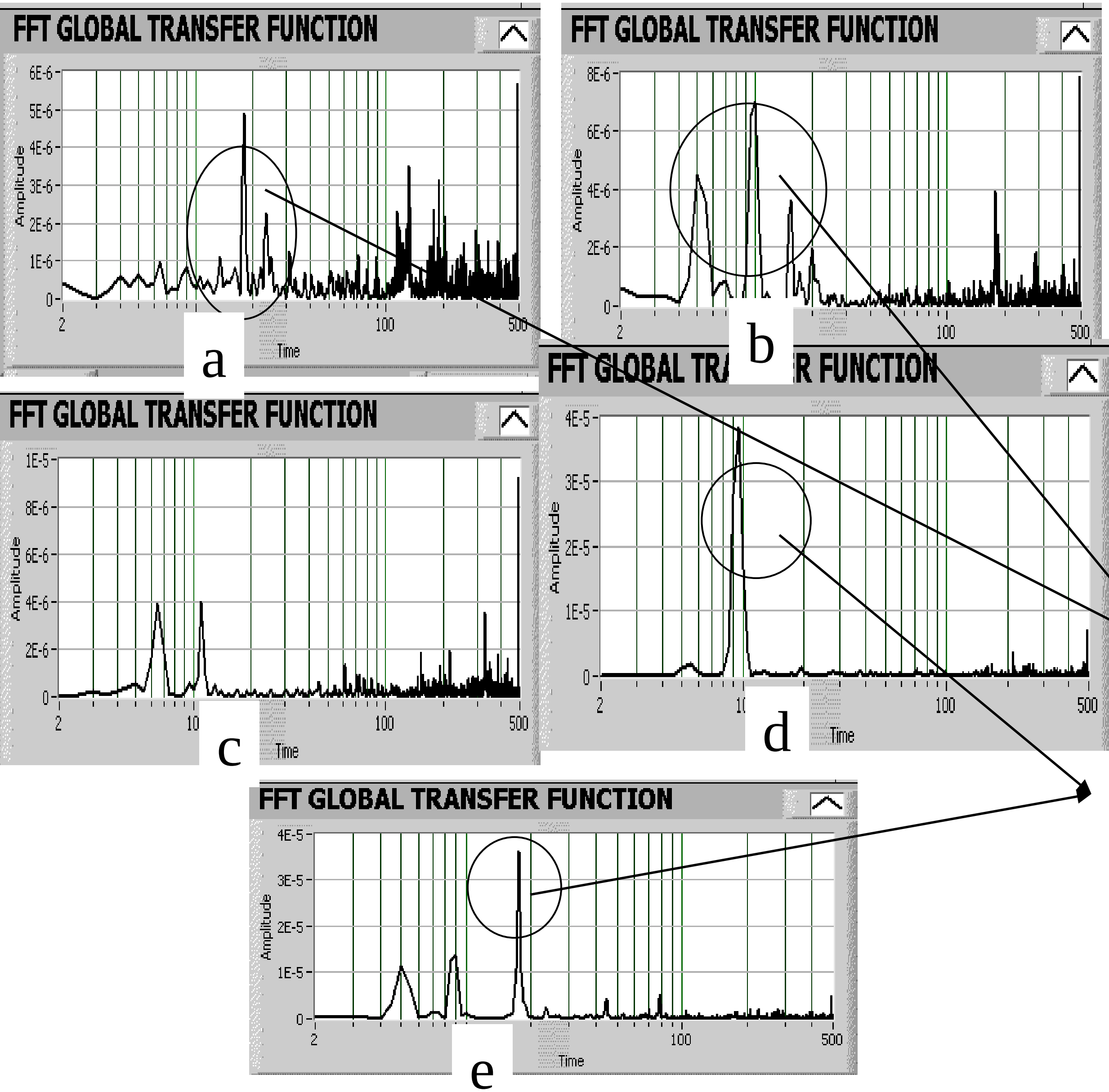

Fourier spectrum for the différents cases:

a- mouvement in up direction with MRD;

b- movement in up direction with air damper;

c-movement in up direction without damper;

d- movement in down direction without damper;

e- movement in down direction with MRD.

After comparative analyze between the using the MRD or without using the MRD. We can see one movements of the frequencies from the Fourier spectrum to the high frequencies and the decrease of the oscillation magnitude.

The research of the global dynamic damper behavior and the global dynamic compliance of the industrial robot with proper smart damper system

The GDC will be:

$$GDC = \frac{1}{k(j\omega)} = \frac{\int_0^T x(t) e^{-j\omega t} dt}{\int_0^T F_s(t) e^{-j\omega t} dt} = \frac{FFT(x)}{FFT(F)} = \frac{E_x(j\omega)}{E_F(j\omega)}$$

Magnitude of the GDC is calculated by:

$$\left| \frac{1}{k(\omega)} \right| = \sqrt{(\mathrm{Re}\{\frac{1}{k(j\omega)}\})^2 + (\mathrm{Im}\{\frac{1}{k(j\omega)}\})^2}$$

The VGDDC, *c* without magnetorheological damper for each resonance frequency can be calculated with:

$$c_i = 2\xi_i \frac{k_i(\omega)}{\nu_{n_i}}$$

The dynamic damper ratio (DDR) for each resonance frequencies ξ_i *can be obtain from Fourier vibration spectrum by:*

$$\xi_i = \frac{\nu_{i1} - \nu_{i2}}{2\nu_{iR}}$$

The viscose dynamic damper equivalent coefficient when was applied the magnetorheological damper c_{eq} we can obtain by:

$$c_{eq} = \frac{E}{\pi\omega x^2}$$

The dynamic damper energy (DDE) can be calculate with:

$$E = \int_0^{2\pi/\omega} F(t)x'(t)dt$$

where: *F(t)* is the damping variable force determined by experimental research, [N]; *x'(t)* - velocity of the response determined by derivation of the displacement characteristic, [m/s].

The VGDDEC after application of the MRD will be:

$$c_f = c + c_{eq}$$

SOME RESULTS OF THE ASSISTED RESEARCH WITH DATA AQUISITION

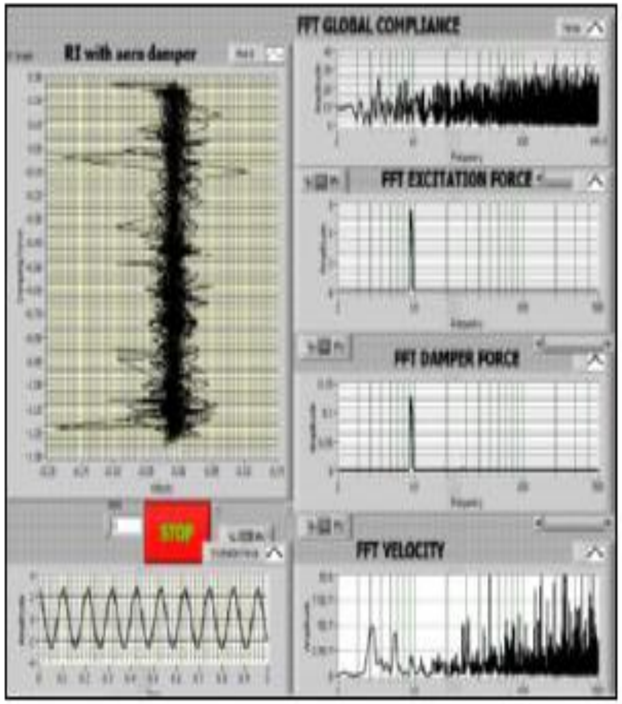

Fig.6. Without damper 5 Hz excitation frequency

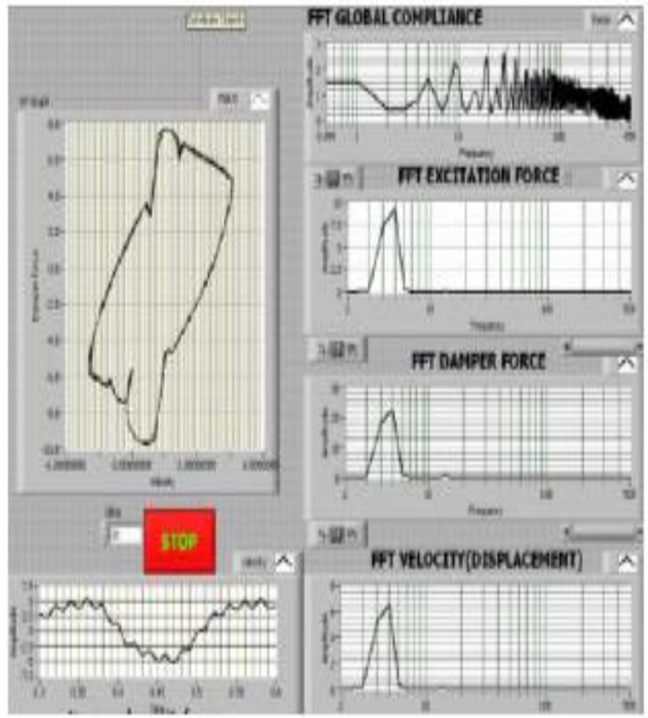

Fig.7. With aero damper 5 Hz excitation frequency

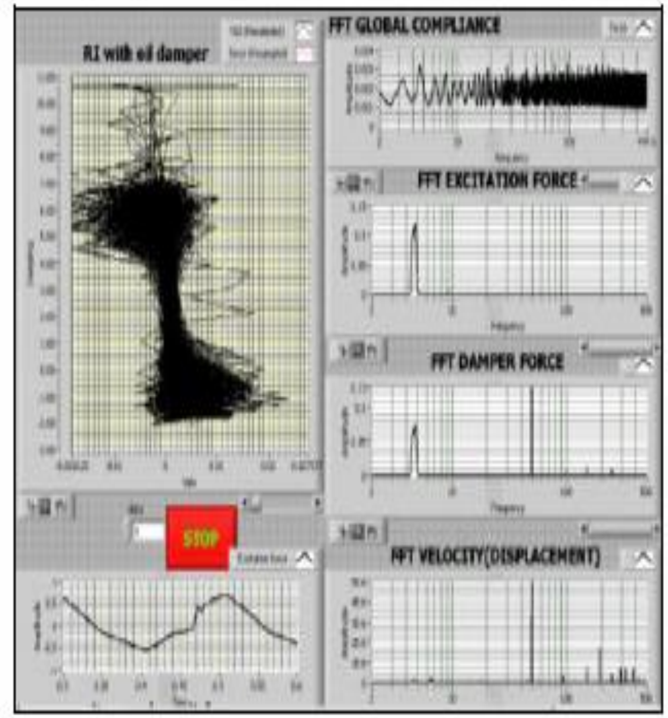

Fig.8. With MRD 5Hz excitation frequency

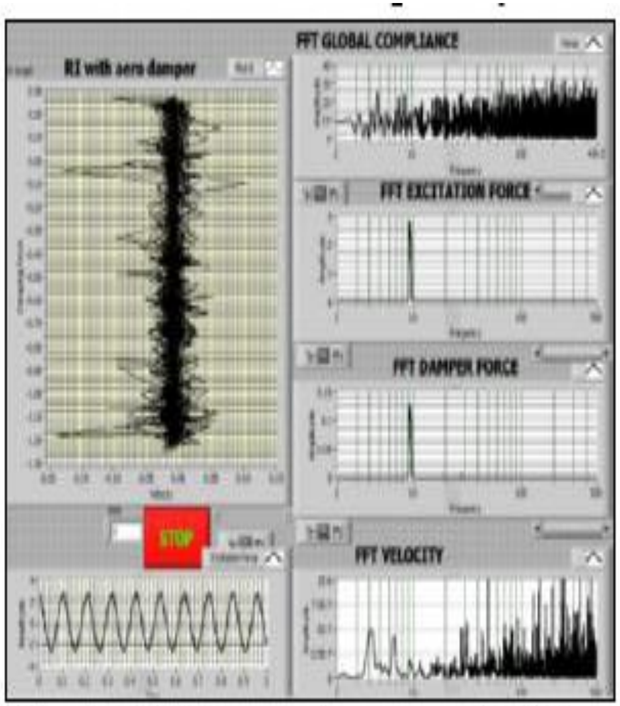

Fig.9. Without damper 12 Hz excitation frequency

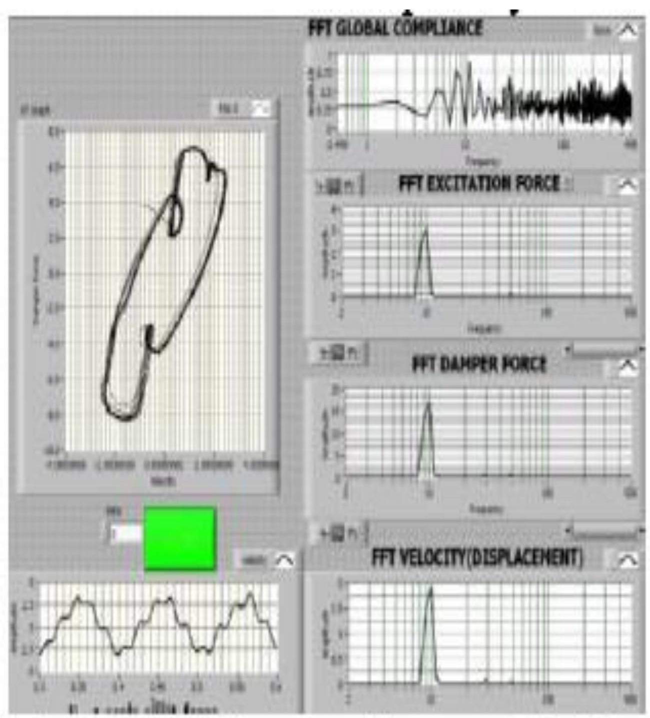

Fig.10.With aero damper12 Hz excitation frequency

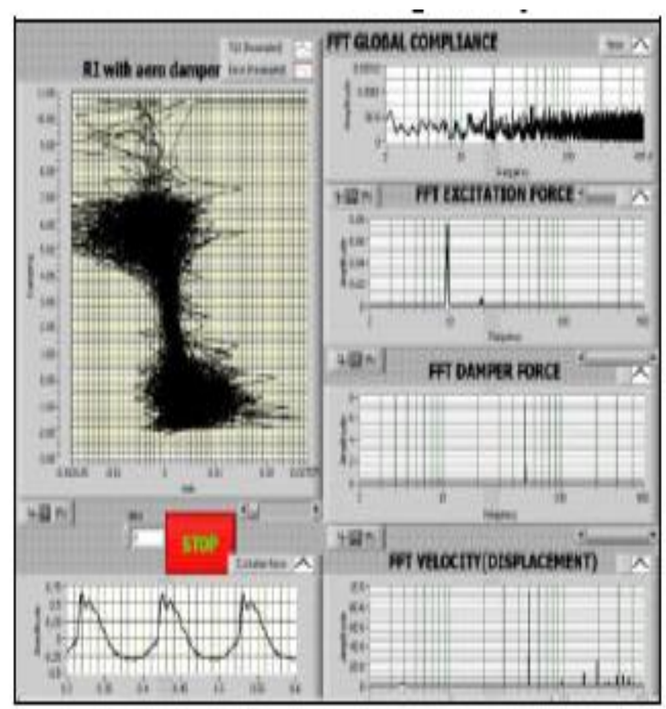

Fig.11. With MRD 12Hz excitation frequency

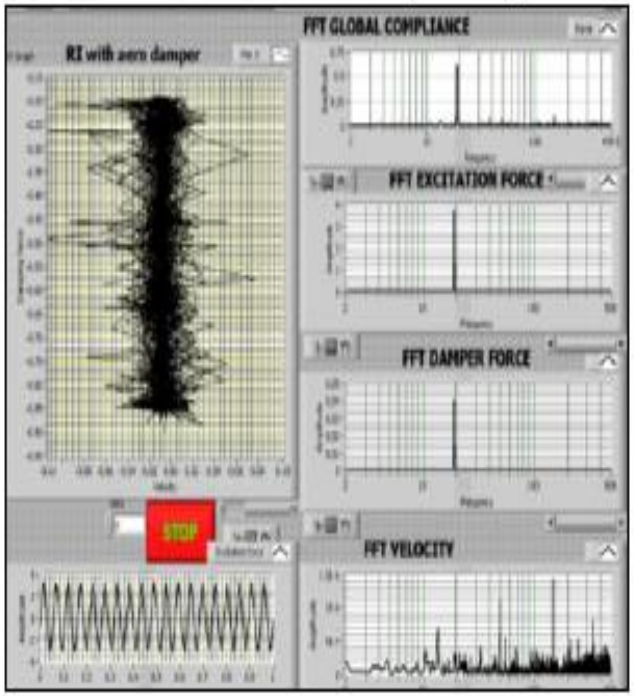

Fig.12. Without damper 25 Hz excitation frequency

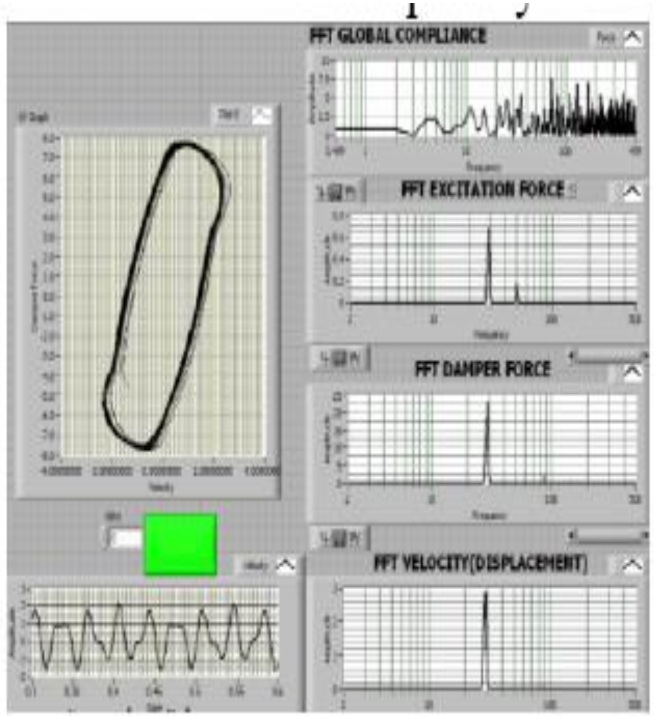

Fig.13.With aero damper25 Hz excitation frequency

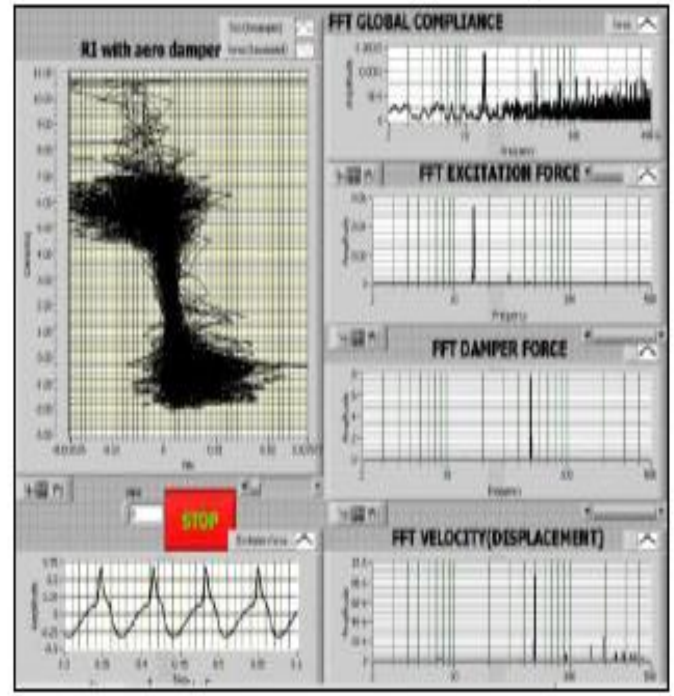

Fig.14. With MRD 25Hz excitation frequency

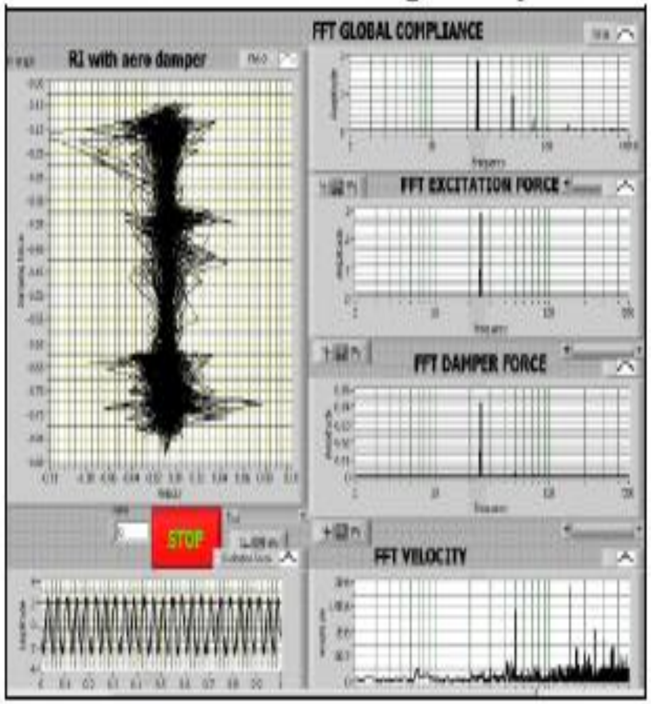

Fig.15. Without damper 38Hz excitation frequency

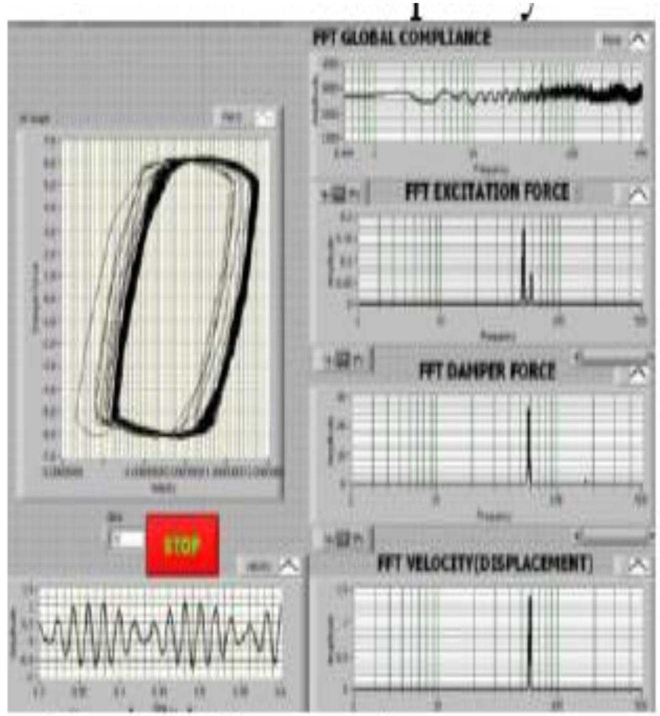

Fig.16.With aero damper 38Hz excitation frequency

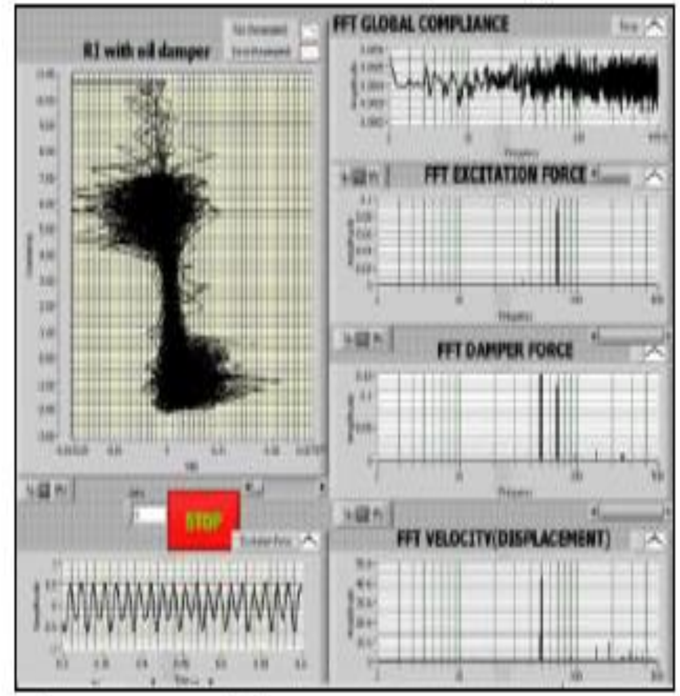

Fig.17. With MRD 38Hz excitation frequency

Experimental results

Table 1

Transmissibility and global dynamic compliance in movement with aero damper (acquisition with 5 simultaneously channels)

Frec Ex. [Hz]	Type Dmp.	Transmisibility	Global Dynamic Compliance	Damper force	Damper force vs. velocity
		[v] /[A]	[v] /[A]	[v] /[A]	$[F_{min-max}]$/ $[v_{min-max}]$
10	Aero damper	10/0.5 10^{-6}; 19/8 10^{-6}; 28/4 10^{-6}	4/20; 7/19; 8/19; 12/18; 14/18; 18/18; 19/18; 20/19; 21/19; 25/18; 28/19; 32/17	9/0.12; 18/0.01; 28/0.01	-1.3 la 0.2/ -0.05 la 0.05 (1.5/0.1) **15**
20	-''-	20/1.5 10^{-5}; 190/3 10^{-6}; 210/1 10^{-6}	20/0.6; 28/0.14; 40/0.14; 150/0.15	20/0.04	-0.9 la -0.2/ -0.04 la 0.04 (0.7/0.08) **8.75**
25	-''-	25/9 10^{-6}; 75/4 10^{-6}; 130/0.5 10^{-6}; 180/5 10^{-6}; 220/1.5 10^{-6}; 420/0.5 10^{-6}	25/1.8; 50/1; 75/0.4; 100/0.2; 150/0.2; 250/0.1	25/0.04; 50/0.002; 75/0.001	-0.8 la -0.1/ -0.04 la 0.02 (0.7/0.06) **11.66**
30	-''-	30/1 10^{-6}; 88/7 10^{-6}; 120/1.4 10^{-6}; 180/3.8 10^{-6}; 200/9 10^{-6}; 220/1.2 10^{-6}	21/0.1; 30/1; 50/0.4; 80/0.1; 88/0.25; 120/0.1; 150/0.3; 250/0.1	30/0.07; 88/0.005	-1 la -0.15/ -0.06 la 0.04 (0.85/0.1) **8.5**
35	-''-		35/4.2; 50/0.5; 70/2; 80/0.1; 100/2; 140/1; 150/0.5; 180/0.5; 250/0.5	35/0.05; 70/0.025; 100/0.05	-0.9 la -0.05/ -0.05 la 0.03 (0.85/0.08) **10.625**
50	-''-	50/1.2 10^{-5}; 150/0.00025 10^{-6}; 200/5 10^{-6}; 250/0.002 10^{-6}	4/120; 7/150; 12/120; 15/120; 18/110; 22/140; 26/130; 30/100; 32/110; 34/110; 40/180; 45/120; 50/120; 52/120; 55/150; 60/140; 63/110; 70/150; 80/90; 85/110; 90/180; 95/110; 100/160; 110/160; 120/150; 130/90; 140/150; 150/150; 200/150	50/0.08;	-1 la 0/ -0.05 la 0.04 (1/0.09) **11.11**
60	-''-	60/0.8 10^{-6}; 180/3.8 10^{-6}	4/0.02; 50/0.05; 60/0.18; 150/0.05; 170/0.04; 230/0.03; 250/0.05; 400/0.05	60/0.014	-0.8 la -0.25/ -0.04 la 0.04 (0.55/0.08) **6.875**

(continuation)

70	-‘’-	70/2.8 10^{-5}; 150/1 10^{-6}; 200/2.5 10^{-5}; 400/1 10^{-6}	25/0.02; 30/0.02; 32/0.03; 40/0.01; 50/0.15; 58/0.03; 68/0.02; 70/0.01; 150/0.08; 250/0.07; 350/0.07	70/0.0035	-0.66 la - 0.36/ -0.05 la 0.04 (0.3/0.09) **3.33**
80	-‘’-	40/0.2 10^{-6} ; 80/3.5 10^{-6}; 120/0.4 10^{-6}; 160/0.5 10^{-6}; 190/0.55 10^{-6}; 220/0.1 10^{-6}	4/0.01; 20/0.01; 32/0.01; 50/0.13; 90/0.01; 100/0.01; 120/0.04; 150/0.075; 220/0.06; 250/0.07; 280/0.02; 320/0.075; 350/0.025; 400/0.06	40/0.00025; 80/0.001; 120/0.00025	-0.62 la - 0.42/ -0.04 la 0.04 (0.2/0.08) **2.5**
90	-‘’-	90/5.5 10^{-6}; 180/0.8 10^{-6}; 220/0.2 10^{-6}	3/0.005; 5/0.005; 8/0.005; 11/0.005; 13/0.005; 15/0.005; 18/0.018; 30/0.01; 43/0.01; 50/0.05; 53/0.005; 80/0.008; 100/0.005; 160/0.04; 200/0.01; 220/0.01; 250/0.03; 280/0.015; 320/0.01; 400/0.03	45/0.0002; 90/5 10^{-5}; 100/2.5 10^{-5}; 120/2.5 10^{-5}; 180/2.5 10^{-5}; 200/1 10^{-5}; 300/1 10^{-5}	-0.58 la - 0.42/ -0.04 la 0.04 (0.16/0.08) **2**
100	-‘’-	100/5 10^{-7}; 120/1 10^{-7}; 200/2.3 10^{-6}; 300/1 10^{-7}; 400/1 10^{-7}; 450/2 10^{-7};	3/0.01; 50/0.12; 60/0.01; 70/0.01; 80/0.01; 90/0.01; 100/0.01; 110/0.01; 130/0.015; 200/0.02; 250/0.05; 270/0.02; 300/0.03; 320/0.01; 350/0.05; 400/0.03; 450/0.04	12/1.25 10^{-5}; 15/2.5 10^{-5}; 50/2 10^{-5}; 100/8 10^{-5} ; 110/2 10^{-5}; 150/1 10^{-5}; 200/1 10^{-5}; 300/1.8 10^{-5}; 400/1 10^{-5};	-0.62 la - 0.38/ -0.05 la 0.04 (0.24/0.09) **2.66**
150	-‘’-	72/0.8 10^{-7}; 95/0.8 10^{-7}; 150/2.2 10^{-7}; 170/0.2 10^{-7}; 180/1.5 10^{-7}; 220/0.5 10^{-7}; 250/0.2 10^{-7}; 270/0.6 10^{-7}; 300/0.5 10^{-7}; 420/5.8 10^{-7};	4/0.01; 5.5/0.01; 15/0.015; 18/0.012; 28/0.01; 30/0.015; 38/0.008; 50/0.05; 100/0.01; 120/0.012; 130/0.015; 150/0.04; 170/0.01; 180/0.01; 190/0.01; 230/0.015; 250/0.03; 260/0.015; 300/0.015; 350/0.025; 360/0.018; 400/0.01; 420/0.045;	4.8/0.5 10^{-5}; 5.5/0.8 10^{-5}; 13/0.2 10^{-5}; 72/1.3 10^{-5}; 98/0.5 10^{-5}; 100/1.8 10^{-5}; 150/2.5 10^{-5}; 160/0.6 10^{-5}; 200/0.6 10^{-5} 250/0.1 10^{-5}; 300/1.8 10^{-5}; 370/0.1 10^{-5}; 400/0.5 10^{-5};	-0.56 la - 0.46/ -0.05 la 0.03 (0.1/0.08) **1.25**
200	-‘’-	190/6 10^{-6}	50/0.06; 150/0.04; 230/0.01; 250/0.03; 270/0.025; 330/0.018; 350/0.02; 420/0.018; 450/0.03;	12/0.00025; 100/0.00001; 300/0.00001;	-0.57 la - 0.45/-0.05 la 0.04 (0.12/0.09) **1.33**
300	-‘’-	4/5 10^{-8}; 100/3 10^{-8}; 180/4 10^{-8}; 190/2 10^{-8}; 200/2 10^{-8}; 270/3.5 10^{-8}; 290/4 10^{-8}; 300/2 10^{-8}; 370/2 10^{-8}; 400/3 10^{-8}; 450/1.7 10^{-7}	50/0.15; 150/0.1; 220/0.02; 250/0.1; 320/0.02; 350/0.08; 450/0.08;	15/8 10^{-5}; 100/2 10^{-5}; 150/1 10^{-5}; 200/1 10^{-5}; 300/1.8 10^{-5}; 400/0.5 10^{-5};	-0.56 la -0.46/ -0.05 la 0.04 (0.1/0.09) **1.11**
400	-‘’-	45/4 10^{-8}; 100/3 10^{-8}; 180/3.5 10^{-8}; 300/4 10^{-8}; 350/2 10^{-8};	3/0.04; 50/0.2; 130/0.05; 150/0.15; 220/0.02; 250/0.05;	6/5 10^{-6}; 13/1.5 10^{-6};	-0.55 la - 0.47/

Table 2

Transmissibility between base and end effector
With base excitation with/ without damper

Type of the damper	Excitation frequency [Hz]	Transmissibility		Type of damper	Transmissibility	
		Spectrum frequency [Hz]	Spectrum magnitude [-]		Spectrum frequency [Hz]	Spectrum magnitude [-]
MRD	10	10	$3.5\ 10^{-6}$	without MRD	10	$5.5\ 10^{-6}$
		20	$2.8\ 10^{-6}$		20	$4.5\ 10^{-6}$
		30	$0.2\ 10^{-6}$		30	$0.3\ 10^{-6}$
		50	$0.15\ 10^{-6}$		50	$0.2\ 10^{-6}$
		130	$0.15\ 10^{-6}$		130	$0.2\ 10^{-6}$
		220	$0.8\ 10^{-6}$		220	$0.8\ 10^{-6}$
		320	$0.9\ 10^{-6}$		320	$0.9\ 10^{-6}$
		420	$0.8\ 10^{-6}$		420	$0.8\ 10^{-6}$
MRD	14	14	$3.8\ 10^{-6}$	Aero damper	6.5	$1.1\ 10^{-6}$
		20	$6.5\ 10^{-6}$		15	$0.25\ 10^{-6}$
		180	$0.5\ 10^{-6}$		20	$1.5\ 10^{-6}$
					26	$0.18\ 10^{-6}$
					50	$0.18\ 10^{-6}$

Table 3

Global Dynamic Compliance with/without damper

Excitation frequency [Hz]	Type of damper	Global Dynamic Compliance		Type of damper	Global Dynamic Compliance	
		Spectrum frequency [Hz]	Spectrum Magnitude [m/N]		Spectrum frequency [Hz]	Spectrum magnitude [m/N]
10	MRD	10	0.6	Without damper	5	1
		20	0.2		11	0.75
		30	0.32		15	0.25
		40	0.52		18	0.37
		60	0.4		25	1.25
		70	0.08		30	0.6
		80	0.3		40	0.55
		90	0.32		45	1.25
		110	0.33		55	0.85
		130	0.28		60	0.5
		140	0.18		62	0.5
		150	0.15		72	1.4
		160	0.22		80	0.4
		180	0.25		90	1.25
		200	0.2		100	0.6
		220	0.28		110	0.35

Conclusion of the experimental results

- GDC, in a function of the IR with MRD is reduced and transfered in to the high frequencies with 6-8 Hz;

- Transmisibility is reduced with more than 35% at the frecquencies between 10-100Hz in the cases with MRD, in comparation with the cases without MRD, and with 20% in comparation with air damper;

- By using MRD, in comparation with the case of the mouvement with air damper or without damper we observe the transfere of the three frequencies from the Fourier spectrum to the high frequencies, respectively 1,6,11 Hz for the cases of the mouvement in up direction without damper, 5,10,16 Hz in up mouvement with air damper, 15, 18, 24 Hz in mouvement in up with MRD, 1,5,9 Hz in down mouvement without damper and 5,9,18Hz in down direction with MRD;

- At the desecquilibrium of the arm, the Fourier spectrum is different in up and down mouvement, the weight force action like one damper. In this case for one up and down mouvement, for the same damper case, frecquencies of the up mouvement in comparation with down mouvement are more, respectively 1,6,11 Hz in comparation with 1,5,9 Hz in mouvement without damper and respectively 15,18,24 Hz in comparation with 5,9,18 Hz in mouvement with MRD;

- Transmisibility is bigger in slow frecquency, frecquncies comparable with rezonance frequency of the structure 14 Hz, at the excitation of 10,20Hz, vezi table 1 and 2;

- Transmisibility between the base and end-effector, at one excitation on the base 10 Hz with MRD is reduced in coomparation with the case without damper, respectively 3.5 10-6 in comparation with 5.5 10-6 at the first frequency from the spectrum 10 Hz and 2.8 10-6 in coomparation with 4.5 10-6 at the frequency 20 Hz, see the table;

- Transmisibility is aproximately the same at the high excitation frequency more that 35 Hz (frequency work domain of the didactical robot);

  10.62 at 35 Hz; 8.75 at 20 Hz; 8.5 at 30 Hz;

- Global dynamic compliance is bigger in the slow frequency excitation domain, exemple 20mm/N at the frecquency 4 Hz from the spectrum, in comparation with 0.2 at one frequency 20 Hz, at one excitation 20 Hz, see the table 1;

- Global dynamic compliance is maximal at one excitation 10 Hz, that mince the structure of the robot have near this value his mechanical rezonance frequency, 14 Hz;

- From the variation raport of the damper force vs. velocity we can determine the damper energy; this energy coefficient calculated by the formule is maximum at 10 Hz- 15; this is at the values: 11.66 at 25 Hz; 11.11 at 50 Hz;

- By using the complex control with proper neural network, the kinematics, dynamics and Fourier spectrum;

Optimization of the space trajectory by using the neural network and the complex controlling of the kinematics, dynamics and Fourier spectrum

Prof.univ.Ph.D.Eng.Adrian OLARU
senior member of IACSIT (Singapore)
International
Association of Computer Sciences and Information Technology
University Politehnica of Bucharest, ROMANIA

Complex mathematical model

$$(r)_i^0 = (r)_{i-1}^0 + [D]_{i-1}^0 (r)_i^{i-1} \qquad (1)$$

$$[D]_{i-1}^0 = [D]_1^0 [D]_2^1 \ldots [D]_{i-1}^{i-2}$$

$$(r)_1^0 = \begin{pmatrix} 0 \\ 0 \\ l_1 \end{pmatrix}; (r)_2^0 = \begin{pmatrix} 0 \\ 0 \\ l_1 + l_2 \end{pmatrix}; (r)_3^0 = \begin{pmatrix} c_1 s_2 l_3 \\ s_1 s_2 l_3 \\ l_1 + l_2 + c_2 l_3 \end{pmatrix};$$

$$(r)_4^0 = \begin{pmatrix} c_1 s_2 l_3 + (c_1 c_2 s_3 + c_1 s_2 c_3) l_4 \\ s_1 s_2 l_3 + (s_1 c_2 s_3 + s_1 s_2 c_3) l_4 \\ l_1 + l_2 + c_2 l_3 + (-s_2 s_3 + c_2 c_3) l_4 \end{pmatrix}$$

$$\begin{pmatrix} F \\ M \end{pmatrix} = \begin{bmatrix} z_u & 0 \\ 0 & z_u \end{bmatrix} \begin{pmatrix} D_{0,i}(F_R^i + f(i)) \\ D_{0,i} M_R^i \end{pmatrix} - diag \begin{bmatrix} sign \frac{v_u^i}{|v_u^i|} m_{u_i} & sign \frac{\omega_u^i}{|\omega_u^i|} J_{g_i} \end{bmatrix} \cdot \begin{pmatrix} (a_{i,0}^i) + [\tilde{\omega}_{i,0}^i]^2 (r_{g_i}^i) \\ (\varepsilon_{i,i-1}^i) + [\omega_{i-1,0}^i](\omega_{i,i-1}^i) \end{pmatrix}$$

$$+ \begin{bmatrix} z_u & 0 \\ 0 & z_u \end{bmatrix} \cdot \begin{pmatrix} (0) \\ [G_{i,k}](\tilde{b}_{i,k}) \left((D_{0,i}(F_R^i + f(i))) - diag \begin{bmatrix} sign \frac{v_u^i}{|v_u^i|} m_{u_i} \end{bmatrix} \cdot [D_{0i}]((a_{i,0}^i) + [\tilde{\omega}_{i,0}^i]^2 (r_{g_i}^i)) \right) \end{pmatrix},$$

$$f(i) = c_0(x' - y') + k_0(0.003 - y) + 100(x - 0.002) + \alpha z$$

$$y' = \frac{1}{c_0 + c_1} [\alpha z + c_0 x' + k_0 (0.003 - y)]$$

$$z' = -747|x' - y'||z|z|^{n-1} - 1047(x' - y')|z|^n + 40000(x' - y')$$

$$\alpha(i) = 0.9 i^3 + 1.1 i^2 + 0.9 i + 0.9$$

$$c_0(i) = 60 i^3 - 70 i^2 + 19 i + 7$$

$$c_1(i) = -i^3 + 300 i^2 + 5 i + 1000$$

$$k_0(i) = 200 i^3 + 100 i^2 + 100 i + 300$$

$$\delta = 50 \sin(10\pi + 0.21) + 1.1 \sin(18\pi + 0.31) +$$

$$+ 1.4 \sin(30\pi + 0.62)$$

$$n_1 = [\underbrace{w^1}_{p_1} + \underbrace{tcg_1}_{p_2} \cdot \varepsilon_1](p - a_2(t - p_3 + 1)) + (b_1 + \varepsilon_1)$$

$$a_1 = \frac{p_4 (1 - e^{-n_1})}{1 + e^{-n_1}}$$

$$\varepsilon_1 = t_1 - a_1$$

$$n_2 = [w^2 + \underbrace{tcg_2}_{p5} \cdot \varepsilon_2](a_1 (t - p_6 + 1)) + (b_2 + \varepsilon_2)$$

$$a_2 = \frac{p_7(1 - e^{-n_2})}{1 + e^{-n_2}}$$

$$\varepsilon_2 = t_2 - a_2$$

$$q_i = p_8(a_2 - \varepsilon_f)$$

$$\varepsilon_{pos} = t_3 - r_i$$

$$n_3 = [w^3 + \underbrace{tcg_2}_{p_5} \cdot \varepsilon_{pos}](q_i) + (b_3 + \varepsilon_{pos})$$

$$a_3 = \frac{p_9(1 - e^{-n_3})}{1 + e^{-n_3}}$$

$$\varepsilon_f = t_2 - a_3$$

$$(U_m) = \frac{L_a}{K_m} \cdot (M) + (\frac{R_a}{K_m} \cdot [J_{red}] + L_a \cdot \frac{b}{K_m})\frac{d}{dt}(\omega_m) + (R_a \cdot \frac{b_m}{K_m} + K_e) \cdot (\omega_m)$$

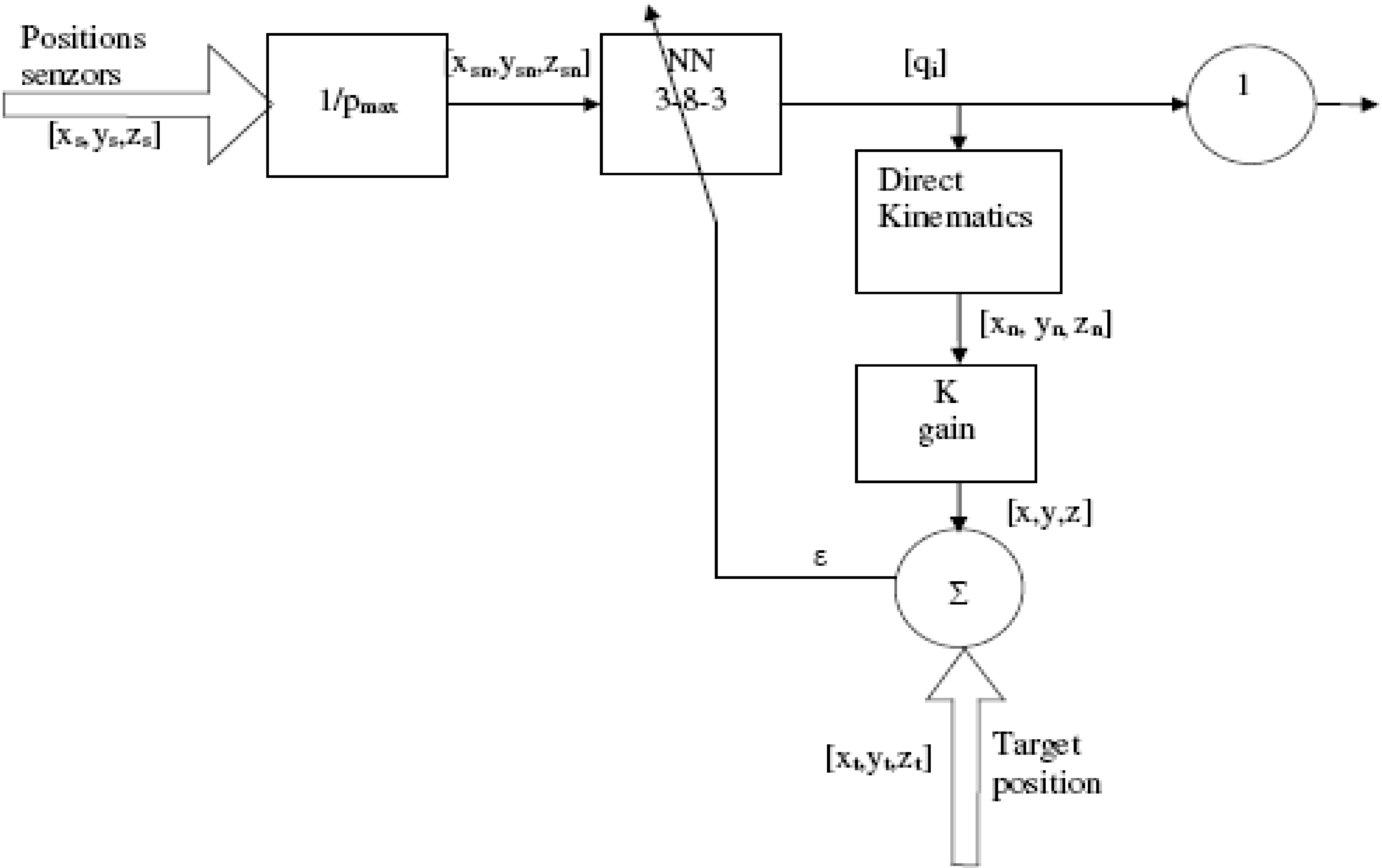

Positions
senzors
$[x_s, y_s, z_s]$
$1/p_{max}$
$[x_{sn}, y_{sn}, z_{sn}]$
NN
3-8-3
$[q_i]$
1
Direct
Kinematics
$[x_n, y_n, z_n]$
K
gain
$[x, y, z]$
ε
Σ
$[x_t, y_t, z_t]$
Target
position

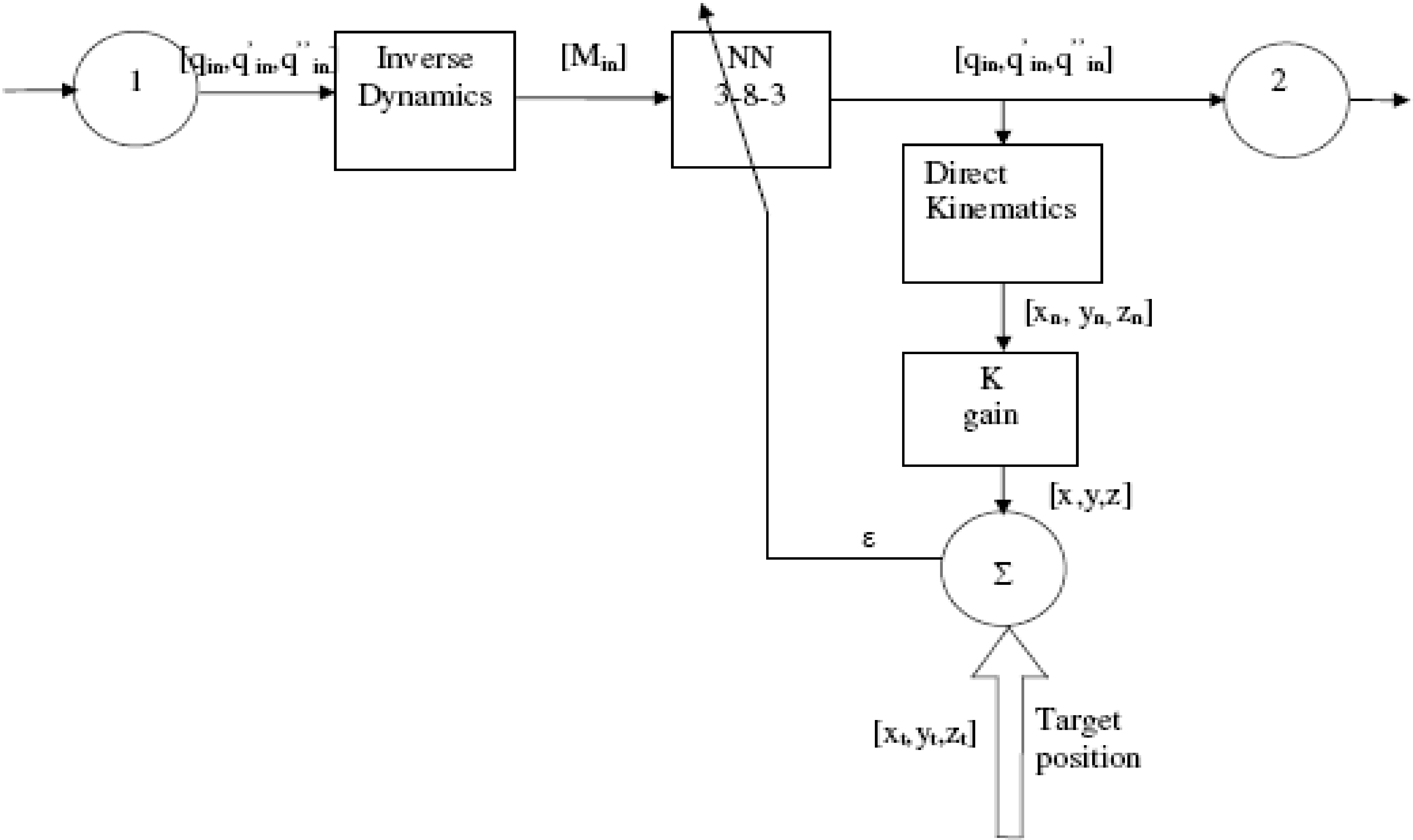
1
[q_in, q'_in, q''_in]
Inverse Dynamics
[M_in]
NN 3-8-3
[q_in, q'_in, q''_in]
2
Direct Kinematics
[x_n, y_n, z_n]
K gain
[x,y,z]
ε
Σ
[x_t, y_t, z_t]
Target position

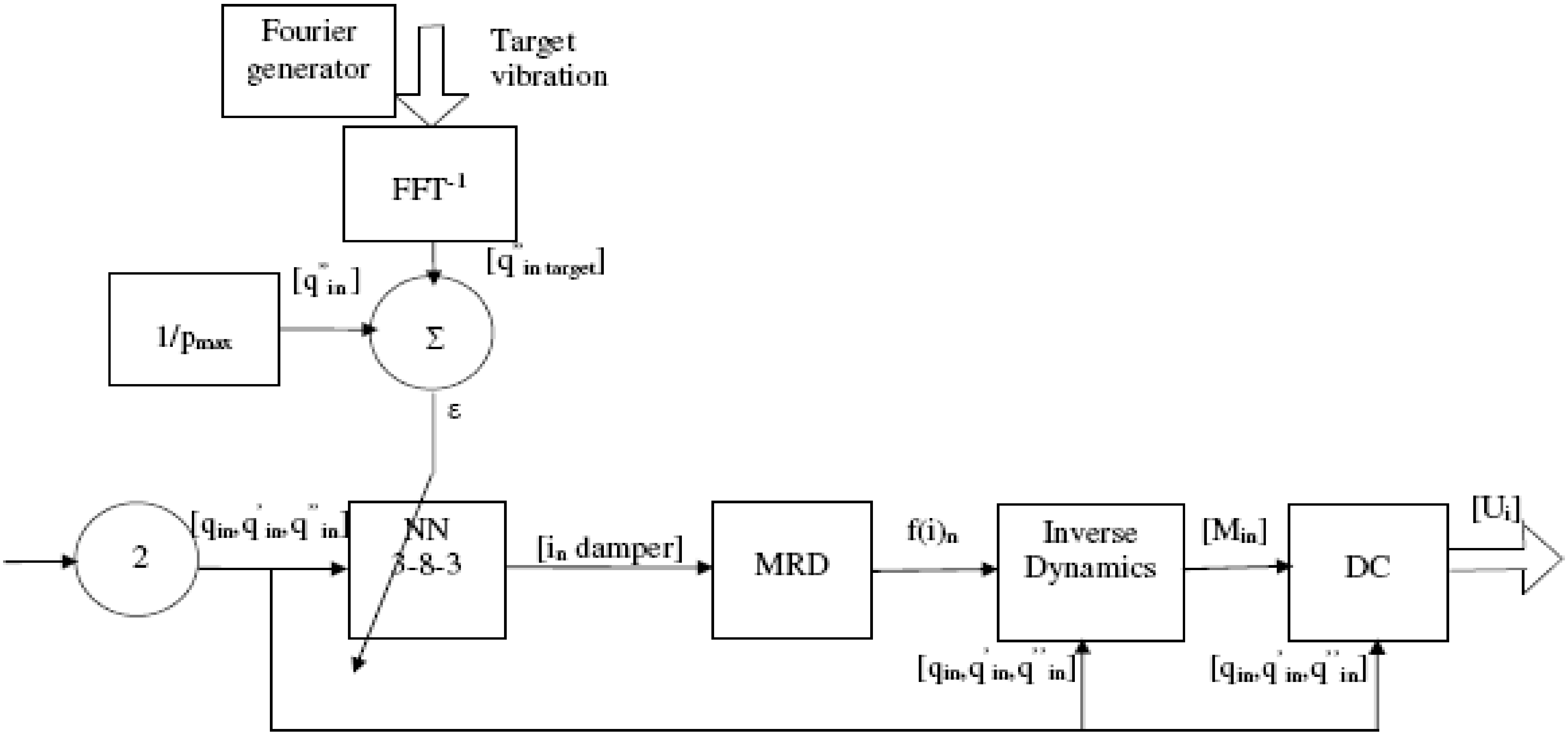

Fourier generator
Target vibration
FFT-1
[q'' in target]
[q'' in]
1/pmax
Σ
ε
2
[qin,q' in,q'' in]
NN
3-8-3
[in damper]
MRD
f(i)n
Inverse Dynamics
[Min]
DC
[Ui]
[qin,q' in,q'' in]
[qin,q' in,q'' in]

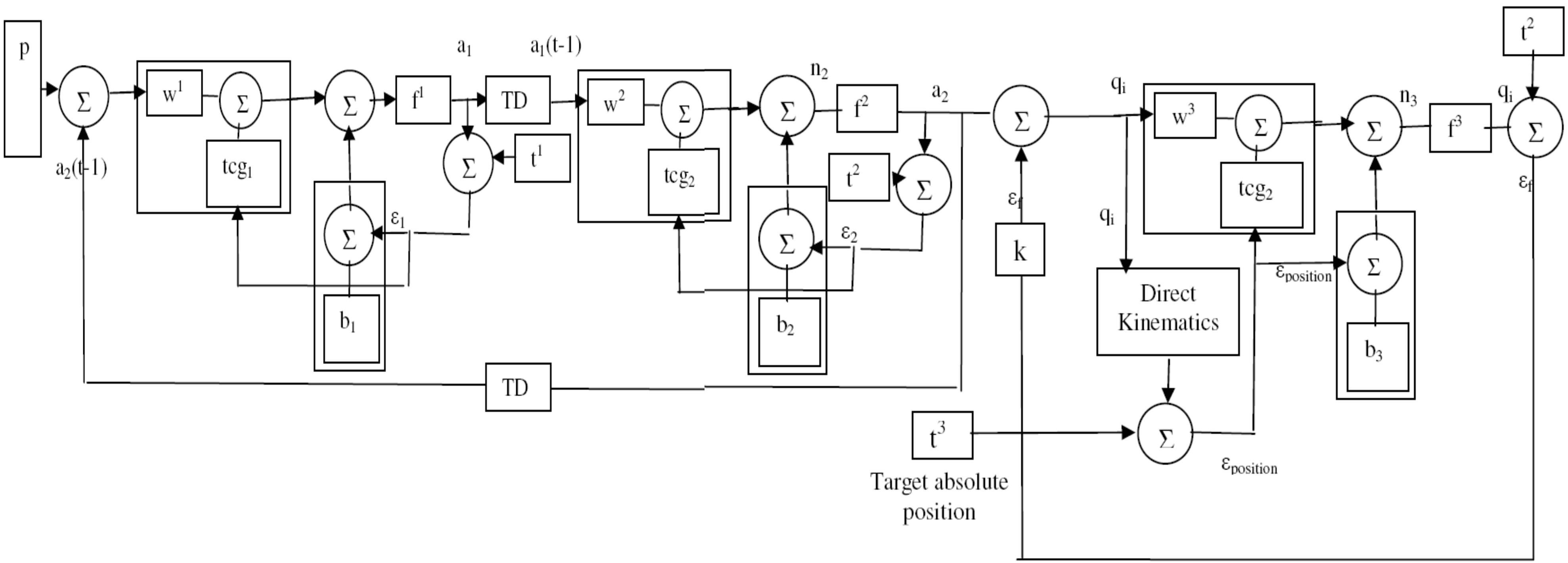
p
Σ
$a_2(t-1)$
w^1
Σ
tcg_1
Σ
Σ
b_1
f^1
a_1
$a_1(t-1)$
TD
Σ
t^1
ε_1
w^2
Σ
tcg_2
n_2
Σ
Σ
b_2
f^2
a_2
t^2
Σ
ε_2
TD
Σ
ε_f
k
q_i
q_i
w^3
Σ
tcg_2
Direct Kinematics
Σ
$\varepsilon_{position}$
t^3
Target absolute position
$\varepsilon_{position}$
n_3
Σ
Σ
b_3
f^3
q_i
t^2
Σ
ε_f

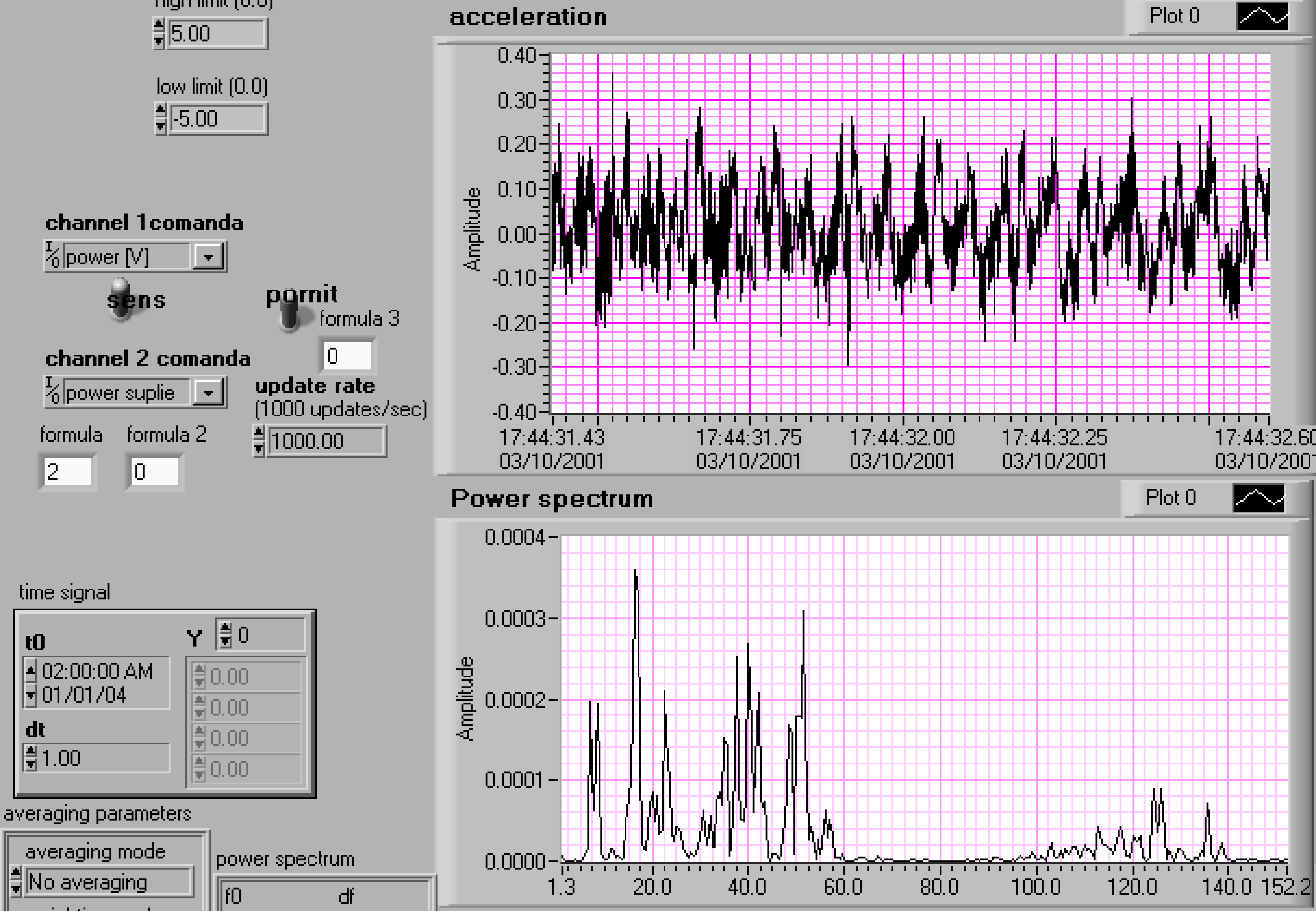
high limit (0.0)
5.00
low limit (0.0)
-5.00
channel 1comanda
power [V]
sens
pornit
formula 3
0
channel 2 comanda
power suplie
update rate
(1000 updates/sec)
1000.00
formula
formula 2
2
0
time signal
t0
02:00:00 AM
01/01/04
dt
1.00
Y
0
0.00
0.00
0.00
0.00
averaging parameters
averaging mode
No averaging
power spectrum
f0
df
acceleration
Plot 0
Amplitude
0.40
0.30
0.20
0.10
0.00
-0.10
-0.20
-0.30
-0.40
17:44:31.43 03/10/2001
17:44:31.75 03/10/2001
17:44:32.00 03/10/2001
17:44:32.25 03/10/2001
17:44:32.60 03/10/2001
Power spectrum
Plot 0
Amplitude
0.0004
0.0003
0.0002
0.0001
0.0000
1.3
20.0
40.0
60.0
80.0
100.0
120.0
140.0
152.2

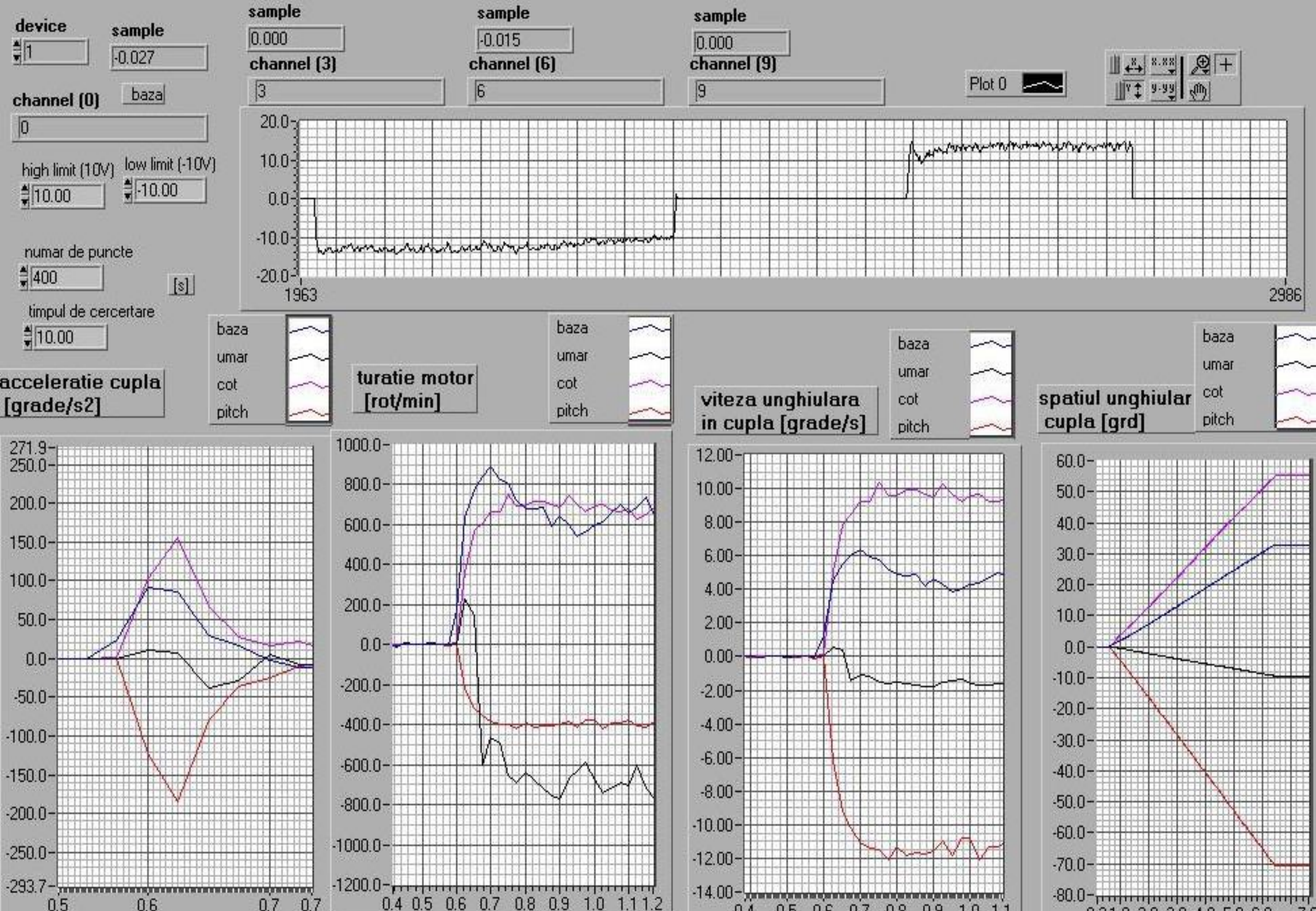
device
1
sample
-0.027
channel (0)
baza
0
high limit (10V)
10.00
low limit (-10V)
-10.00
numar de puncte
400
[s]
timpul de cercertare
10.00
sample
0.000
channel (3)
3
sample
-0.015
channel (6)
6
sample
0.000
channel (9)
9
Plot 0
1963
2986
baza
umar
cot
pitch
acceleratie cupla [grade/s2]
turatie motor [rot/min]
viteza unghiulara in cupla [grade/s]
spatiul unghiular cupla [grd]

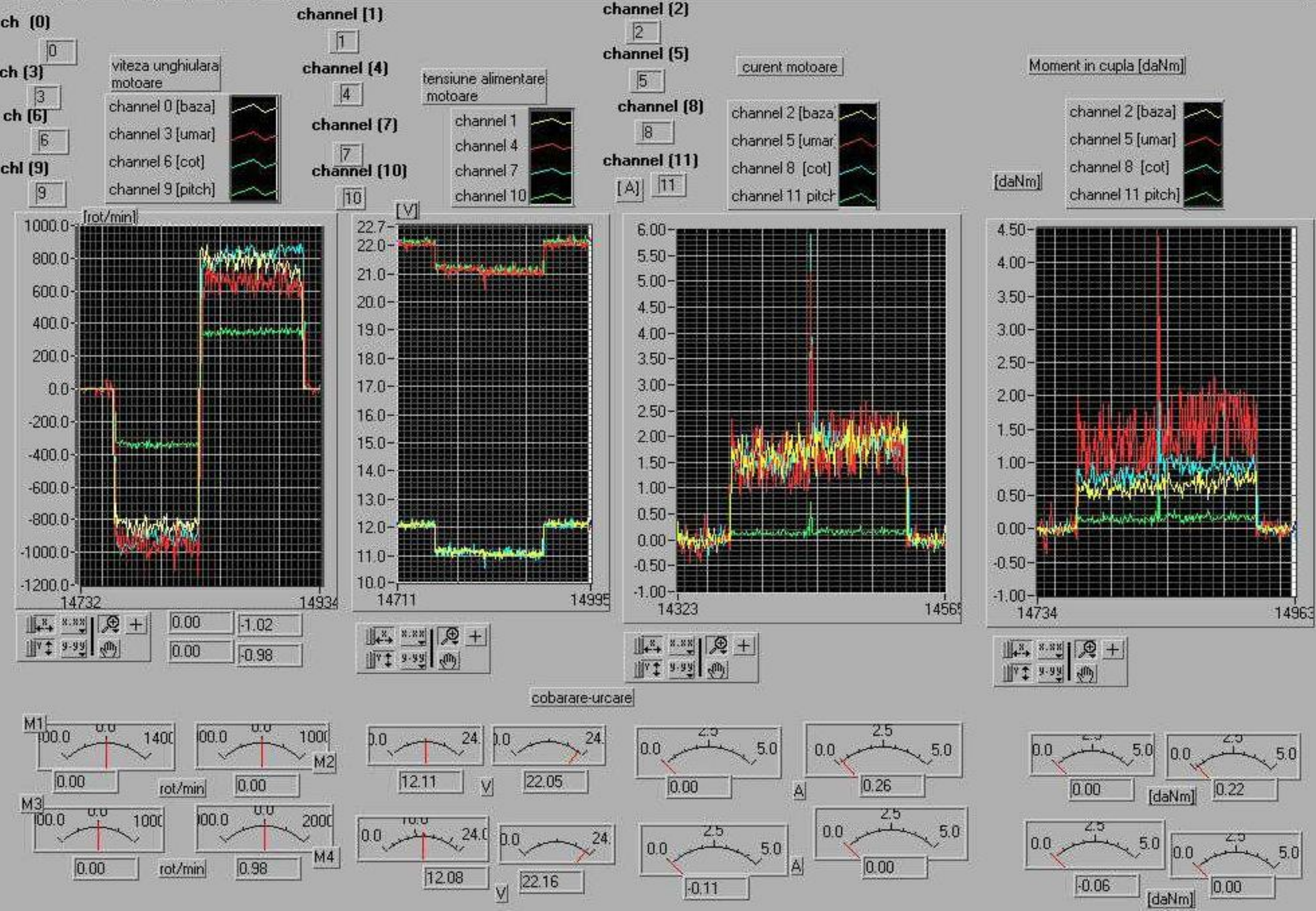

ch (0)
ch (3)
ch (6)
chl (9)
viteza unghiulara motoare
channel 0 [baza]
channel 3 [umar]
channel 6 [cot]
channel 9 [pitch]
channel (1)
channel (4)
channel (7)
channel (10)
tensiune alimentare motoare
channel 1
channel 4
channel 7
channel 10
channel (2)
channel (5)
channel (8)
channel (11)
curent motoare
channel 2 [baza
channel 5 [umar
channel 8 [cot]
channel 11 pitch
Moment in cupla [daNm]
channel 2 [baza]
channel 5 [umar]
channel 8 [cot]
channel 11 pitch]
[rot/min]
[V]
[A]
[daNm]
cobarare-urcare
M1
M2
M3
M4
rot/min
V
A
[daNm]

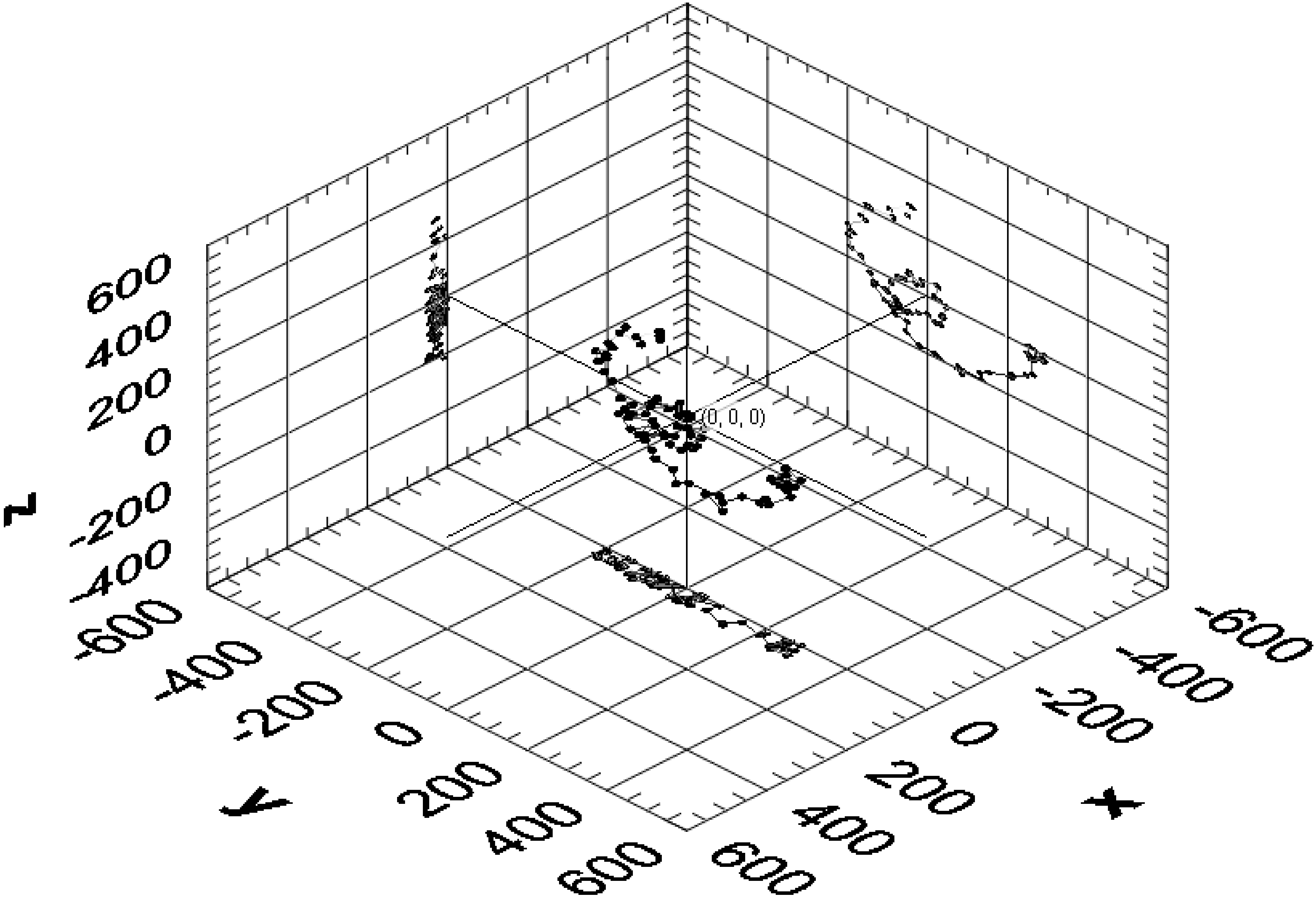

600
400
200
0
-200
-400
z
-600
-400
-200
0
200
400
600
y
-600
-400
-200
0
200
400
600
x
(0, 0, 0)

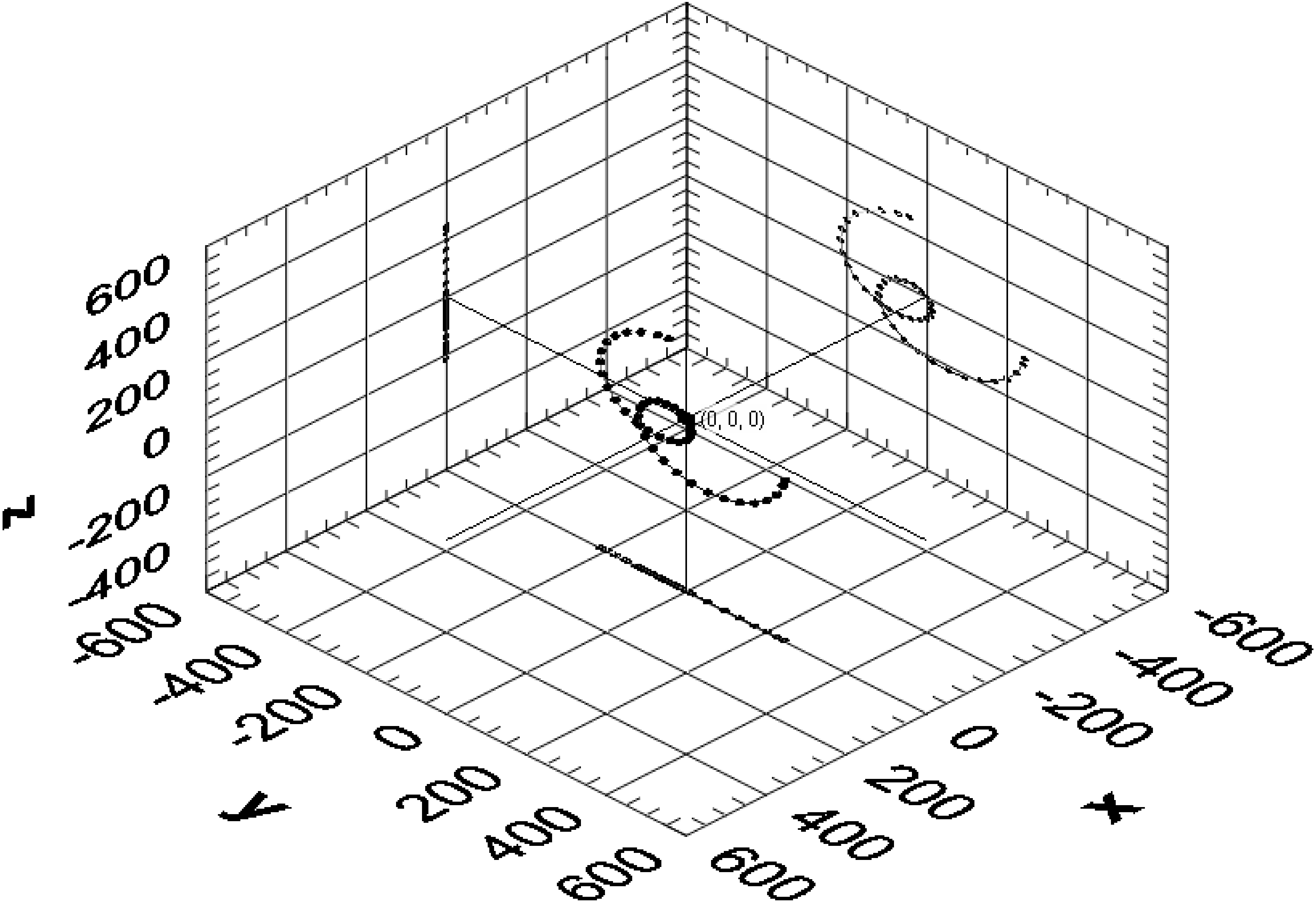

600
400
200
0
-200
-400
z
-600
-400
-200
0
200
400
600
y
-600
-400
-200
0
200
400
600
x
(0, 0, 0)

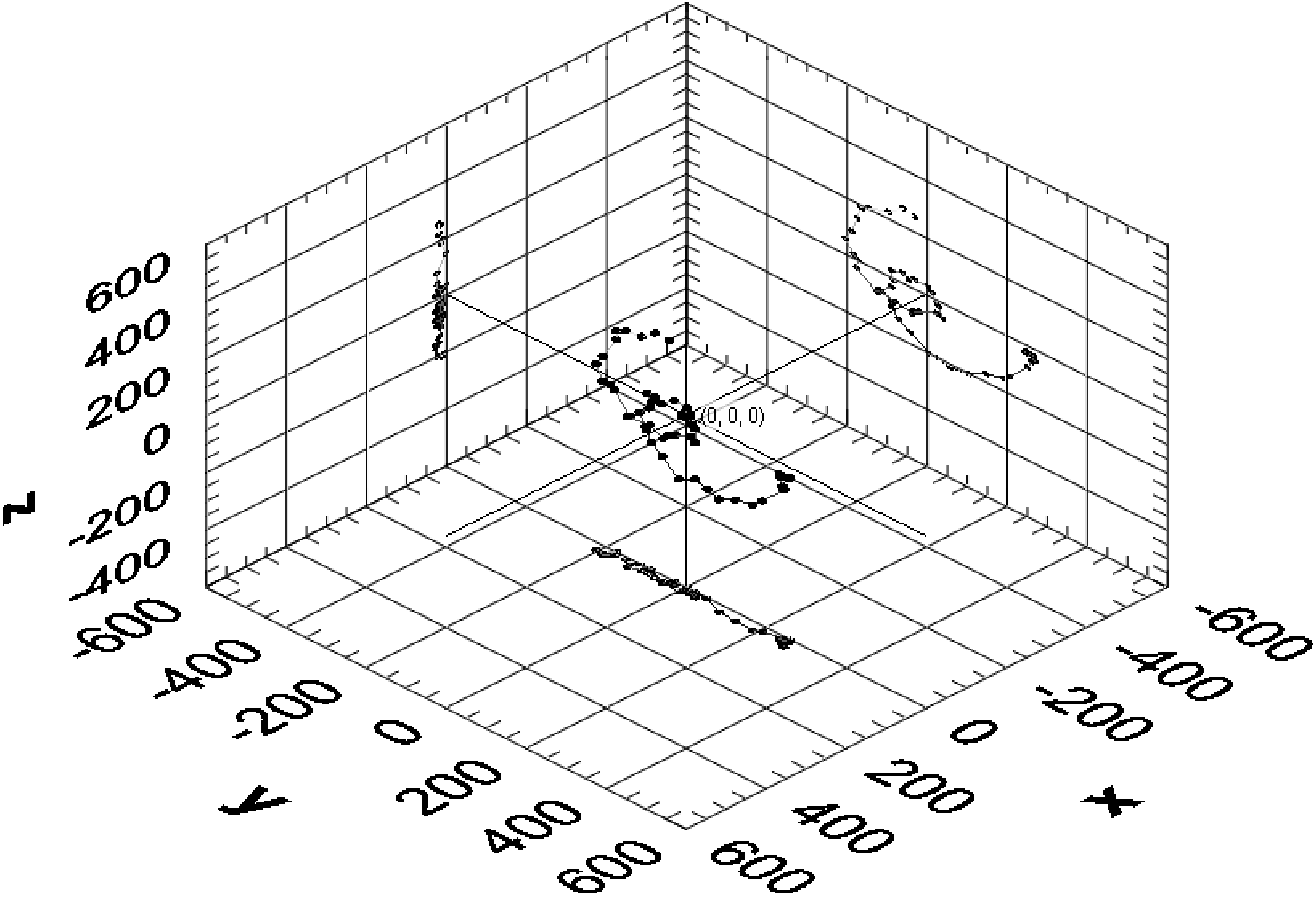

600
400
200
0
-200
-400
z
-600
-400
-200
0
200
400
600
y
-600
-400
-200
0
200
400
600
x
(0, 0, 0)

FINAL CONCLUSIONS

- The assisted method of the research open the way to optimize the global dynamic behaviour of the robots by on-line application of the LabVIEW *VI*;

- We can see that by changing, on-line, some of the system parameters, will be possible to change the characteristics of the simulated space trajectory;

- The assisted method and the virtual LabVIEW instrumentation are generally, we can apply in many other mechanical applications.

References

•P.J.Alsina, N.S.Gehlot, Direct and inverse kinematics of robot manipulator based on modular neural networks, *ICARCV*, *IEEE*, pp. 1743-7, **3**, 1994.

•R. Manseur, D.Keith, A fast algorithm for reverse kinematics analysis of robot manipulator, *International Journal of Robotics Research,* **7** (3), 1998, pp. 622-648.

•D. Gorinevsky, T.Connoly, Comparations of some neural network and scattered data approximations: The inverse manipulator kinematics example, *Neural computation*, **3** (6), pp.521-542.

•L.Lee, Training feedforward neural networks: An algorithm givin improved generalization, *Neural Networks*, **10** (1), pp.61-68, 1997.

•C. Schittenkopf, G.Deco and W. Brauner, Two strategies to avoid overfitting in feedforward networks, *Neural Networks*, **10** (3), pp.505-516, 1997.

•Olaru, A., Olaru S., Ciupitu, L. Assisted research of the neural network by bach propagation algorithm, OPTIROB 2010 International Conference, Calimanesti, Romania, *The RPS Singapore Book*, pp.194-200 , 2010.

•Olaru, A., Olaru, S., Paune D., Ghionea A. Assisted research of the neural network, OPTIROB 2010 International Conference, Calimanesti, Romania, *The Research Publishing Services Singapore Book*, pp.189-194 , 2010.

•Olaru, A., Olaru, S. Assisted research of the neural network with LabVIEW instrumentation, *IEEE ICMENS-2010 Proceedings*, Changsha, China, pp.1-8, 2010.

•Olaru, A., Oprean, A., Olaru, S., Paune, D. Optimization of the neural network by using the LabVIEW instrumentation, *IEEE ICMERA 2010 Proceedings*, ISBN 978-1-4244-8867-4, IEEE catalog number CFP1057L-ART, pp.40-44, 2010.

•Olaru, A., Olaru, S., Paune, D. Assisted research dynamic neural network with time delay and recurrent links, *IEEE ICMERA 2010 Proceedings*, ISBN 978-1-4244-8867-4, IEEE catalog number CFP1057L-ART, pp.284-288, 2010.

•M. Minsky and S. Papert, *Perceptrons: an introduction to computational geometry,* The MIT Press, Cambridge MA, 1969.

•J. J. Hopfield, “Neural networks and physical systems with emergent collective computational abilities”, *Proc. of the National Academy of Sciences,* 81, 1984, pp.3088-3092.

•Hajduk, M., Semjon, J., Vagaš, M.: *Design of the Welding Fixture for the Robotic Station for Spot Weldind Based on the Modular Concept.* In: Acta Mechanica Slovaca No. 3/2009, volume 13, p. 30-35, ISSN 1335-2393.

•Hajduk, M., Sukop, M., Baláž, V., Semjon, J., Vagaš, M.: *Improving the performance of manufacturing systems based reconfiguring and computer integration.* Košice, 2006.

•Páchniková L., Šalátová, M.: *Ciele a efekty pružných výrob*. In: Acta Mechanica Slovaca, roč. 12, č. 2-A, 2008, p. 451- 454, ISSN 1335-2393.

•Páchniková L.: *Profiling production cells based on simulation*. In: Modelling and designing in production engineering, Lublin 2009, p. 132 -137, ISBN 978-83-87833-91-6.